[redacted] Original Vol. 53, No. 1, July, 1982

January, 1983

PEEL HERE

1

SATEAZ 53(1) 443-514 (1982)

SOVIET ATOMIC ENERGY

АТОМНАЯ ЭНЕРГИЯ
(ATOMNAYA ÉNERGIYA)

TRANSLATED FROM RUSSIAN

[redacted]

CONSULTANTS BUREAU, NEW YORK

PEEL HERE

SOVIET ATOMIC ENERGY

Soviet Atomic Energy is abstracted or indexed in *Chemical Abstracts, Chemical Titles, Pollution Abstracts, Science Research Abstracts, Parts A and B, Safety Science Abstracts Journal, Current Contents, Energy Research Abstracts,* and *Engineering Index.*

Mailed in the USA by Publications Expediting, Inc., 200 Meacham Avenue, Elmont, NY 11003.

POSTMASTER: Send address changes to *Soviet Atomic Energy,* Plenum Publishing Corporation, 233 Spring Street, New York, NY 10013.

Soviet Atomic Energy is a translation of *Atomnaya Energiya,* a publication of the Academy of Sciences of the USSR.

An agreement with the Copyright Agency of the USSR (VAAP) makes available both advance copies of the Russian journal and original glossy photographs and artwork. This serves to decrease the necessary time lag between publication of the original and publication of the translation and helps to improve the quality of the latter. The translation began with the first issue of the Russian journal.

Consultants Bureau journals appear about six months after the publication of the original Russian issue. For bibliographic accuracy, the English issue published by Consultants Bureau carries the same number and date as the original Russian from which it was translated. For example, a Russian issue published in December will appear in a Consultants Bureau English translation about the following June, but the translation issue will carry the December date. When ordering any volume or particular issue of a Consultants Bureau journal, please specify the date and, where applicable, the volume and issue numbers of the original Russian. The material you will receive will be a translation of that Russian volume or issue.

Subscription (2 volumes per year)
Vols. 52 & 53: $440 (domestic); $489 (foreign)
Vols. 54 & 55: $500 (domestic); $555 (foreign)

Single Issue: $50
Single Article: $7.50

CONSULTANTS BUREAU, NEW YORK AND LONDON

c/b
233 Spring Street
New York, New York 10013

Published monthly: Second-class postage paid at Jamaica, New York 11431.

SOVIET ATOMIC ENERGY

A translation of *Atomnaya Énergiya*

January, 1983

Volume 53, Number 1 July, 1982

CONTENTS

CONTENTS

(continued)

The Russian press date (podpisano k pechati) of this issue was 6/23/1982. Publication therefore did not occur prior to this date, but must be assumed to have taken place reasonably soon thereafter.

PROBLEM OF HELIUM IN THE STRUCTURAL MATERIALS OF A THERMONUCLEAR REACTOR

A. S. Nikiforov, A. P. Zakharov,
V. I. Chuev, A. G. Zaluzhnyi,
Yu. N. Sokurskii, V. D. Onufriev,
V. N. Tebus, A. E. Gorodetskii,
V. Kh. Alimov, I. V. Al'tovskii,
and V. M. Cherednichenko-Alchevskii

UDC 669.14.018.8:621.039.5

Under the action of high-energy neutrons, because of (n, α)-reactions, a large quantity of helium can be accumulated in the structural materials of a thermonuclear reactor (TNR); in particular, the content of helium in the material of the primary wall, after 10 years of operation, can attain 0.2 to 0.5 at. % [1]. The presence of helium causes high-temperature radiation embrittlement (HTRE) [2-6], imposing the most rigid limitations on the choice of material for the primary wall of a thermonuclear reactor. Therefore, a study of the resistance of materials to helium embrittlement is of great interest. In recent years, the investigations of the behavior of helium solids have been extended [6, 7].

Helium Buildup

At the present time, together with the experimental study of the buildup of helium in structural materials as the result of neutron irradiation [8-13], theoretical calculations of the helium concentration formed are being used successfully. Thus, in the Kharkov Physicotechnical Institute of the Academy of Sciences of the Ukrainian SSR, using perturbation functions obtained experimentally [14] and calculated by means of the ALICE program [15], the buildup of helium in 30 steels was calculated, in the conditions of water-graphite, fast, and future thermonuclear reactors [16].

Table 1 shows the quantitative estimates of the rate of formation of displaced atoms and the buildup of helium, for a number of structural materials, for the condition of a neutron loading of 1 MW·y/m^3 [16-18]. It was established [19], that the nature of the radiation damage is determined to a considerable degree by the relation between the rate of buildup of helium atom c, and the rate of formation of displacements d, expressed by the coefficient K. The value of K depends on the neutron spectrum, the cross section of the (n, α)-reactions, and the elastic scattering cross sections. With large values of K, the tendency to the formation of helium bubbles increases, the number of interstitial atoms avoiding recombination is increased, and the growth of a loop of interstitial atoms is intensified. According to Table 1, K amounts to approximately 3 to 35 for TNR and high-flux reactors, and 0.01 to 0.1 for fast reactors. Therefore, it will be advantageous to use high-flux reactors with a thermal neutron spectrum, e.g., SM-2, in order to verify the radiation resistance of nickel-containing alloys and steels, proposed for the material of the primary wall of a thermonuclear reactor.

Table 2 shows certain data about the buildup of helium as a result of irradiation in a number of reactors. The higher concentration of helium in materials irradiated in reactors with a thermal spectrum of the neutron flux, is explained by the course of the two-stage reaction $^{58}Ni(n, \gamma)^{59}Ni(n, \alpha)^{56}Fe$, leading to a parabolic dependence of the helium concentration on the fluence [9, 13, 16]. Moreover, the formation of helium in structural materials as the result of neutron irradiation, can be caused [16] by the presence of impurities of silicon, phosphorus and sulfur, for which the (n, α)-reaction cross sections in the region up to 5 MeV is a factor of ten greater than for iron isotopes. All this indicates the necessity for verifying the theoretical calculations by means of direct experiments on irradiation with high-energy neutrons.

Translated from Atomnaya Énergiya, Vol. 53, No. 1, pp. 3-13, July, 1982. Original article submitted January 12, 1982.

0038-531X/82/5301-0443$07.50

TABLE 1. Rate of Formation of Helium, c (10^{-4} at. %/y) and Displaced Atoms, d (displ./atom) in Certain Materials

Material	TNR						EBR-II [18]			HFIR [1]		
	c *		d †		K		c	d	K	c	d	K
Steel 316	147	200	11	10	13	20	4,7	44	0,11	4200	140	30
Nb	29	24	7	7	4,1	3,4	1	28	0,04	1,8	41	0,04
Mo	—	47	—	8	—	5,9	1,8	30	0,06	3,1	44	0,07
V	—	57	—	12	—	4,7	0,5	54	0,009	—	—	—
5—10% Al_2O_3 в Al	—	410	—	17	—	24	7,9	76	0,1	—	—	—
Al	310	—	14	—	23	—	—	—	—	—	—	—
Nimonik RE-16	240	—	12	—	20	—	—	—	—	—	—	—

*The values of c in columns 1 and 2 are from the data of [17, 18], respectively; for steel 316 according to [16], c = 350.
†The values of d and K in columns 3, 4 and 5, 6, respectively, are according to the data of [17 and 18]; for steel 316 according to [16], K = 35.

TABLE 2. Concentration of Helium, Formed in Certain Structural Materials during Irradiation in Reactors, with E > 0.1 MeV, at. %

Material	ITR-2000 *			BOR-60†			SM-2 ‡
	c_e	c_c	$\frac{c_e}{c_c}$	c_e	c_c	$\frac{c_e}{c_c}$	c_e
Fe (99,97%)	$2,5\cdot10^{-4}$	$1,5\cdot10^{-6}$ [9]	160	$1\cdot10^{-3}$	$7,7\cdot10^{-4}$ [9]	1,3	—
Ni (99,98%)	$9,5\cdot10^{-4}$	$8,8\cdot10^{-5}$ [9, 10]	4	—	—	—	$1\cdot10^{-2}$
OKh16N15M3B	$9,5\cdot10^{-4}$	$1,4\cdot10^{-5}$ [9, 10]	70	$3,8\cdot10^{-3}$	$9,2\cdot10^{-4}$ [9]	4,1	$4,1\cdot10^{-4}$
Kh26N6T	—	—	—	$1,2\cdot10^{-2}$	$1,5\cdot10^{-3}$ [9]	8,0	—
KhN77TYu	—	—	—	$4\cdot10^{-3}$	$1,1\cdot10^{-3}$	3,6	—
Steel 304	$3,0\cdot10^{-4}$	$9,4\cdot10^{-6}$ [9, 10]	32	—	—	—	—
OKh17N40B	—	—	—	—	—	—	$3\cdot10^{-3}$

*$\Phi t = 4.8\cdot10^{19}$ neutrons/cm^2, $T_{irr} \approx 450$°K.
†$\Phi t = 7.8\cdot10^{22}$ neutrons/cm^2, $T_{irr} \approx 800$°K.
‡$\Phi t = 2.4\cdot10^{21}$ neutrons/cm^2, $T_{irr} \approx 340$°K.

Effect of Helium on the Mechanical Properties

It is well known that the presence of helium in austenitic stainless steels leads to a reduction of plasticity at $T > 0.55_m$ [3, 5, 6], and in many cases the degree of embrittlement is independent of the degree of radiation damage, d, displ./atom. Figure 1 shows how the mechanical properties of samples of austentitic steel OKh16N15M3B depend on the temperature, after irradiation in the SM-2 reactor by neutrons, and helium ions in a cyclotron. It can be seen that the plasticity at a temperature above 600°C for samples irradiated in the reactor and saturated with helium in the cyclotron, varies identically. A similar high-temperature helium embrittlement (HTHE) was observed for samples of this steel irradiated with high-energy electrons at a temperature of 700°C and above [4].

When investigating the dislocation structure and the nature of failure of irradiated samples of steel OKh16N15M3B, it was established that during deformation at 800°C, polygonization and recrystallization occurred, which is confirmed by the serration of the grain boundaries (Fig. 2a), and the polygonal dislocated structure (Fig. 2e). In samples saturated with helium, tested at 800°C, the serration of the grain boundaries is absent (Fig. 2b) and formation of dislocated walls is not observed (Fig. 2f), which indicates a retardation of polygonization and recrystallization processes. Samples with a content of 10^{-3} to 10^{-1} at. % of helium, fail through the grain boundaries (Fig. 2b, d) in contrast from unirradiated samples, or samples containing a small (10^{-5}-10^{-4} at. %) amount of helium, which fail transcrystallitely (Fig. 2a). The size of the helium bubbles at the grain boundaries in all cases did not exceed 10 nm.

The retardation of climbing and gliding of the dislocations in samples saturated with helium can be explained either by a reduction of the effective concentration of free vacancies, because of their bonding with free helium atoms in a solid solution, or by the retardation of the dislocations by minute helium bubbles. In this case, the body of the grain is strengthened and becomes less plastic. The helium bubbles weaken the boundaries between

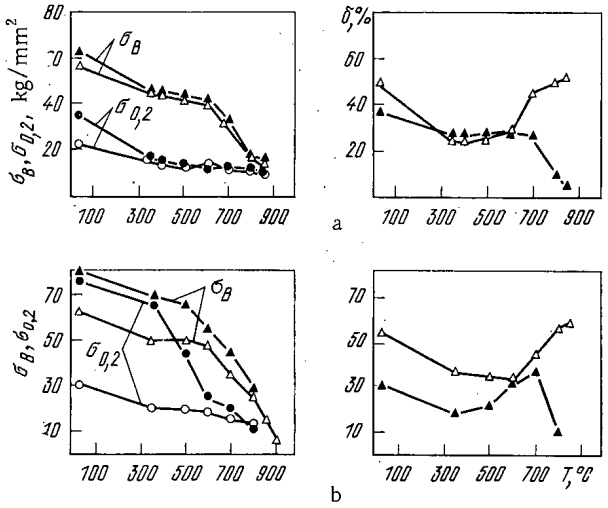

Fig. 1. Temperature dependence of the tensile strength σ_B, the yield stress $\sigma_{0.2}$, and the total expansion of samples of steel OKh16N15M3B, irradiated (●, ▲) with helium ions up to a concentration of 10^{-2} at. % (a), and with neutrons up to a fluence of $1 \cdot 10^{22}$ neutrons/cm^2 with E > 0.1 MeV, and up to a helium concentration of $\sim 2 \cdot 10^{-3}$ at. % (b); ○, △) unirradiated samples.

grains and additionally increase the difference between the relative strength and plasticity of the body and of the grain boundaries, increasing the tendency to intergrain failure and reduction of plasticity of the materials.

A reduction of the rate of deformation from $5 \cdot 10^{-2}$ to $5 \cdot 10^{-3}$ min^{-1} leads to a retardation of the movement of the dislocations, formed in samples of steel OKh16N15M3B in the case of high-temperature (700-800°C) deformation, with dispersed (~10 nm) particles of Nb(C, N), and to an additional embrittlement (Fig. 3). The contribution of this embrittlement is more marked at a low (10^{-5}-10^{-4} at. %) concentration of helium.

An increase in the helium injection temperature from approximately 100 to 700°C leads to a reduction of plasticity at a testing temperature of 400°C and above (Fig. 4). This is due to the formation, under irradiation at a temperature of 550-700°C, of relatively large bubbles (~20 nm) at the grain boundaries and in the solid.

Thus, the mechanism of the embrittlement effect of helium on structural materials during tests at $T \geq 0.55T_m$ is clear. The helium retards polygonization and recrystallization, disturbs the relation between the strength of the body and the boundaries of the grains, and leads to intergrain failure with low plasticity. The concentration of helium and the conditions of testing (irradiation temperature, rate of deformation, etc.), at which the embrittlement effect of helium appears, of course, are peculiar to each material. Heterogeneous phase decay, leading just like helium to the formation of barriers for the movement of dislocations in the body of the grain, and to the appearance of large layers over the grain boundaries, also causes embrittlement at elevated temperature.

Effect on Stainless Steels, Iron and Nickel

As a significant reduction of plasticity of Fe—Cr—Ni alloys, saturated with helium, is observed at a temperature in excess of 600°C, and the effect of helium on the strength properties at this temperature is insignificant, then we shall derive only the values of the total expansion of the samples at 800°C (Fig. 5a). Samples saturated with helium in the cyclotron, of iron and nickel, ferrite—martensitic steel 1Kh13M2, steel OKh16N15M3B, and the alloys DKh17N40B, KhN77T, and KhN77TYu [20], were investigated. It can be seen from Fig. 5 that, with a given helium concentration all the materials, except ferrite—martensitic steel 1Kh13M2, showed a very considerable tendency toward HTHE. This applies particularly to alloys with 40-80% nickel and, first and foremost, to KhN77TYu, alloyed with titanium and aluminum.

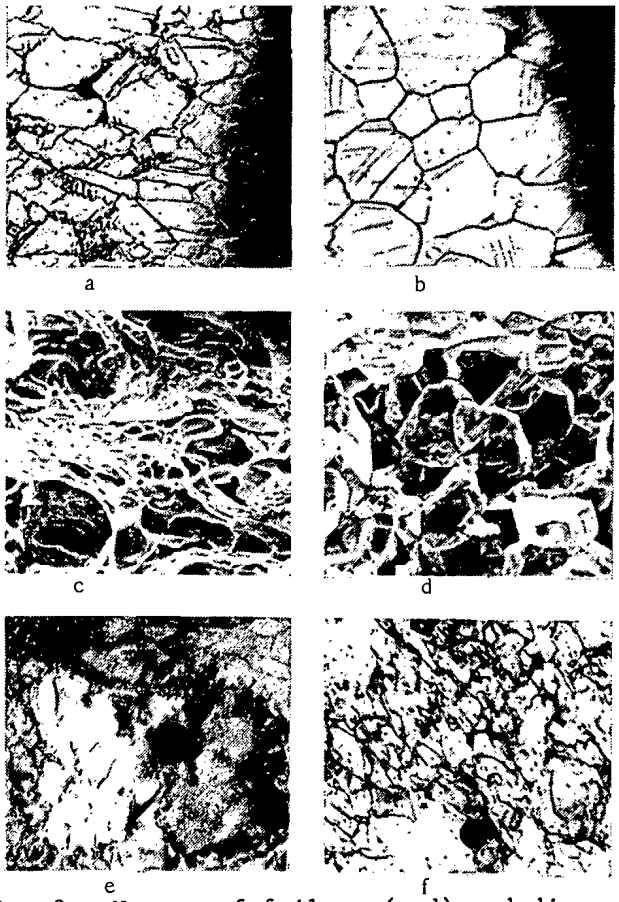

Fig. 2. Nature of failure (a-d) and dislocated structure (e, f) of samples of steel OKh16N15M3B, unirradiated (a, c, e) and irradiated by helium ions up to a concentration of 10^{-2} at. % (b, d, f), after testing at 800°C: a-d) ×1000; e, f) ×40,000.

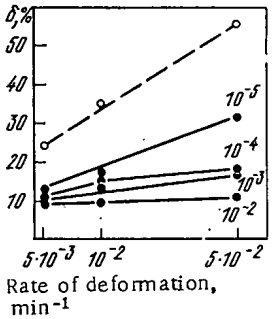

Fig. 3

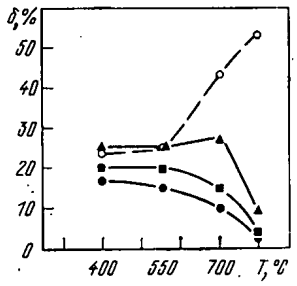

Fig. 4

Fig. 3. Dependence of the total expansion on the rate of deformation at 800°C of samples of steel OKh16N15M3B before (○) and after (●) irradiation with helium ions up to a concentration of 10^{-5} to 10^{-2} at. % (figures at the curves represent the helium concentration, at. %): ----) initial sample; ○, ●) experiment.

Fig. 4. Temperature dependence of the total expansion of samples of steel OKh16N15M3B, irradiated with helium ions up to a concentration of 10^{-2} at. %, for different temperatures: ○) original sample; ▲) $T_{irr.} < 100°C$; ■, ●) $T_{irr.} = 550°$ and 700°C.

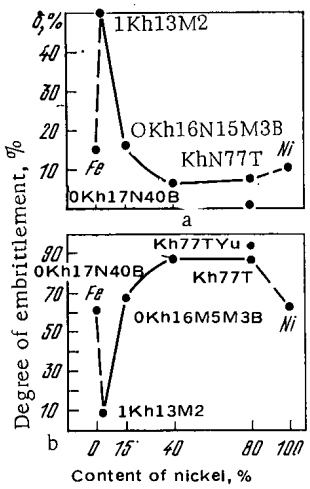

Fig. 5

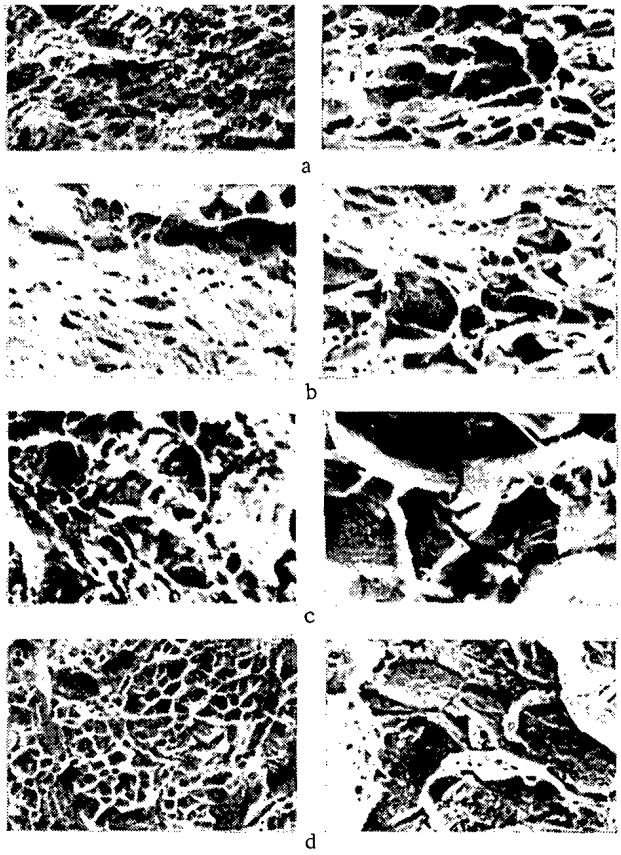

Fig. 6

Fig. 5. Dependence of relative expansion (a) and degree of embrittlement $\frac{\delta_{init}-\delta_{irr.}}{\delta_{init}}$ (b) of materials saturated with helium, investigated up to a concentration of 10^{-3} at. % and tested at 800°C, on the content of nickel.

Fig. 6. Fractograms of samples of steel 1Kh13M2 (a), OKh16N15M3B (b), alloys 0Kh17N40B (c) and KhN77TYu (d) (×1000), deformed at 800°C, unirradiated (left) and saturated with helium to a concentration of 10^{-3} at. % (right).

According to the data of metallographic and fractographic investigations, irradiated samples of iron, steels OKh16N15M3B and 1Kh13M2, fail at 700-800°C through the body of the grains, samples of nickel through the grain boundaries, and alloys with 40-80% nickel have a mixed nature of failure (Fig. 6).

It was established by an electron-microscopic investigation that helium, as already mentioned earlier, retards polygonization and recrystallization, and intensifies the tendency toward intergrain failure of samples of all the materials investigated, with the exception of steel 1Kh13M2. With increase of the content of nickel, the embrittlement action of helium is intensified. In the case of the deposition of dispersed particles of γ'-phase in the alloy KhN77TYu during deformation at 700-800°C, the embrittlement of samples saturated with helium is a maximum.

The very low capability of ferrite—martensitic steel 1Kh13M2 towards HTHE may be related with the special features of the composition (strengthening of the body and boundaries of the grains with carbon), high mobility of the grain and subgrain boundaries, and the low diffusion mobility of helium. We note that the degree of HTHE of this steel was not increased with increase of the helium concentration up to 10^{-2} at. %.

Thus, it may be noted that in the range of helium concentrations of 10^{-3} to 10^{-2} at. %, of the Fe—Cr—Ni steels and alloys, only ferrite—martensitic steel 1Kh13M2 was found to be almost uninclined towards HTHE. According to the mechanism given for HTHE, a reduction of

TABLE 3. Sensitivity of a Number of Materials to Helium Embrittlement [22]

Material	C_{He}, at. % 10^2	δ, %	$S^* = \frac{\delta_{init.}}{\delta_{irr.}} \frac{1}{c}$
Nb	0	47	—
	1,5	40	80
	2,5	31	60
Ti-70A	0	50	—
	1,5	43	80
	3,0	33	50
Ti-6Al-4V	0	35	—
	1,5	15	160
	3,0	11	110
Steel 316	0	28	—
	0,05	17	3300
	0,2	11	1300

*Parameter of sensitivity to HTHE.

TABLE 4. Chemical Composition of Samples of Titanium and its Alloys

Material	Composition, mass %				Impurities, mass %					
	Ti	Al	Mn	Zr	C	N	Fe	Si	H	O
Titanium	Base material	0,05	—	—	0,02	0,01	0,05	0,02	0,0003	0,07
Titanium alloys										
№ 1	Same	5,1	—	—	0,02	0,02	0,04	0,03	0,0003	0,05
№ 2	»	2,0	—	2,1	0,03	0,0004	0,08	0,01	0,005	0,06
№ 3	»	0,7	0,6	—	0,04	0,01	0,04	0,02	0,005	0,03

the embrittlement effect of helium on austenitic steels and alloys can be expected in the case of alloying, ensuring stronger and more plastic grain boundaries.

Effect on Titanium and its Alloys

The effect of irradiation on the properties of titanium, and more so of the HTHE of titanium, have been studied insufficiently. According to a number of papers, titanium and α-titanium alloys possess a higher resistance to radiation swelling and HTHE, than stainless steels. Thus, Jones et al. [21] did not detect radiation swelling of α-alloys of titanium Ti-70A and Ti-6Al-4V during their irradiation with Ni^{++} ions with an energy of 5 MeV, up to doses corresponding to 50 displ./atom [21]. Data have been published [22] about the effect of ^3He injected into titanium by means of a "tritium trick" on the transient mechanical properties at 20 and 450°C. It can be seen from Table 3, that alloys of titanium, Ti-70A and Ti-6Al-4V, are considerably less damaged by HTHE than stainless steels.

An investigation was conducted of the effect of ^4He injected in a cyclotron up to a concentration of $1 \cdot 10^{-2}$ at. %, on the transient mechanical properties of titanium and the alloys Ti–Al Nos. 2 and 3 (Table 4). Irradiation leads to a marked hardening of all materials in the temperature range 20–400°C. The degree of hardening is decreased with increase of the temperature of testing, and at 500°C and above, the hardening disappears completely. At the same time, irradiation reduces the plasticity of all materials. It is shown in Fig. 7 how the total and uniform expansion depends on the testing temperature. It can be seen that irradiation does not have an identical effect on the plasticity of difference alloys; however, the general properties are:

1. independence of the reduction of plasticity on the testing temperature in the range 20–400°C;
2. reestablishment of plasticity at a temperature above 500°C (this is especially noticeable from the data on uniform expansion);
3. a sharp increase of plasticity with T > 500°C, which is due, obviously, to recrystallization processes and not to the limited presence of helium.

It should also be noted that in the irradiated materials at all temperature values, a satisfactory reserve of plasticity is retained ($\delta_p \geqslant 8\%$) and, as shown by investigations on the optical and scanning electron microscope, failure during testing to fracture is of a ductile nature, just as for the original materials.

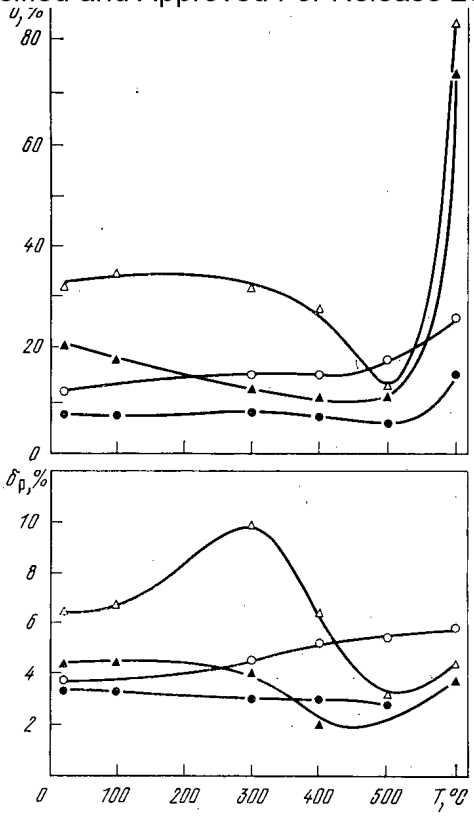

Fig. 7

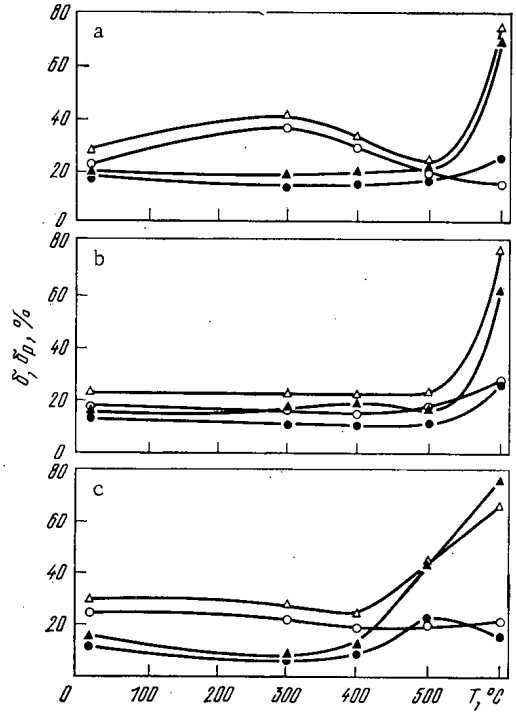

Fig. 8

Fig. 7. Variation of the total and uniform δ_p expansion of titanium and the alloy Ti — 5% Al, by the effect of irradiation: △, ▲) original and irradiated titanium; ○, ●) same, for Ti — Al.

Fig. 8. Dependence of the variation of plasticity of titanium (a) and titanium alloys Ti—2%Al—2%Zr (b) and Ti—0.7%Al—0.8%Mn (c) on the testing temperature: △, ○) δ and δ_p (original samples); ▲, ●) δ and δ_p (irradiated samples).

TABLE 5. Plasticity of Al—Li Alloys with a Different Content of Radiogenic Gases, %

Temperature of testing, °K	Concn. of gas ($^4He + {}^3H$), at. %			
	0	$1{,}5 \cdot 10^{-2}$	$2{,}8 \cdot 10^{-2}$	$23{,}5 \cdot 10^{-2}$
77	23	33	26	20
296	26	25	13	22
523	69	10	8	1

Investigations were conducted also on the joint effect of reactor irradiation (fluence $\sim 1 \cdot 10^{20}$ neutrons/cm², E > 0.1 MeV) and ^3He (concentration $\sim 5 \cdot 10^{-4}$ at. %), implanted by means of the "tritium trick," on the transient mechanical properties of titanium and Ti—Al alloy No. 1. Figure 8 shows how the total and uniform expansion depends on the testing temperature. It can be seen, that just as in the case of helium, implanted by the cyclotron method, the plasticity of the materials is retained at quite a high level ($\delta \geqslant 6\%$) and with $T \geqslant 500°C$ is completely reestablished (for titanium), or has a tendency to reestablishment (for the alloy) at a higher temperature.

Thus, it can be said definitely that titanium and titanium alloys are considerably less inclined to HTHE than stainless austenitic steels, and this factor can serve as the limitation for the use of titanium as the material for the primary wall of a TNR, in the case of loadings up to 5MW·yr/m².

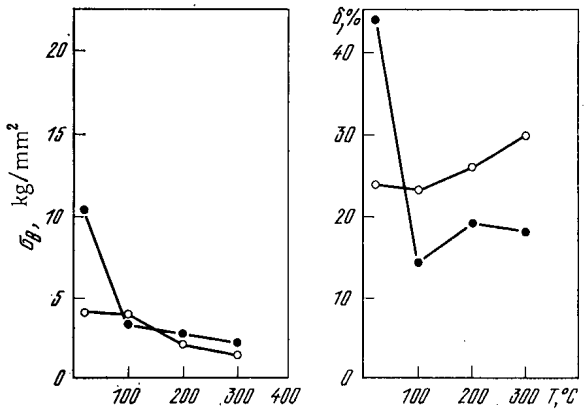

Fig. 9. Dependence of the change of mechanical properties of aluminum on the testing temperature: ○, ●) unirradiated and irradiated samples.

TABLE 6. Calculated Values of the Energy of Dissolution, or the Formation of Interstitial Helium Atoms, Activation of the Migration Process, and the Link between Helium and Vacancies for Certain Metals, eV/atom

Metal	$Q^{He}_{diss.}$	E^{He}_{M}	E^{He}_{B}	Metal	$Q^{He}_{diss.}$	E^{He}_{M}	E^{He}_{B}
Cu	2,03	0,5	1,88*	Mo	4,91	0,23	3,0
Ni	4,52	0,08	2,3	W	5,47	0,24	4,05
Pd	3,68	1,74	3,0*	V	4,61	0,13	3,20*
Au	1,53	0,86	1,53*	Ta	4,23	0,00	3,44*
α-Fe	5,36	0,17	3,98*				

*Calculated values, other — experimental.

Effect on Aluminum and Its Alloys

There are even more limited data about HTHE for aluminum and its alloys. It is known that HTHE has been observed in aluminum alloys irradiated up to high fluence values [23], and it has been assumed that it was due to the effect of helium atoms generated in these alloys because of (n, α)-reactions. However, direct experimental evidence was not obtained.

No appreciable joint effect of reactor irradiation (fluence up to $5\cdot10^{21}$ neutrons/cm², E > 0.1 MeV) and ^{4}He formed by (n, α)-reactions up to a concentration of 0.17 at. % was detected, on the plasticity of baked aluminum alloys in the temperature range 20-500°C [24]; however, the plasticity of the original materials was extremely low (less than 0.5%, for T = 400°C). Embrittlement of Al–Li alloys, irradiated in the reactor, was observed by Smith et al. [25] and Farrell et al. [26]. They explained the loss of plasticity by a weakening of the strength of the grain boundaries in consequence of the formation in them of large helium bubbles (Table 5).

The results of the investigations of the effect of ^{4}He, implanted in pure aluminum in the cyclotron, up to a concentration of $1\cdot10^{-2}$ at. %, on the transient mechanical properties of aluminum in the range 20-300°C are shown in Fig. 9. It can be seen that the expansion of aluminum saturated with ^{4}He in the temperature range 100-300°C is approximately a factor of 1.5 less than the expansion of the original material. This experiment shows unambiguously that aluminum is subject to HTHE for $T \geqslant 0.5T_m$.

Helium in the Crystalline Lattice

Helium is almost insoluble in metals. The energy necessary for transferring an atom of helium from the gas phase into an interstitial position in the metal lattice, i.e., in the

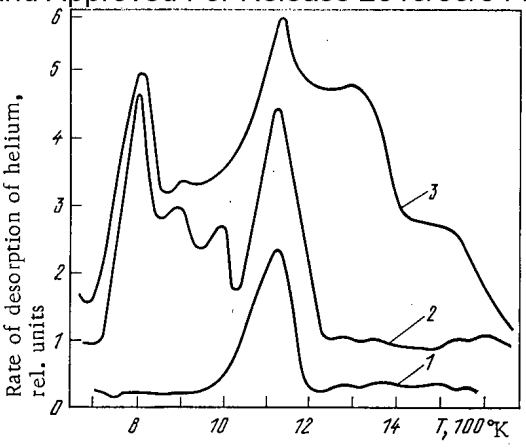

Fig. 10

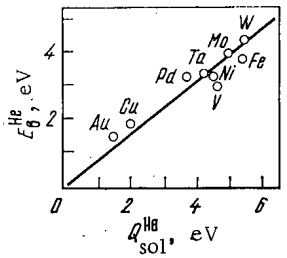

Fig. 11

Fig. 10. Occupation by helium of helium-vacancy complexes: 1) desorption spectrum of Mo(110), containing $1.5 \cdot 10^{12}$ cm^{-2} HeV. The sample was previously irradiated with 1 keV He^+ with a dose of $2 \cdot 10^{13}$ ions/cm^2, and then annealed up to 1050°K; 2, 3) previous treatment just as in 1), but with subsequent irradiation with 150 eV He^+, with a dose of $1 \cdot 10^{14}$ and $2 \cdot 10^{14}$ ions/cm^2, respectively.

Fig. 11. Correlation link between the thermal dissolution of helium in metals, and the binding energy of helium with vacancies.

dissolved state, according to computer calculations [7, 27] is quite large (2-6 eV), and is comparable with the energy of formation of inherent interstitial atoms (Table 6).

It is quite complicated to determine experimentally the energy of dissolution. The results of measurements of the coefficient of helium capture η as a result of irradiation by ions with energy below the threshold for the creation of point defects, i.e., with energy 5-25 eV, can serve as a rough estimate. In this range of energies, the capture coefficients are reduced sharply to 10^{-4}, and the mean free path amounts to one interatomic distance [28].

According to computer calculations [27], atoms of helium entering the lattice can migrate quite rapidly by an interstital mechanism, with an energy of activation of 0.1 to 0.3 eV for the majority of metals (see Table 6). Low values of E_M^{He} were observed experimentally in thermodesorption experiments with W [29], Mo [30] and Ni [31], and also in experiments with the ion projector [32].

According to calculation [27], complexes of the type HeV_2 also are quite mobile, whereas the complex HeV is only slightly mobile. The contribution of multivacancy complexes HeV_n, where $n > 2$, to the migration of helium also is small. The migration of helium to considerable distances throughout the body of the metal can be observed at a temperature in excess of $0.5\text{-}0.6T_m$, when self-diffusion processes are activated [33-35]. One of the possible mechanisms for this migration is based on the dissociation of HeV complexes with the ejection of an He atom into the intergrain position, with rapid migration through the interstices, and with a new capture of vacancies. In this case, the effective diffusion coefficient must depend on the vacancy concentration.

When studying the release of helium from the matrix by heating at a constant rate (thermodesorption procedure), the nature of the disposition of the helium in the crystal lattice can be estimated [29, 35-37]. The quantitative thermal desorption spectrometer, developed by Kornelsen [29] and Caspers [30] and coworkers, has become one of the principal methods for obtaining information about the behavior of helium in metals. The essential conditions in these experiments are low concentration of the helium being investigated, and of the radiation defects interacting with the helium. The latter must be disposed close to the surface at a distance of not more than 10 nm from it, in order to exclude recapture processes of helium by the traps. An important feature is the use of beams of helium atoms with subthreshold energy. The investigation of the system He—Mo (Fig. 10) can serve as an

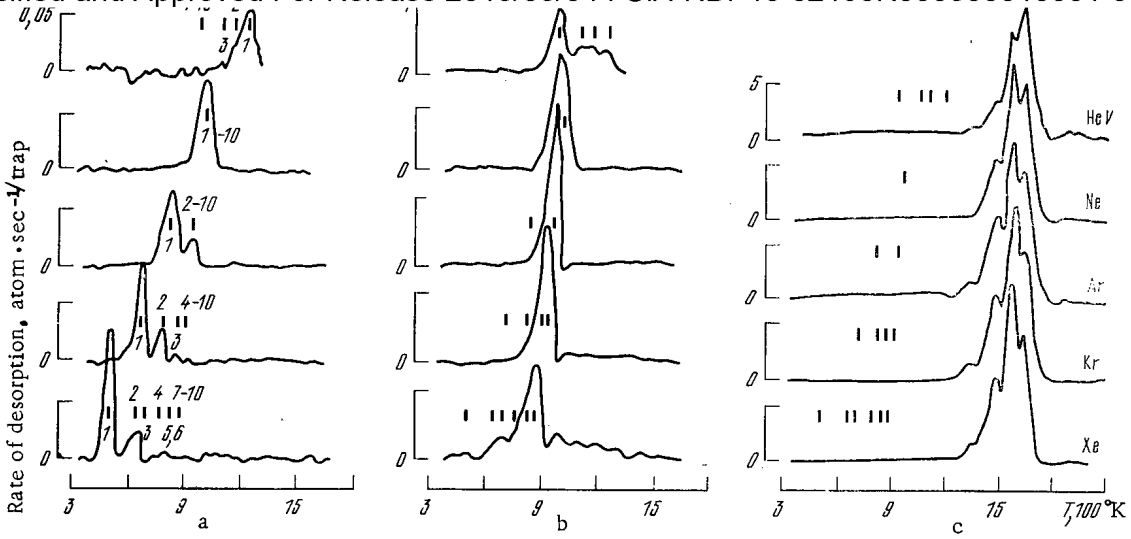

Fig. 12. Desorption spectrum of W(100) with five different types of collectors, created by previous irradiation with ions of He^+, Ne^+, Ar^+, Kr^+, and Xe^+, and subsequent annealing. The collectors were filled by means of irradiation with He^+ ions with an energy of 250 eV, up to a dose of $1 \cdot 10^{12}$ ions/cm^2. The vertical lines on each spectrum show the temperature of the peaks, and the figures show the number of atoms of helium in the dissociating complex: a) average number of captured helium atoms per single collector (0.17); b) same, as in a), but after irradiation by He^+ up to a dose of $2 \cdot 10^{13}$ ions/cm^2, average number of captured helium atoms per single collector 5.6; c) same as in a), but with a dose of $1.2 \cdot 10^{14}$ ions/cm^2, average number of captured helium atoms per single collector 62.

example. Analysis of the experimental results led the author of [38] to the conclusion that the gas release peak at 1100°K is related with the dissociation of HeV complexes. The peaks lying to the left of it and appearing at a lower temperature, were interpreted as dissociations of He_nV complexes, and the peaks located to the right are dissociations of HeV_n complexes. Thus, it was possible to determine the binding energy of the He_nV_m complexes in tungsten [28], nickel [39], and stainless steel [40].

According to Table 6, a definite correlation is observed between the energy of formation of interstitial helium atoms and the binding energy of the helium with vacancies (Fig. 11). This makes it possible to estimate the energy of dissolution of helium from the thermodesorption spectra. In consequence of the quite large values of the binding energy, the vacancy secures an atom of helium, converting it into a nonmobile defect up to a temperature of $\sim 0.5T_m$. Another important consequence was the discovery of the fact of nonsaturability of the collectors during irradiation with helium ions in the temperature range less than $(0.4\text{-}0.5)T_m$. The property of nonsaturability means that in proportion to the entry of helium into the metal, new collectors cannot originate, but the old ones will serve as infinite sinks for the helium, continually increasing their size, due to the transfer of metal atoms to the interstitial positions.

The collector centers, previously created in monocrystals of tungsten, of the type HeV, NeV, ArV, KrV, and XeV, to the amount of 10^{11} cm^{-2}, were filled with helium without the injection of additional defects [41]. It was found that with an average filling of the collectors equal to 0.2, the radius of capture amounts to 2.5-3 Å (1 Å = 10^{-10} m), and the gas release peaks on the thermodesorption spectra are displaced to the region of lower temperature with transition from HeV to XeV (Fig. 12). With an average filling of the collectors equal to 6, the radii of capture are increased to 5-7 Å, and the thermodesorption spectra are similar to that obtained for the He_6V complexes. Finally, with a collector filling equal to 60, all the low-temperature peaks disappear and peaks appear which are related with the release of helium from gas bubbles with a radius of 12 Å (see Fig. 12).

These experiments show that in proportion with the buildup of helium in the metal (even at a temperature less than the temperature of the start of movement of the vacancies), the collectors continually increase their radius of capture, having been converted into helium

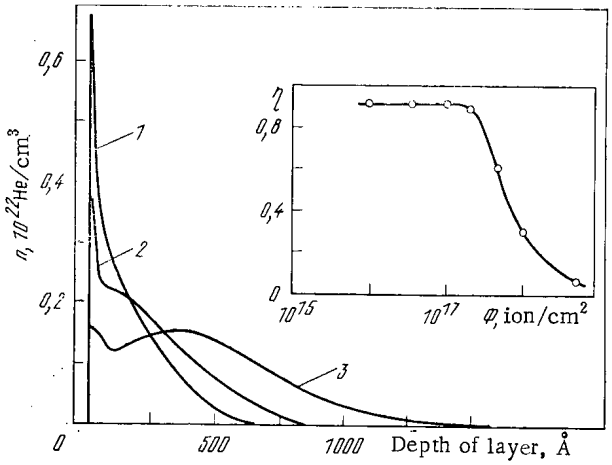

Fig. 13. Distribution of implanted helium in molybdenum (dose 10^{17} ions/cm^2) with energy of 1.5 (1); 3(2), and 9 keV (3) and a temperature of 300°K. Inset, dependence of the capture coefficient of helium on the dose for 9-keV He^+.

bubbles. The process of increasing the radius of the bubble, as a result of filling with helium, can lead to seepage, playing the role of an additional mechanism of helium release from the metal [42]. In proportion with the increase of helium concentration (in the case when the bombarding ions have a broad energy spectrum), the bubbles can join up with one another, forming "dynamic" channels for the outlet of helium at the surface.

Modeling on the computer has shown that the collectors for helium can be not only vacancies, but also boundary dislocations [43] (especially steps in them), implantation loops [44], and also accumulations of impurity implantation atoms, e.g., carbon [45]. Finally, somewhat closely disposed helium atoms can collapse, expelling a metal atom into an internode and forming complexes He_nV_m [46].

An investigation of the distribution of helium in metals, implanted by irradiation with ions with an energy of 1-10 keV and with a different backing temperature, gives very important information about the helium buildup mechanism [47]. These experiments showed, that in Mo, Ni, Cu, and α-Fe in the temperature range 77-600°K, the depth of penetration of helium coincides mainly with the mean free path of the helium ions of this energy (Fig. 13). There are similar data for niobium [48], vanadium [49], and stainless steels. The thermal migration of slowed-down helium atoms and their capture by lattice defects affect the distribution [47]. When annealing the samples, it was established that with a dose of 10^{16}-10^{17} ions/cm^2 the helium is found predominantly in the compound high-temperature complexes He_nV_m, where n and m > 2. A significant reduction of the helium content in the metals being considered can be achieved only by heating the samples up to $(0.4\text{-}0.6)T_m$.

With doses preceding blistering, the relative concentration of helium near the surface of the metal can attain 0.3 to 2 atoms of gas per atom of metal (Fig. 14), so that gas bubbles are formed, the pressure in which reaches several tens of kilobars (1 bar = 10^5 Pa). After rupture of the blister caps, the helium distribution curves assume the normal form (Fig. 15), and the capture coefficient becomes close to zero. The observed enhanced penetration of helium through a diaphragm of molybdenum, irradiated from one side with helium and hydrogen ions, is of great interest [50]. This phenomenon, in the first place, is due to the origination of a high helium concentration in the irradiated near-surface layer and, secondly, to the formation of radiation defects. It will be interesting, in particular, to analyze the possibility of the release of helium from the metallic matrix during interaction of the interstitial atoms with HeV complexes. The energy of formation of the interstitial atoms usually exceeds the energy of an atom of helium occupying an interstitial position and, therefore, the reaction of the displacement of helium into the interstitial position can be accomplished even at a low temperature. This reaction was observed in the case of a molybdenum target irradiated with ions of xenon [30] or hydrogen, and previously irradiated with helium ions. In any case, experiments will be necessary, in which a high rate of helium buildup would be combined with a high rate of generation of defects.

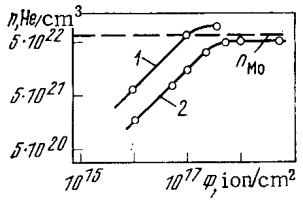

Fig. 14

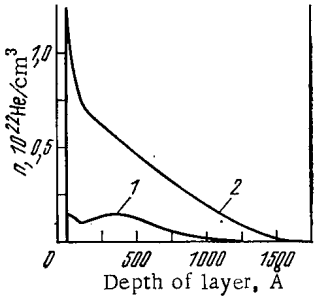

Fig. 15

Fig. 14. Dependence of the change of concentration of helium in the maximum distribution in molybdenum, on the irradiation dose, for an energy of the incident ions of 1.5 (1), and 9 keV (2); ----) atomic density of molybdenum.

Fig. 15. Distribution of implanted 9-keV He^+ in molybdenum, with a dose of 10^{17} (1) and $5\cdot10^{18}$ ions/cm^2 (2), at a temperature of 20°C.

Change of Structure of Metals by the Implantation of Helium

As the result of the implantation of helium into the metallic matrix, the crystal structure of metals is changed significantly, especially with high helium concentrations. As the production of a high concentration of helium by irradiation in a reactor or on a cyclotron requires high costs, methods have been developed for using electrostatic accelerators. The uniform saturation with helium achieved with samples of thickness ∿10 μm has allowed the physical properties to be studied and x-ray structural investigations to be carried out, neglecting surface effects [52].

In the case of low-temperature irradiation [$<(0.3\text{-}0.4)T_m$], the helium atoms remain implanted in the lattice, forming a metastable solid solution and submicroscopic complexes, which were mentioned above. The x-ray investigations revealed a sharp increase of the lattice period with small doses (Fig. 16a), which is characteristic for the formation of solid solutions of helium in the metal. The appearance of a saturation stage is due to the formation of complexes. The increase of the width of the lines (Fig. 16b) further confirms this. The maximum on the B_s curve for nickel indicates consolidation of the depositions and the formation of noncoherent depositions or the process of formation of new complexes, because of recombination of vacancies. The number of these vacancies is increased in proportion with an increase of the dose, which can be judged by the increase of the number of interstitial atoms, enclosed in dislocation loops (Fig. 17c). The size and concentration of the loop in nickel and steel OKh16N15M3B differ strongly (see Fig. 17). The loops in steel remain small for all radiation doses; their concentration is maintained and the number of defects enclosed in them. It follows from the results quoted that the nature of the structure with defects depends strongly on the chemical composition of the material. On annealing, the x-ray lines converge; the value of the lattice period is restored. The dislocation loops are enlarged and their concentration decreases. It was established by a comparison electron-microscopic investigation [53] of the structure of a molybdenum foil, through which α-particles passed, and foils in which these particles were stopped, that the implanted helium atoms have a significant effect on the growth of the loop of interstitial atoms. The atoms of helium, forming the HeV complexes, reduce the probability of recombination of Frenkel pairs and increase the rate of growth of dislocation loops of interstitial atoms.

With increase of the annealing temperature up to $T > (0.44\text{-}0.54)T_m$, gas bubbles are formed. The principal experimental facts about this process were described briefly in [8, 34], however many details of the mechanism of their generation and growth remain unclear. It is necessary only to emphasize that irradiation at a given temperature T more effectively affects the development of the helium bubbles than low-temperature irradiation with subsequent annealing at this same temperature [54]; as in the first case radiation acceleration of diffusion appears.

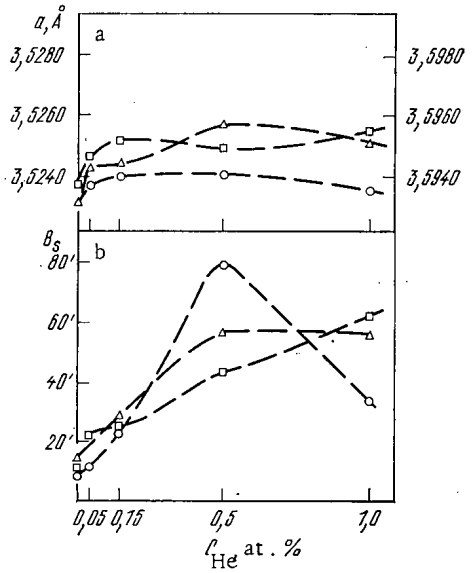

Fig. 16

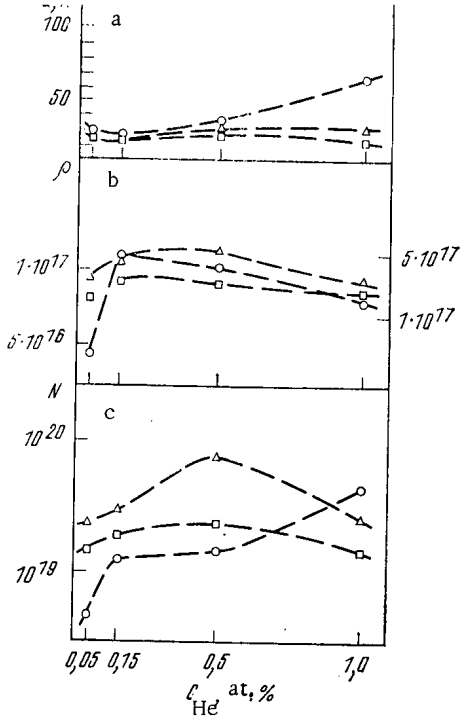

Fig. 17

Fig. 16. Dose dependence of the lattice period (a) and the integral line width (331) B_s (b) for Ni (○), steel OKh16N15M3B (□) and alloy Kh20N40M5B (△); along the ordinate axis to the left is the lattice period of nickel, and to the right — that of OKh16N15M3B and Kh20N40M5B.

Fig. 17. Dose dependence of the size (a), concentration of dislocation loops (b), and the number of point defects (c), enclosed in the dislocation loops (symbols the same as in Fig. 16); in b along the ordinate axis, to the left the concentration of loops in nickel, and to the right in OKh16N15M3B and Kh20N40M5B.

In the case of irradiation with helium ions with an energy of 1-10 keV up to doses of 10^{16}-10^{17} ions/cm^2, a lattice of pores was observed in many metals [54, 55], which was destroyed with increase of helium concentration, and channels were formed which promoted the release of helium. Irradiation with high doses of helium ions with an energy of 30-50 keV of sprayed-on thin films of a number of transition metals [56], led to phase transformations with a change of structure: in nickel, fcc→hcp; in iron, bcc→hcp; in molybdenum and vanadium, bcc→fcc→hcp, and in titanium, hcp→fcc.

Similar transformations were observed also in the case of irradiation with other ions. It is assumed that in this case that the "new" structure is stabilized not by "the foreign" implanted atoms, and the radiation point defects, but more likely by atoms of the natural lattice, ejected into the interstices. However, the sputtered films usually contain a large number of atoms of impurity gases, which under the action of irradiation can promote stabilization of structures, typical for implantation phases.

There are certain indications of a significant change of material properties as the result of implantation of helium atoms in the crystal lattice. In particular, BeO irradiated in a reactor and containing atoms of helium, formed because of (n, α)-reaction, possesses an enhanced surface activity and is capable of being sintered at a lower temperature than unirradiated BeO [57].

CONCLUSIONS

The volume of the publication does not allow an exhaustive review of the problem to be made, because only certain aspects have been considered, which are important for the development of radiation-resistant materials for the primary wall of a thermonuclear reactor and

which represent the maximum scientific interest. According to the theoretical estimates, in the majority of structural materials during the operation of a thermonuclear reactor a large quantity of helium is accumulated. Because of this, the buildup of helium obtained in the course of experiments in fission reactors, usually exceeds the calculated amount by a factor of several. This problem may yet prove to be more serious.

Stainless steel has a tendency to high-temperature helium embrittlement (HTHE). A similar tendency is observed also with aluminum and its alloys; however, in the latter case further investigations are necessary. A significantly less tendency to HTHE is found with ferrite–martensitic steels, titanium and its alloys. It must be emphasized here that the limiting concentration of helium achieved in experiments is still below the expected values during the operation of a thermonuclear reactor.

LITERATURE CITED

1. G. Kulcinski, D. Doran, and M. Abdou, Comparison of Displacement and Gas Production Rates in Current Fission and Future Fusion Reactors, ASTM STP-570 (1975), p. 329.
2. J. Dupouy, J. Lehmann and J. Boutard, in: Reactor Material Behavior [in Russian], Vol. 5, Izd. TsNIIatominform, Moscow (1978), p. 280.
3. N. P. Agapova et al., At. Énerg., 41, No. 5, 314 (1976).
4. V. F. Zelenskii et al., in: Reactor Material Behavior [in Russian], Vol. 2, Izd. TsNIIatominforn, Moscow (1978), p. 192.
5. N. P. Agapova, in: Reactor Material Behavior [in Russian], Vol. 5, Izd. TsNIIatominform, Moscow (1978), p. 177.
6. E. Bloom, J. Nucl. Mater., 85/86, 795 (1979).
7. D. Reed, Radiat. Effects, 31, 129 (1977).
8. Yu. N. Sokurskii et al., Problems of Nuclear Science and Technology Series. Physics of Radiation Damage and Radiation Material Behavior [in Russian], Moscow, Vol. 2, Issue 13, 39 (1980).
9. A. G. Zaluzhnyi, in: Reactor Material Behavior [in Russian], Vol. 2, Izd. TsNIIatominform, Moscow (1978).
10. N. Dudey, S. Harkness, and H. Farrar, Nucl. Appl. Technol., 9, 700 (1970).
11. A. Bauer and M. Kagilaski, J. Nucl. Mater., 42, 91 (1972).
12. A. G. Zaluzhnyi et al., At. Énerg., 48, 4, 260 (1980).
13. F. Holmes and J. Straalsund, Nucl. Mater., 85-86, 447 (1979).
14. G. Dolya et al., Preprint of the Kharkov Physicotechnical Institute 16-50 [in Russian], Kharkov, p. 23 (1976).
15. M. Blann, Overlaid ALICE. Report COO-3494-29 (1976).
16. B. A. Shilyaev, V. A. Kuz'menko, and V. A. Yamnitsskii, in: Problems of Nuclear Science and Technology. Series Physics of Radiation Damage and Radiation Material Behavior [in Russian], Vol. 2, Issue 13 (1980), p. 43.
17. S. Harkness and B. Cramer, J. Nucl. Mater., 85/86, 135 (1979).
18. G. Kulcinski, in: Plasma Physics and Controlled Nuclear Fusion Research, Vol. 2, IAEA, Vienna (1975), p. 251.
19. Sh. Sh. Ibragimov et al., in: Problems of Nuclear Science and Technology. Series Physics of Radiation Damage and Radiation Material Behavior [in Russian], Vol. 1, Issue 4 (1977), p. 71.
20. N. P. Agapova et al., in: Reactor Material Behavior [in Russian], Vol. 2, Izd. TsNIIatominform (1978), p. 214.
21. R. Jones et al., Trans. Am. Nucl. Soc., 33, 258 (1979).
22. R. Jones and A. Charlott, J. Nucl. Mater., 85/86, 877 (1979).
23. R. King and J. Weir, in: Trans. Am. Nucl. Soc., 11, 146 (1968).
24. P. Maziasz and K. Farrell, J. Nucl. Mater., 85/86, 913 (1979).
25. T. Smith and B. Russel, J. Nucl. Mater., 38, No. 1, 1 (1971).
26. G. Farrell, J. Nucl. Mater., 37, 96 (1970).
27. V. V. Kirsanov, in: Defects in Crystals and their Computer Modeling [in Russian], Nauka, Moscow (1980), p. 115.
28. A. Van Gorkum and E. Kornelsen, Radiat. Effects, 52, 25 (1980).
29. E. Kornelsen, Rad. Effects, 13, 227 (1972).
30. L. Caspers et al., Phys. Status Solidi, A37, 371 (1976).
31. E. Kornelsen and D. Edwards, in: Applications of Ion Beams to Metals, Plenum Press, New York (1973), p. 521.

32. A. Wagner and P. Seidman, Phys. Rev. Lett., 42, 515 (1979).
33. A. A. Babad-Zakhryapin and M. I. Lagutkin, Fiz. Met. Metalloved., 47, 858 (1979).
34. N. P. Agapova et al., Izv. Akad. Nauk SSSR. Ser. Fiz., 38, 11, 2337 (1974).
35. N. P. Agapova et al., At. Énerg., 40, 490 (1976).
36. V. S. Karasev et al., Problems of Nuclear Science and Technology. Series Physics of Radiation Damage and Radiation Material Behavior [in Russian], Vol. 2, Issue 13, (1980), p. 82.
37. V. S. Karasev et al., At. Énerg., 34, 4, 251 (1973).
38. A. Van Veen and L. Caspers, in: Proc. Seventh Int. Vacuum Congress and Third Int. Conf. on Solid Surface, Vienna, 12-16th September (1977), p. 2637.
39. D. Reed, D. Armour, and G. Carter, Vacuum, 24, 10, 455 (1974).
40. R. Rantanen and E. Donaldson, Radiat. Effects, 23, 37 (1974).
41. E. Kornelsen and A. Van Gorkum, J. Nucl. Mater., 92, 79 (1980).
42. W. Wilson, M. Baskes, and C. Bisson, Phys. Rev., 1313, 2470 (1976); L. Caspers et al., Phys. Status Solidi, A46, 541 (1978).
43. F. Berg et al., Solid State Commun., 24, 193 (1977).
44. L. Caspers et al., Phys. Status Solidi, A52 (1979).
45. G. Van der Kolk and A. van Veen, Delft. Prog. Rep., 4, 19 (1979).
46. L. Caspers, A. van Veen, and H. van Dam, Phys. Lett., 50A, 5, 351 (1974).
47. V. Kh. Alimov, A. E. Gorodetskii, and A. P. Zakharov, Zh. Tekh. Fiz., 49, No. 6, 1273 (1979).
48. J. Roth et al., J. Nucl Mater., 63, 120 (1976).
49. R. Blewer and R. Langley, J. Nucl. Mater., 63, 337 (1976).
50. A. P. Zakharov, V. M. Sharapov, and A. E. Gorodetskii, Dokl. Akad. Nauk SSSR, 251, No. 6, 1388 (1980).
51. D. B. Bogomolov et al., Pis'ma Zh. Tekh. Fiz., 5, 22, 1389 (1979).
52. V. D. Onufriev, Yu. N. Sokurskii, and V. I. Chuev, Preprint IAE-3070 [in Russian], Moscow (1978).
53. Sh. Sh. Ibragimov et al., Problems of Nuclear Science and Technology. Series Physics of Radiation Damage and Radiation Material Behavior [in Russian], Vol. 1, Issue 4 (1977), p. 71.
54. Sh. Sh. Ibragimov et al., Problems of Nuclear Science and Technology. Series Physics of Radiation Damage and Radiation Material Behavior [in Russian], Vol. 1, Issue 4 (1977), p. 65.
55. W. Jäger and J. Roth, J. Nucl. Mater., 93/94, 756 (1980).
56. V. N. Bykov et al., in: Reactor Material Behavior [in Russian], Vol. 3, Izd. TsNIIatominform, Moscow (1978), p. 197.
57. A. V. Khudyakov, Izv. Akad. Nauk SSSR, Ser. Neorg. Mater., 9, 1192 (1973).

MODULE OF ANGARA-5 FACILITY

E. P. Bol'shakov, E. P. Velikhov,
V. A. Glukhikh, O. A. Gusev,
E. V. Grabovskii, V. I. Zaitsev,
Yu. A. Istomin, Yu. V. Koba,
G. M. Latmanizova, G. M. Oleinik,
A. M. Pasechnikov, V. P. Pevchev,
A. S. Perlin, O. P. Pecherskii,
L. I. Rudakov, V. P. Smirnov,
V. I. Chernobrovin, V. I. Chetvertkov,
and I. R. Yampol'skii

UDC 621.039.6

Advances made in the technique of high-power pulsed accelerators and in research on the physics of the interaction of intense fluxes of charged particles with matter have made it possible to proceed with the construction of a demonstration thermonuclear facility with inertial plasma confinement, the Angara-5. Scientists of the D. V. Efremov Scientific-Research Institute of Electrophysical Apparatus jointly with scientists of the I. V. Kurchatov Institute of Atomic Energy have developed a design for the accelerating complex of the Angara-5 facility, which consists of separate modules, radially arranged around the reactor chamber which contains the thermonuclear target.

The module is a pulsed electron accelerator with a design energy of 2 MeV and a current of 0.8 MA with a pulse full-width at half-maximum of 85 nsec. At the end of 1980, in operation with an equivalent load, the main module of the Angara-5 was brought up to near-design conditions.

Description of Module. The accelerator is installed in a horizontal multisectional cylindrical tank (Figs. 1, 2). The first storage device is a surge generator based on a circuit with bipolar charging. The generator consists of three parallel branches, each of which has 14 cascades of four series-parallel connected 0.4-μF capacitors with a nominal voltage of 100 kV. The generator is switched by gas dischargers with field "distortion" which are arranged on the outer perimeter of the generator to reduce its internal inductance. The control pulses enter the discharges through longitudinal and transverse resistive connections. The generator is set up in a section of a 3-m-diameter tank filled with transformer oil. The energy stored in the generator is transmitted along a coaxial dual shaping line, whose geometric dimensions are given in Fig. 2. The intermediate electrode of the dual shaping line is connected to a high-voltage electrode generator by two symmetric conductors which pass through dielectric diaphragms located between the sections of the tank. With the actuation of five gas-filled commutators radially arranged between the intermediate and inner electrodes a nanosecond electromagnetic pulse is formed and is transported along a transmission line to the load.

Two-gap commutators with distortion of the electric field are mounted in the module [1]. The middle electrode is made in the form of two segments, turned with their bases to each other. It has a central through-hole 60 mm in diameter. One of the gaps controls the delivery of a triggering pulse to the igniting electrode while the second gap is irradiated through the hole in the intermediate electrode.

Calculations of the commutator electric fields showed that the maximum value of the field at the surface of the intermediate electrode in the prebreakdown stage is 392 kV/cm while after breakdown in one of the gaps it is 614 kV/cm. The field intensity tangent to the surface of the insulator in the gas does not exceed 105 kV/cm in the first regime and 180 kV/cm in the second regime.

Translated from Atomnaya Énergiya, Vol. 53, No. 1, pp. 14-18, July, 1982. Original article submitted February 26, 1982.

 0038-531X/82/5301-0458$07.50

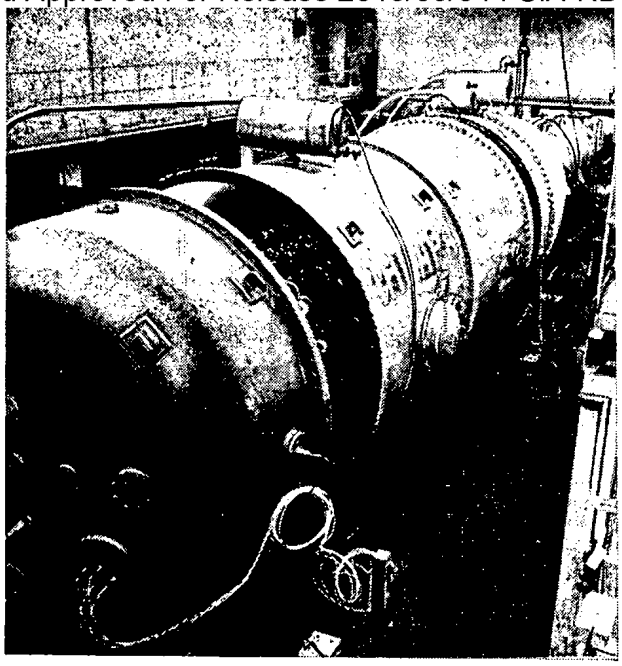

Fig. 1. Accelerator module of Angara-5 facility.

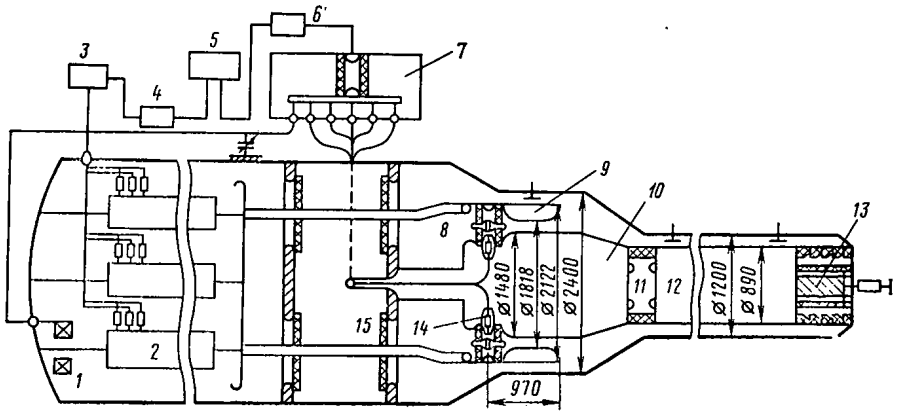

Fig. 2. Schematic of Angara-5 facility: 1) current transformer; 2) branches of surge generator; 3) generator of igniting pulses; 4, 6) thyratron amplifiers; 5) synchronizer; 7) commutator-triggering unit; 8, 9, 10) commutator and intermediate and inner electrodes, respectively, of dual shaping line; 11) prepulse discharger; 12) transmission line; 13) load equivalent; 14) protective resistor; 15) high-voltage diaphragm.

The main design characteristics of the module are:

Surge generator:	
surge capacitance, nF	78.7
operating voltage in surge, MV	up to 2.3
operating energy store, kJ	up to 210
Dual shaping line:	
operating charging voltage, MV	up to 2.1
wave resistance of inner line, Ω	1.35
wave resistance of outer line, Ω	0.86
capacitance of intermediate electrode, nF	77
Wave resistance of transmission line, Ω	2

Maximum electric field intensity, kV/cm:	
at high-voltage electrode of generator	132
at surface of insulation diaphragms	79
at positive electrode of dual shaping line	155
at rounded parts of negative electrode of dual shaping line	220

The dischargers of the generator and the commutators of the dual shaping line are controlled by a special synchronization scheme whose elements are indicated in Fig. 2. The surge generator is triggered by an auxiliary ignition generator built on ceramic capacitors. An ignition pulses (70 kV) is delivered through six cables to the dischargers of the first three cascades of each parallel branch. Pulses which control the commutators of the dual shaping line are produced by a generator with coaxial-cable shaping lines. The control pulses, with a voltage of 150-200 kV and a leading edge of ∿20 nsec, are formed when the cable lines are closed with the aid of a gas-filled thyratron discharger. The cables are charged in step with the intermediate electrode of the dual shaping line from a pulsed current transformer, connected into the circuit of one branch of the surge generator. Smooth regulation of the amplitude of the charging voltage of the controlling cables is attained by connecting a variable capacitor to the input of the triggering unit.

Damping resistors protect the cables from overvoltages arising when the commutators of the dual shaping lines are actuated. The ignition generator and the capacitor triggering unit are triggered by 50-kV pulses, with a leading edge of ∿20 nsec, which come from pulse amplifier-shapers. Control is effected by the synchronizer.

The current in the apparatus was measured with Rogowski loops with integration in coaxial foil resistors. These pickups make it possible to resolve signals with a leading edge of about 10 nsec. The voltage in the apparatus was measured with the aid of capacitive dividers in which a foil capacitor with a low stray inductance was the secondary capacitance. The time resolution of these dividers was about 2 nsec.

Results of Measurements. In the accelerator the electrical strength of the principal units was checked under actual operating conditions, the regimes of stable switching of the surge generator and the dual shaping line were ascertained, and the energy balance of the facility was studied with the dual shaping line being charged at voltages of up to 2.1 MV. During the experiments an equivalent load with a built-in voltage divider was installed at the end of the transmission line in order to absorb the energy of the module and to enhance the reliability of the measurements of the output power. A solution of potassium chloride was used for the resistor.

The switching characteristics of the generator were investigated while the dual shaping line was being charged. The mean switching time of the generator is 600 ± 30 nsec with an asynchronism of 100-150 nsec in the triggering of the individual branches, which can be considered to be allowable with a total charging time of 1.4 μsec for the dual shaping line (Fig. 3).

Processing of the current oscillograms for five controls of the cables by the commutators reveals that the spread of their switching-on times does not exceed ±2.6 nsec. As shown by comparison of the current rise time with the values calculated for the ignition time, the first breakdown occurs between the control and intermediate electrodes. The oscillogram of the commutator current (Fig. 4c) shows an oscillation of frequency ∿26 MHz. Analysis of the oscillations indicates that in the gap between the intermediate and high-voltage electrodes the overvoltage reaches a threefold value, which is quite sufficient for a reliable breakdown in the gap under illumination. On processing a series of such oscillograms, we used the damping decrement to estimate the average resistance of the discharge channel as being $R_c = 0.325\ \Omega$. This value is roughly half that calculated form the theory of Braginskii [2] with the assumption that each discharger has ten discharge channels. From the same measurements we estimated the average inductance of one commutator as $L_c = 64$ nH.

Figures 4a and b show the voltage pulses at the end and beginning of the transmission line with the dual shaping line being charged at 1.6 MV. The parameters of the output pulse were measured with the aid of two capacitive voltage pickups. From the values of the voltage we isolated the reflected and incident waves, which enabled us to calculate the current, voltage, and impedance of the load. Figure 4d gives the oscillogram of the voltage across the resistance divider built into the load. The dashed line shows the voltage pulse calculated from the values of the voltage at the end and the beginning of the transmission line

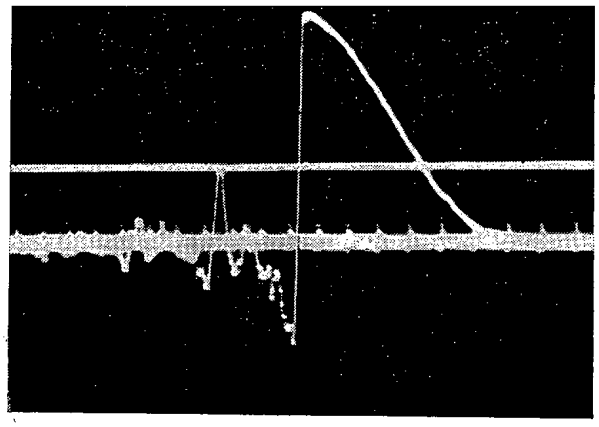

Fig. 3. Oscillogram of charging of capacitance of dual shaping line (the period of the calibration markers is 200 nsec while the amplitude calibration is 700 kV).

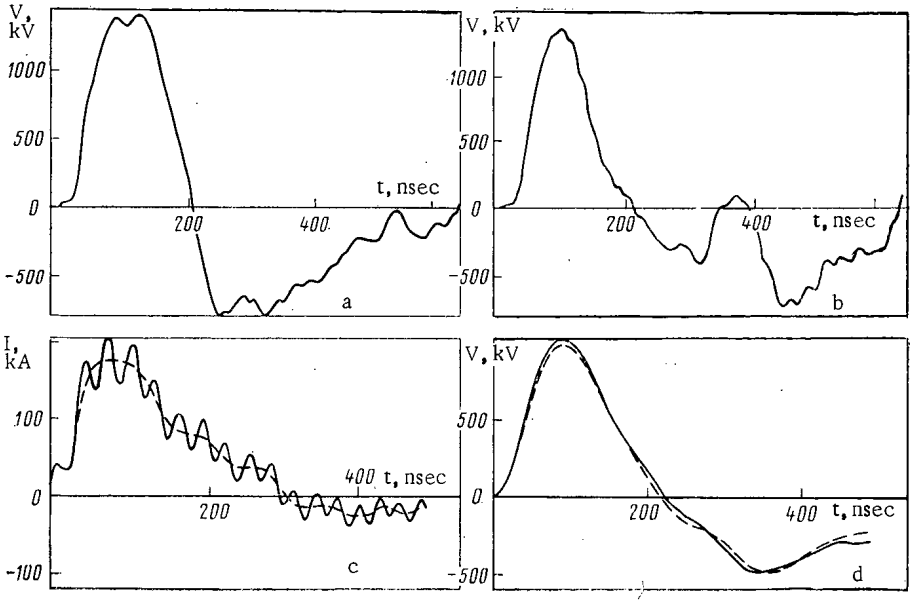

Fig. 4. Current and voltage pulses in various elements of module with the dual shaping line being charged at 1600 kV: a, b) voltage pulse at end and beginning of transmission line, the distance to the load being 1.5 and 4.8 m, respectively; c) current in one commutator of the dual shaping line; d) voltage pulses in equivalent load; dashed lines and solid lines, respectively, are the curves calculated from oscillograms *a* and b and the curves plotted according to the measured values.

(Figs. 4a, b). The agreement (to within 3%) indicates that the calibration of the capacitive pickups was correct since the division ratio of the resistance divider is determined only by geometric factors.

Figure 5 gives the oscillogram of the voltage pulse in the transmission line at a charging voltage of 2.1 MV in the dual shaping line; the time calibration is 40 nsec and the voltage calibration is 550 kV. The pulse energy up to the time of polarity reversal is 105 kJ ± 10%.

Comparison of the Calculated and Experimental Characteristics. To obtain reliable results concerning the energy transfer coefficient and also to ascertain if it can be increased, we calculated the process of recharging the surge generator by the dual shaping line and compared the results with experiment. The calculations were performed by using the

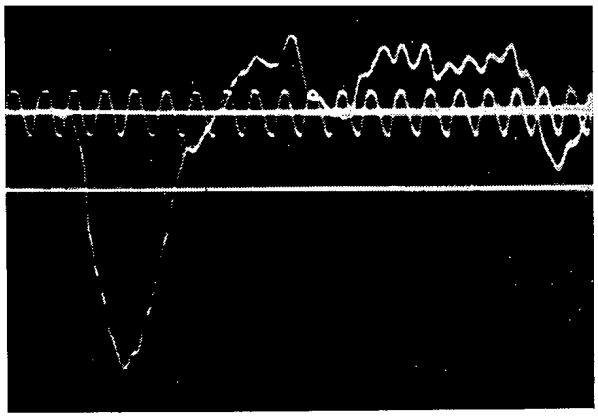

Fig. 5. Oscillogram of voltage at beginning of transmission line at a voltage of 2100 kV in the dual shaping line.

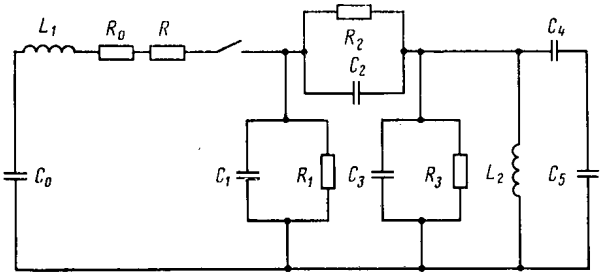

Fig. 6. Equivalent circuit for calculation of recharging of surge generator by dual shaping line.

equivalent circuit shown in Fig. 6. The values of the circuit parameters were obtained from the results of experimental measurements on the module. The loss resistance of the capacitors, determined from the damping decrement for a single capacitor at the operating frequency of the surge generator, was $R_0 = 0.57\ \Omega$. The surge capacitance of the generator ($C_0 = 78.7$ nF) was calculated from the measured values of the capacitances of the capacitors installed in the generator and was corrected by allowing for the fact that the dynamic capacitance of the capacitors, determined at the operating frequency, is 4% smaller than the static capacitance. The pattern of the electrostatic fields was used to determine the outer and inner partial capacitances of the dual shaping line, $C_1 = 48.5$ and $C_2 = 28.5$ nF, and the junction capacitance $C_3 = 13$ nF.

The inductance of the charging circuit, calculated from the results of measurements in the short-circuit regime, is $L_1 = 5.6$ μH. The charging inductance of the inner capacitance of the dual shaping line is $L_2 = 0.44$ μH.

The resistance of the spark channel in the dischargers of the generator was measured in a separate experiment from the damping of the oscillations in an auxiliary high-frequency circuit, incorporating a discharger ($f_0 = 11$ MHz, $\rho = 30\ \Omega$, $r_0 = 0.13\ \Omega$). The main circuit, with a natural frequency of 330 kHz and $\rho = 2\ \Omega$, ensured the operating current of the discharger spark. Within the limits of the measurement accuracy the experimental results are in agreement with the resistance values calculated from the Braginskii formula. The good agreement is apparently attributable to the fact that there was one-channel switching in these experiments.

The results of the calculation of the efficiency of energy transfer by the dual shaping line during one charging half-period and the distribution of the losses are as follows (in %):

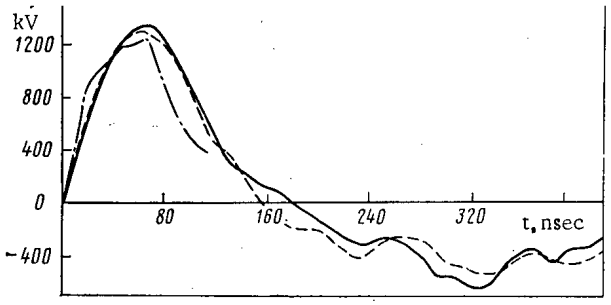

Fig. 7. Voltage of incident wave in transmission line with dual shaping line being charged at 1600 kV; the solid line is the experimental curve while the dot-and-dash and the dashed lines are the preliminary and refined calculated curves, respectively.

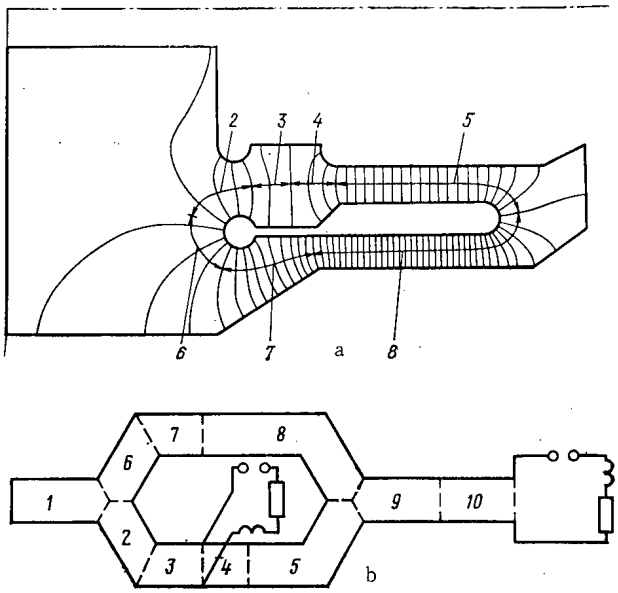

Fig. 8. Diagram for refined calculation: a) distribution of electric field in dual shaping line; b) equivalent circuit: 1) delay 30 nsec, wave resistance 14.5 Ω; 2) 9 nsec, 2.58 Ω; 3) 5 nsec, 2.25 Ω; 4) 6 nsec, 2.25 Ω; 5) 26 nsec, 1.3 Ω; 6) 9 nsec, 2.58 Ω; 7) 12 nsec, 1.2 Ω; 8) 30 nsec, 0.86 Ω; 9) 17 nsec, 2.68 Ω; 10) 17 nsec, 2.5 Ω, respectively.

Losses:	
in capacitors	6.2
in water (ρ_{water} = 3 MΩ·cm)	4.5
in contacts	4.7
in dischargers	1.1
Residual energy in capacitors	1.3
Efficiency of energy transfer by dual shaping line	81.3

It is of interest to compare the values of the incident wave in the transmission line with the calculation made during the designing of the facility [3]. The main characteristics of the pulse, i.e., the amplitude and length, coincide but the shape of the curve differs (Figs. 7 and 8). The calculations are refined substantially by using data on the distributions of the electric field (Fig. 8a) in the dual shaping line to select the equivalent parameters of the segments of the lines (Fig. 8b). In this case the length of the segments

TABLE 1. Efficiency of Charge Transfer in the Accelerator Module

Characteristic	Energy	
	kJ	%
Initial energy of generator	210	100
Energy losses in recharging of generator and dual shaping line	40	19
Losses in commutators of dual shaping line	15.5	7.4
Energy losses due to nonideal geometry of dual shaping line (inequality of lengths and wave resistances of outer and inner lines, charging inductance, stray capacitances, etc.)	46.3	22.1
Energy losses in prepulse discharger	3.2	1.5
Useful energy in load	105	50

is chosen to be equal to the mean equipotential length while the capacitance is chosen from the number of tubes of force. In Fig. 8 each tube of force corresponds to 1 nF. The resistance of the commutators was chosen to be 0.325:5 Ω. Their inductance is estimated from the two-dimensional approximation of the magnetic field pattern. It was L_c = 17 nH. The losses in the prepulse discharger were determined [3] for eight one-channel discharges developing in the discharger.

The satisfactory agreement of the calculated results with experiment makes it possible to calculate the losses in the individual elements of the pulse-shaping system and to determine the efficiency of energy transfer of the surge generator to the load. Table 1 gives the energy balance in the Angara-5 module with the capacitors of the surge generator being charged at ±82 kV according to the results of refined calculation.

When the voltage in the dual shaping line is raised to 1.8-1.9 MV the module operates stably and no breakdowns are observed either in the liquid insulation or in the structure of the insulators, diaphragms, and dischargers. A further increase of the voltage to 2.1 MV led to a decrease in the stability of the generator triggering owing to the small amplitude of the commutators of the dual shaping line. We did record individual cases of breakdowns in the water insulation between the intermediate and outer electrodes. The operating stability can be enhanced by increasing the charging voltage of the generator to 180 kV and appropriately shortening the charging time of the dual shaping line.

The authors express their thanks to the workers of the I. V. Kurchatov Institute of Atomic Physics, the D. V. Efremov Scientific-Research Institute of Electrophysical Apparatus, and the Institute of High-Current Electronics, Siberian Branch of the Academy of Sciences of the USSR, who participated inthe experimental investigations.

LITERATURE CITED

1. V. V. Vecherkovskii et al., Abstracts, Second All-Union Conference on Engineering Problems of Thermonuclear Reactors [in Russian], Leningrad (1981).
2. S. I. Braginskii, Zh. Eksp. Teor. Fiz., 34, 1548 (1958).
3. E. P. Velikhov et al., Preprint D-0301, D. V. Efremov Scientific-Research Institute of Electrophysical Apparatus, Leningrad (1976).

FLAW DETECTOR FOR THE INSIDE SURFACES OF PIPES IN A NUCLEAR POWER STATION

A. A. Madoyan, V. G. Kantsedalov,
V. P. Samoilenko, and P. B. Samoilenko

UDC 620.179.1(08.8)

Present-day methods of monitoring the inside surfaces of pipelines can only be used on straight runs. Therefore, the best and most promising way of solving the problems involved in monitoring the metal of the pipelines in a nuclear power station is to create remote-monitoring systems able to cover the whole of the lines, including bends and parts that are difficult to get at. Such equipment must be able to cope with sections having complex arrays of pipes with bends of various radii of curvature and remote control of the transducers under conditions in which the shapes of the surfaces being monitored are not constant.

Analysis and simulation of the technical process of remote monitoring shows that these difficulties can be overcome if the unit for moving the transducer is made up of flexibly articulated members, each of which is capable of being deployed in a plane passing through the center of curvature of the bend, normal to the plane containing its axis. Furthermore, the transport mechanism as a whole must possess axial symmetry and be controlled only by the commands "Forward" and "Reverse."

It is also necessary to adapt compact transducers to the geometry of the surfaces being monitored, which be achieved by pneumatic drive of the parts in contact with the pipe, by taking advantage of the damping properties of compressed air. In this case, the contact force does not depend upon the "path" of the transducer when it moves from its initial to its working position. To adapt a noncontact transducer, such as a telemetric, photographic or optical-fiber type, involves an increase in the depth of focus of the optical system.

The Southern branch of the Dzerzhinskii Institute of Heat Engineering has investigated a prototype for a production version of equipment for monitoring the inside walls of pipes on nuclear power stations equipped with water-cooled water moderated reactors type VVÉR-440, developed and approved for the Armyansk nuclear power station. The type DTL-500 equipment can deliver the surface-treatment and the testing and measurement units to the check zone. This latter unit consists of various units of nondestructive testing equipment which are assembled on the transport in the form of modules. The composition of these modules will depend upon the subject of the investigation and the demands placed on the reliability of the metal in the pipeline. The transporter consists of the following assembles and units: the transport mechanism, a system for controlling the transport mechanism in the automatic mode, equipment for preparing the inner surface of the pipe, a scanning system, a system for controlling the angular orientation, a fiber-optics system for checking the metal of the pipe, a control desk, a power line, and a communications system for control signals and information.

The present article examines a transport mechanism consisting of two support belts and units for coupling and displacement (Fig. 1). Each support belt takes the form of a cup, the outer surface of which carries an elastic annular chamber. The coupling and displacement units take the form of a bellows attached between the bottoms of the cups, the internal cavity of which, together with the chamber, are connected to a compressor via a reversing valve and automatic control equipment. The mechanism is set in motion by the compressor, compressed air from which is applied through a system of regulators so that each link of the mechanism operates in sequence, ensuring that the device moves automatically.

The transport mechanism for flaw detection of the inside surface 1 of tube 2 comprises two support belts in the form of cups 3 and 4, on the outer wall of which is mounted an elastic cylindrical collar 5 and annular chambers 6 and 7. The bottoms 8 of the cups are

Translated from Atomnaya Energiya, No. 1, pp. 18-21, July, 1982. Original article submitted May 12, 1981.

0038-531X/82/5301-0465$07.50

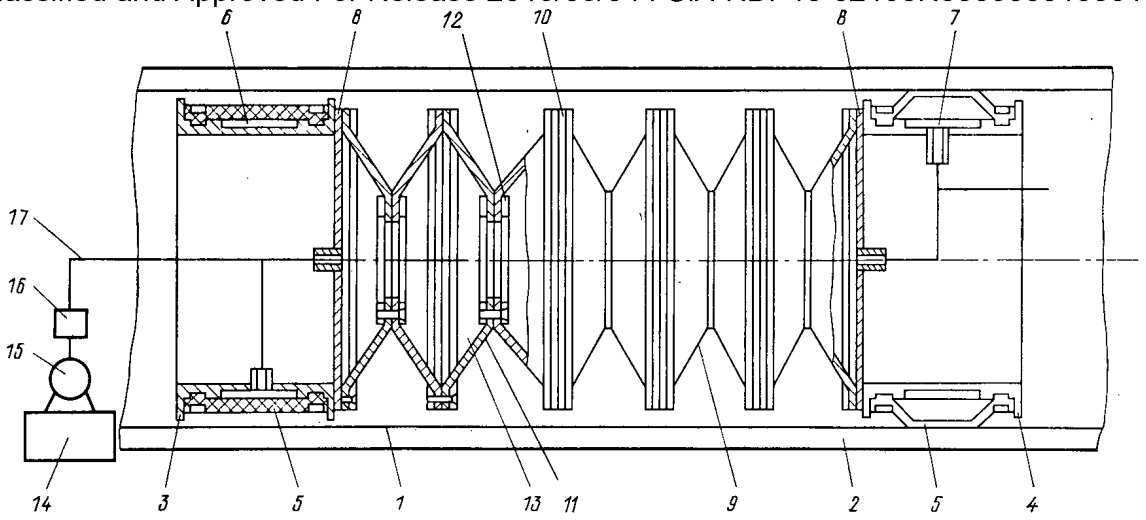

Fig. 1. Transport mechanism.

Position	Positions of displacement mechanism along cycles	Pressure 1	2	3
a	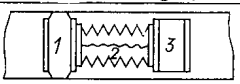	p	0	0
b	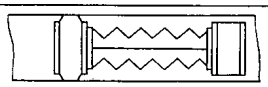	p	p	0
c	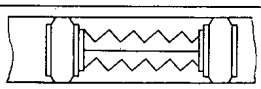	p	p	p
d	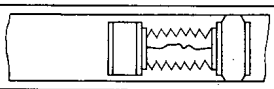	0	0	p
e	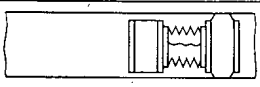	0	-p	p
f	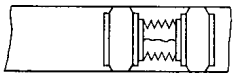	p	-p	p

Fig. 2. Positions of mechanism during the elements of a single step: 1) chamber; 2) cavity.

connected by a coupling and displacement mechanism taking the form of a bellows 9 made of a set of rigid rings 10 connected together by elastic members 11 in the form of truncated cones attached to each other by small flanges 12. The inside cavity 13 of the bellows and the cavity of the annular chambers are connected to compressor 14 via reversing valve 15 and automatic equipment for controlling the mechanism. Air is applied to feed main 17.

The mechanism operates as follows. Compressor 14 applies compressed air through changeover valve 15, which initially acts to pressurize the feed main 17. Air is applied to chamber 6 of cup 3. The elastic collar is deformed by the increased pressure in the chamber, to become convex. This brings it into contact with surface 1 of pipe 2, locating it in place by friction. The air in the internal cavity 13 of the bellows and chamber 7 is at atmospheric pressure (see Fig. 2, position *a*). The automatic equipment then connects the discharge chamber 13 to the main, so that the pressure builds up, expanding the bellows so that it elongates, pushing cup 4 forward relative to 3 (see Fig. 2, position b). With a further increase in pressure in cavity 13, the automatic equipment connects chamber 7 of cup 4, the air pressure in which deforms the collar and fixes cup 4 to the inner surface 1 of pipe 2 in the same way as with cup 3. Chambers 6 and 7 of both cups, together with internal cavity 13, are now pressurized (see Fig. 2, position c). The next cycle starts with a drop

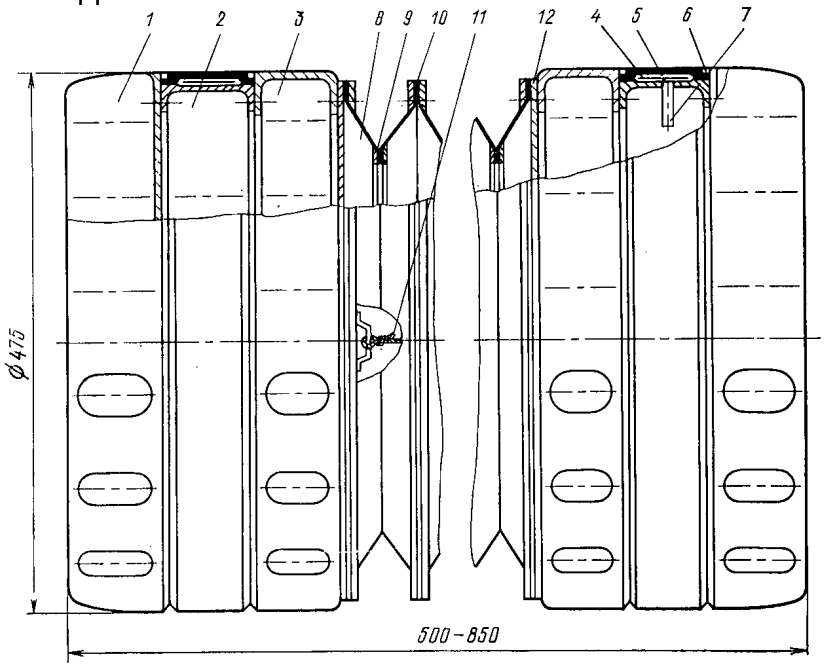

Fig. 3. Design of transport mechanism.

in the pressure of chamber 6 of cup 3 and in cavity 13, so that the friction between the elastic collar of the cup and the inside surface of the pipe disappears (see Fig. 2, position d). The automatic equipment then connects cavity 13 to the suction pipe of the compressor, causing the pressure in 13 to drop below atmospheric. The bellows collapses under atmospheric pressure. Since cylinder 4 is fixed in place, cup 3 is drawn along behind cup 4 (see Fig. 2, position e). The automatic equipment then connects the air supply to chamber 6 and fixed cup 3 in the pipe (see Fig. 2, position f). The pressure in cavity 13 and chamber 7 equalizes with that of atmosphere (see Fig. 2, position a) and the process is repeated. If need be, the mechanism can move in reverse simply by reversing the sequence of operation of cups 3 and 4.

The transport mechanism Fig. 3 is simple to operate. It enables a system of transducers for flaw detection of the inside surface of the pipe to be delivered to site regardless of the configuration and position in space of the pipes. It is extremely reliable and economic, since a small pressure head created by a compressor will produce a large tractive force, increasing as the diameter of the pipe increases. Therefore, the mechanism can carry a large payload.

The support belt (cup) consists of guides 1, shell 2, insert 3, and bottom 12. The guide and insert take the form of thin-walled perforated cases with abutting end faces. The perforations only serve to reduce weight. The shell comprises a thin-walled cylindrical case on the outer face of which there is an annular slot for the rubber toroid 4. To prevent accidental damage during contact with the inner face of the pipe, the toroid is covered by collar 5 made of dense wear-resistant rubber. Ring-shaped projections are formed at the sides of the shell to grip the collar with the aid of wire ring 6, the elastic toroid has a union for connecting to the pressure main.

Since the guide and insert have different heights, the shell (and, consequently, the collar, the outer surface of which clamps the device in the pipe when the toroid is pressurized) is displaced to the end of the mechanism. This disposition of the fixing surface ensures reliable clamping of the mechanism in the tube and reduces the toppling moment exerted from outside the confines of the cup by the transducers being carried. The assembly of the support belt (cup) out of guide, shell, inert, and bottom is completed by means of rubber connectors.

The connection and displacement assembly (bellows) is formed with a periodic structure. The members of the bellows comprise truncated cones 8 made out of rubber. The ends of the cones about the perimeter are fixed to rigid metal rings 9, 10. The number of members is determined by the geometry of the "most difficult" bend and the geometry of the member it-

self (∿20). The number of sections is also determined by the preset length of each step of the mechanism. The members are assembled into a bellows with the aid of a glued-rubber connection, in order to ensure that the joint is airtight. The end sections of the bellows are fixed to the bottoms of the cups.

To limit the step and prevent the bellows from bursting by overextension or by an accidental increase in pressure inside the bellows, a cable 11 is attached between the bottoms 12 of the cups. The final stage in the assembly of the transport mechanism is the rubber connections of the bellows to the support belts.

Laboratory and site tests at the Armyansk nuclear power station have shown that the transport mechanism has good traction properties, enabling it to pass along pipes with any spatial configuration, containing bends with radii of curvature of $R \geqslant 1.25D_B$, where D_B is the internal diameter of the pipe. The presence of branch lines with $D = 0.2\ D_B$ presents no problems for the mechanism. The technical data of the transport mechanism are as follows:

Tractive force (with gauge pressure of p = 0.04 MP in the bellows)	3500 N
Range of action	100 m
Payload	250 kg
Speed:	
on the straight	0.005 m/sec
round bends	0.003 m/sec
Weight	100 kg
Drive	Pneumatic with P_g = 0.25 MPa
Power connectors	One

CONCLUSIONS

Equipment type DTL-500 has been developed for flaw detection on the inner surfaces of pipes on nuclear and thermal power stations involving the remote monitoring of the state of the base metal and welded joints. The equipment consists of a transport mechanism and systems for preparing the pipe surface and checking on the state of the metal. The flexible displacement unit and axisymmetrical design of the transport mechanism enables the equipment to negotiate bends of any spatial orientation and maximum curvature.

The tractive forces generated by the transport mechanism at an excess pressure in the supply main of ∿0.25 MPa is 3-4 kN, which enables the DTL-500 to carry any check-measurement apparatus. Laboratory and site test have shown that the equipment is simple to manufacture and operate, and that it possesses good performance characteristics.

PROPERTIES AND BEHAVIOR OF THE HIGH-ACTIVITY WASTES FROM THE EXPERIMENTAL GAS-FLUORIDE REPROCESSING OF SPENT URANIUM–PLUTONIUM AND URANIUM FUEL OF THE BOR-60

A. P. Kirillovich, Yu. G. Lavrinovich,
M. P. Vorobei, and Yu. I. Pimonov

UDC 621.039.59:621.039.75

The development of the gas-fluoride method for reprocessing fuel elements [1, 2], which is considered to be one of the most promising for the reprocessing of spent fast reactor fuel, requires investigations of the properties and behavior of the high-activity wastes formed. The purpose of these investigations is the development of safe methods of processing and the long term storage of the wastes. It was reported earlier [3] about the behavior of the high-activity wastes obtained from spent uranium oxide fuel of the BOR-60 reactor, with a cooling of 3 and 6 months.

In the present paper, the results are given of an investigation of certain radiation and physicochemical properties of high-activity wastes, obtained during the gas-fluoride reprocessing of spent uranium-plutonium oxide fuel, and also the behavior of these wastes (initial radioactivity ∿6130 TBq/kg) during six years of monitored storage.

Investigational Procedure

The investigations were conducted on a special test rig, mounted in a shielded chamber. The energy release of the spent fuel and of the high-activity wastes was determined in a calorimeter of the heat-conducting type [4]. The error of the measurements, taking account of the preparation of the average sample did not exceed ±5%, with a confidence coefficient of 0.95. The radiation gas release, degree of contamination of the gas phase, and the thermal stability of the samples were studied by the procedures described previously in [3].

The composition of the gas phase in the waste containers was determined by a mass-spectrometric method for both a uniform temperature of self-heating of the highly active products and for the containers heated externally to 700°C [5].

In order to study the leaching-out of the radionuclides from the wastes, the recommendations given in [6] were used: the ratio of the volume of distilled water to the surface area of the sample amounted to 9 cm, and water samples were taken over 30 days. The quantitative yield of ^{137}Cs was determined by the γ-spectrometric method. The error of the measurements amounted to ±20% with a confidence coefficient of 0.95.

The thermophysical characteristics of the solid fluoride wastes were found by the method of differential thermographs with a quasisteady heating regime. The facility and the procedure for measuring the thermal conductivity are described in [7]; the error of the measurements in remote handling conditions was ±10%.

Results of Investigations and Discussion

Table 1 shows the characteristics of uranium–plutonium oxide spent fuel, taken for the experimental reprocessing, and the highly-active solid wastes obtained as a result. As shown by the investigations, approximately one-half (44.8-60.9%) of the fission product radioactivity is concentrated in the fluorination residues (cinders), for which the specific heat release amounted to 50-52 W/kg, and the β-activity was in excess of 550 TBq/kg. The main contribution to the β-activity was made by cerium, ^{144}Pr, ruthenium, ^{106}Rh, zirconium, ^{95}Nb, and ^{137}Cs. It was shown earlier in [3], that more than 99% of the ^{90}Sr is concentrated in the cinders. The solid wastes formed by the gas-fluoride reprocessing of the fuel, are highly active powdery (cinders) or granulated (sorbent, chemical absorber) materials with a saturated density of 800-1200 kg/m^3.

Translated from Atomnaya Énergiya, Vol. 53, No. 1, pp. 22-25, July, 1982. Original article submitted July 6, 1981.

0038-531X/82/5301-0469$07.50

TABLE 1. Forms and Characteristics of the Wastes from the Reprocessing of Spent Oxide Uranium–Plutonium Fuel

Form of mixture	Duration of cooling, months	Specific heat release W/kg	Specific β-activity, TBq/kg	Radioactivity of fuel, % initial	Activity of radionuclides, TBq/kg							
					$^{144}Ce-^{144}Pr$	$^{106}Ru-^{106}Rh$	^{103}Ru	^{137}Cs	^{134}Cs	^{95}Zr	^{95}Nb	^{141}Ce
Mechanical mixture												
UO_2	6	20,0	222	100	110	4,7	—	0,8	—	24	30	—
PuO_2	170	2,9	32,2									
Fluorination residues	12	50,8	564	60,9	510	6,3	0,56	1,2	—	44	27	1,2
Powder from forecondensate	12	52,0	580	4	160	120	5,6	14	0,4	32	170	0,48
Sorbent basic	12	0,37	4,1	1,8	0,004	0,093	0,003	0,0002	0,00008	0,0007	0,040	0,0002
Sorbent	12	0,15	1,6	1,4	0,0007	0,017	0,0005	0,00007	0,00002	0,00007	0,0008	0,00001
Chemical absorber	12	0,52	5,8	22,5	0,0006	0,07	0,0015	0,00008	0,00002	0,00006	0,0006	0,00002
Actual mixture												
UO_2-PuO_2	8	21,44	238	100	87	2,4	—	0,28	—	6,7	3,3	—
Fluorination residues	8	51,8	580	44,8	240	2,5	—	0,09	—	8,9	3,7	—
Powder from forecondensate	8	73,4	810	16,0	260	16	—	0,93	—	5,2	9,3	—
Sorbent basic	8	0,08	0,89	0,9	0,10	0,20	—	0,0003	—	0,003	0,05	—
Sorbent	8	0,44	4,9	17,3	0,27	0,05	—	0,001	—	0,006	0,013	—
Chemical absorber	8	0,05	0,57	4,0	—	0,06	—	—	—	—	0,0002	—

Note. ^{90}Sr was not determined.

TABLE 2. Forms and Characteristics of Wastes from the Experimental Reprocessing of a Consolidated Portion of Spent Uranium Oxide Fuel

Form of product	Saturated density, kg/m³	Specific heat release, W/kg	Specific β-activity, TBq/kg	Radioactivity of fuel, % initial	Activity of radionuclides, TBq/kg							
					$^{144}Ce-^{144}Pr$	$^{106}Ru-^{106}Rh$	^{137}Cs	^{95}Zr	^{95}Nb	^{125}Sb	^{103}Ru	^{134}Cs
Spent fuel	—	13,00	144	100	60,60	2,50	0,88	3,30	5,40	0,016	0,012	0,005
Fluorination residues	1050	78,70	874	86,0	436	16,9	7,0	16,2	12,0	0,15	0,09	0,08
Sorbent scrubber	800	0,61	6,8	1,1	0,11	0,11	0,009	0,0007	0,006	0,002	—	—
Sorbent	800	0,1	1,1	1,0	0,015	0,004	0,003	0,0004	0,003	0,002	0,003	0,00006
Chemical absorber	1000	0,1	1,1	1,0	0,005	0,22	0,0006	—	—	—	0,014	—

Note. ^{90}Sr was not determined.

Table 2 shows the forms and characteristics of the wastes obtained from the experimental reprocessing of a consolidated portion of spent uranium fuel with an aging time of 5-48 months and a burnup of 4.4-12.8%. A comparison of these data with the results previously obtained from reprocessing uranium oxide fuel with an aging time of 3 months [3], shows that, almost independently of the aging of the fuel, as a result of its gas-fluoride treatment, more than 80% of the fission products is concentrated in the fluorination residues.

In order to work out safe conditions for the long-term monitored storage of the highly-active fluoride wastes and to prepare them for burial, the temperature and energy release of the wastes, the radiation gas release, degree of contamination of the gas phase and its chemical composition, thermal stability, leaching out of ^{137}Cs, and the thermal conductivity were studied.

The variation of temperature and heat release of the cinders from the reprocessing of uranium fuel aged for 3 months, is shown in Fig. 1, from which it follows that the main fall in temperature and energy release is observed during the first 200-300 days of storage;

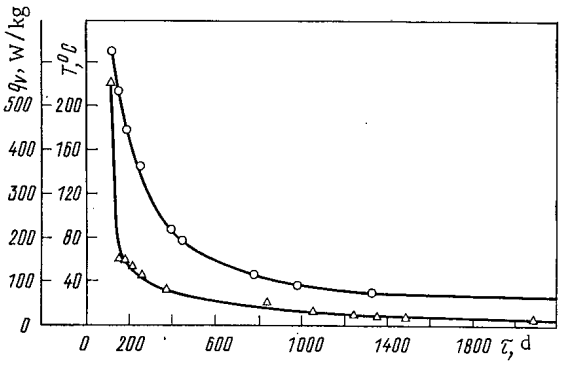

Fig. 1

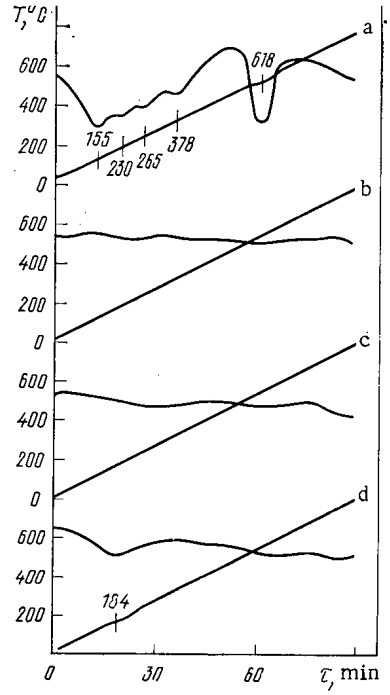

Fig. 2

Fig. 1. Dependence of temperature (○) and specific heat release (△) of cinders, obtained from reprocessed fuel, aged for 3 months, on the duration of storage with natural cooling of the container (volume of container 1 liter, diameter 105 mm, wall thickness 2.5 mm, and mass of cinders 0.280 kg).

Fig. 2. Thermograms of cinders: a) from the reprocessing of uranium fuel, aged for 3 months; b) same, but after a three-year sotrage of the wastes; c) from the reprocessing of fuel, aged for 1.3 y; d) from reprocessed uranium–plutonium fuel (figures at the curves are the transformation temperature).

after 6.5 years, the specific heat release of the cinders has been reduced by a factor of 60.

The thermal conductivity of the fluoride wastes is slightly dependent on the form of the reprocessed fuel and in the temperature range 100-700°C it amounts to 0.220-0.450 W/(m·deg C) for the cinders, and 0.330-0.460 W/(m·deg C) for the sorbent. For the chemical absorber it varies from 0.280 to 0.435 W/(m·deg C) in the range 100-500°C.

The radiation gas release was measured periodically for all forms of wastes from both the reprocessed mixed and uranium fuels. An increase of pressure ($6.08 \cdot 10^3$ Pa, V = 0.23 cm^3/g) in the container with the cinders and with a heat release of 552.3 W/kg, was recorded only at the start of the experiment [3]. A qualitative analysis of the gas phase, released from the wastes, indicated in it the presence of fluorine, hydrogen fluoride, and fluorocarbon. Subsequently, the pressure was determined during 3.5 years. In no case was its increase detected; in the container with the cinders, a vacuum was observed. No excess pressure was detected in the containers filled with the wastes, obtained by reprocessing both uranium and uranium–plutonium fuels (Table 3) with a lower specific energy release, i.e., radiation–chemical processes in the wastes die down in proportion with the decrease of the radioactivity of the wastes, which is well illustrated by the thermal analysis data.

Figure 2 shows the thermograms of the cinders obtained by the fluorination of uranium and uranium–plutonium fuel. An analysis of the thermograms confirms the thermal instability of the cinders, most characteristic for a product with a high specific energy release (see Fig. 2a). By comparing the thermograms of one and the same cinders, taken at the initial instant and over 3.5 years, a completely definite conclusion can be drawn, that the thermal stability of the cinders increases in proportion with the decrease of energy release and radioactivity. This is well supported by the data for the wastes obtained by reprocessing

TABLE 3. Composition of Gas Phase in Containers with Highly-Active Fluoride Wastes*

Form and characteristics of wastes	Expt. conditions: T, °C	Expt. conditions: time of aging at temperature of invest., h	Vol. of gas released with normal cond., cm^3/kg	Gas pressure, Pa ($\cdot 10^2$)	Content, vol. %: N_2	CO	NO	O_2	Ar	CO_2	NOF	SiF_4	ΣN_2F_2, COF
Cinders from fluorination of a consolidated portion of uranium oxide fuel (mass 1.5 kg; radioactivity $1.4 \cdot 10^{14}$ Bq/kg)	100 Self-heating	192	—9,80	—42,10	84,20	—	—	11,0	1,25	3,53	—	—	—
	200	18	13,30	57,60	75,80	—	18,00	0,11	1,13	4,96	—	—	—
	300	18	126,80	580,0	50,10	41,00	0,05	0,04	0,75	8,1	—	—	—
	400	18	57,70	266,00	62,80	28,60	—	0,06	0,94	7,6	—	—	—
	600	18	120,00	550,0	50,9	3,4	—	0,05	0,76	0,46	0,67	41,80	2,00
	700	18	5,5	24,4	79,2	10	—	—	1,04	0,04	—	9,72	—
Cinders from the fluorination of a mixed uranium – plutonium fuel (mass 0.290 kg, radioactivity $1.4 \cdot 10^{14}$ Bq/kg)	38	72	—	—	82,70	—	—	15,90	1,10	0,30	—	—	—
	300	1	—	—	77,90	—	5,20	0,90	1,05	14,95	—	—	—

*Capacity of container 1 liter, diameter 105 mm, and wall thickness 2.5 mm.

fuel with a long aging (see Fig. 2c). Thermal processing of the wastes promotes an increase of their thermal stability.

The mass-spectrometric analysis of the gas phase in the container with the cinders (see Table 3) also indicates the relative instability of the latter: with external heating, a very slight gas release is observed (up to 126.8 cm^3/kg), obviously due to the decomposition of a number of thermally unstable complexes of the type $NOUF_6$, $NOMoF_6$, $FM(CO)_5$, $SrSiF_6$, and $BaSiF_6$ [8], with the release of NO, CO, and SiF_4.

It was established that the radioactivity of the gas phase is due to the presence of the same radionuclides as are in the solid wastes. The rate of volatilization of the radionuclides from the end surface, calculated by the formula $\frac{a'}{a}\tau^{-1}F^{-1}$ (here a' is the radioactivity of the nuclides, passing into the gas phase, Bq; a, specific radioactivity of the product being investigated, Bq/g; τ, time of the tests; and F, end surface area of the wastes, cm^2) increases slightly with increase of temperature and for the most toxic radionuclide ^{137}Cs in the range 20-600°C, for the chemical absorber it amounts to $1.8 \cdot 10^{-5}$ to $1.3 \cdot 10^{-4}$, for the sorbent $3.1 \cdot 10^{-7}$ to $4.7 \cdot 10^{-6}$, and for the cinders $1.8 \cdot 10^{-10}$ g/($cm^2 \cdot$dis), respectively. As it was shown earlier [3], with increase of the aging time of the wastes, the fraction of the radioactivity removed with the aerosols, decreases because of consolidation of the aerosol particles and settling on the container walls, and also because of the gradual depletion of the surface layer of wastes with the radionuclides.

The investigations of the leaching-out of the radionuclides showed that the rate of transfer into water of ^{137}Cs from the sorbent and chemical absorber amounted to $1.9 \cdot 10^{-2}$ to $8.0 \cdot 10^{-2}$ and $1.4 \cdot 10^{-3}$ to $6.9 \cdot 10^{-3}$ g/($cm^2 \cdot$dis), respectively, and from the cinders obtained by reprocessing both uranium and uranium–plutonium fuel, it is equal to $7.5 \cdot 10^{-6}$ to $2.3 \cdot 10^{-5}$ g/($cm^2 \cdot$dis). The data obtained are comparable with leaching-out of ^{137}Cs for borosilicate glasses [10^{-5} to 10^{-6} g/($cm^2 \cdot$dis)]. This allows the assumption that the cesium in the cinders is present not in the form of CsF, which is well soluble in water, but in the form of complexes with the fluorides of fission products which, obviously, have a lower solubility.

The results of the investigations carried out can be used for calculating the conditions for the radiation-safe storage of solid, high-activity fluoride wastes, and for optimization of the technological process for the gas-fluoride reprocessing of spent fuel.

LITERATURE CITED

1. L. J. Anastasia et al., USA Patent No. 3753920, Cl.252-301.1P (COI 43/06) (1973).
2. N. K. Kikoin, Scientific-Research Institute of Nuclear Reactors (NIIAR) Preprint, P-18 (284) [in Russian], Dimitrovgrad (1976).
3. A. P. Kirillovich et al., At. Energ., 42, 2, 94 (1977).
4. A. P. Kirillovich, P. S. Gordienko, and V. P. Bruntushkin, At. Énerg., 40, 5, 427 (1976).
5. A. P. Kirillovich et al., Preprint [in Russian], Scientific-Research Institute of Nuclear Reactors, Preprint No. 31 (439), Dimitrovgrad (1980).
6. Procedure for Choosing the Safe Conditions of Storage of Consolidated Wastes, as a Function of the Properties and Specific Activity [in Russian], Council for Mutual Economic Aid (SÉV), Moscow (1973), p. 31.
7. M. P. Vorobei, A. P. Kirillovich, and Yu. G. Lavrinovich, in: Data of the Fourth SEV Symposium. Investigations in the Field of Irradiated Fuel Reprocessing [in Russian], Prague, Vol. 2 (1977).
8. B. V. Nekrasov, Principles of General Chemistry [in Russian], Vol. 2, Khimizdat, Moscow (1969).

TWO-DIMENSIONAL ANALYSIS OF THE STABILITY OF THE NEUTRON DISTRIBUTION IN A REACTOR

V. N. Konev and B. Z. Torlin

UDC 621.039.512:621.039.512.45

In developing a method of determining the stability of the neutron distribution from the principal eigenvalues of the two-dimensional problem of regulating slow processes in the spatial dynamics of a reactor, a series of previously explained assumptions have been adopted. It follows from [1, 2], e.g., that the mutual positions of the control rods (CR) and sensors have a strong influence on the radial–azimuthal stability of the reactor, stronger than their influence on the stability over the height [3]. Therefore, in studying the stability of systems for stabilizing the neutron distribution, it is necessary to ensure accurate CR and sensor spacing in the reactor lattice corresponding to the investigated object in the calculation. It is this which primarily determines the calculation scheme. On this basis, a regular quadratic or hexagonal lattice is proposed, with a number of cells equal to the number of channels.

The large dimensionality of the units determines the choice of calculational method. For example, to solve a system of equations with of the order of 10^3 unknowns, it is necessary to resort to an iterative method. To ensure the stability and reliability of these procedures, it is worth ensuring in advance, for example, that the spectrum of the transformed operator is positive.

How these principles are realized in the analytical algorithms and the BASIRA program for which they provide the basis will not be considered. Since interest focuses on the analysis of reactor stability in slow processes, the regulators are assumed to be fast-acting, and the lifetimes of instantaneous and delayed neutrons and the lag time of those rapid feedback systems which are due to the change in fuel temperature and heat-carrier enthalpy are neglected. The change over time in the ^{135}Xe concentration and the temperature of the graphite moderator is taken into account, using precisely the same linearized equations as in [4]. After Laplace transformation, these equations are found to include a Laplacian parameter, which will also play the role of eigenvalue — generally speaking, a complex and often nominally complex eigenfrequency ω.

The basic, or principal, eigenvalue, with a maximum real component, is the most important from the viewpoint of stability. A simple power-law method (external iteration) similar to that used in [4] is expedient for its determination. Isolating the required eigenvalue involves a shift of the spectrum in which the basic complex frequency becomes the

Translated from Atomnaya Énergiya, Vol. 52, No. 1, pp. 25-29, July, 1982. Original article submitted November 3, 1981.

0038-531X/82/5301-0473$07.50

largest in modulus [4]. The basic — generally speaking, also complex — eigenmode is then calculated. This involves determining, at each step of the iterative process, the deviation of the neutron distribution φ from its steady value Φ_0 under the action of the reactivity perturbation x, which is a result of the action of all the feedbacks, both fast and slow. In a single-group approximation, the relation of φ with x in the presence of N fast-acting regulators is described by the linearized equation

$$\left.\begin{aligned} &\Delta\varphi + B_0^2\varphi + \frac{\Phi_0}{M_0^2}\left(\sum_{i=1}^{N}\rho_i F_i + x\right) = 0; && \text{(1a)}\\ &\sum_{j=1}^{M} a_{ij}\varphi_j = 0 \quad (i = 1,\ 2,\ \ldots\ N) && \text{(1b)} \end{aligned}\right\}$$

with homogeneous boundary conditions on φ. Here ρ_i is the change in CR effectiveness; F_i, spatial-localization function of the CR; a_{ij}, weighting factors forming the off-balance signal for the i-th CR from all M sensors; $\varphi_j = \varphi(\mathbf{r}_j)$, where $\mathbf{r}_j$ is the point at which the neutron distribution is recorded by the j-th sensor; B_0^2, M_0^2, respectively, the unperturbed values of the material parameter and the area of neutron migration; Φ_0 is determined from the equation

$$\Delta\Phi_0 + B_0^2\Phi_0 = 0 \tag{2}$$

with boundary conditions on Φ_0 of the same form as in Eq. (1a). If each i corresponds to a particular group of sensors for which $a_{ij} \neq 0$, and the groups for each i do not intersect, then the local-automatic-regulator (LAR) model is obtained.

The solution of Eq. (1a) may be written as a sum

$$\varphi = A\Phi_0 + \sum_{i=1}^{N}\rho_i\psi_i + \psi_x \tag{3a}$$

with the condition in Eq. (1b) and

$$\sum_{i=1}^{N}\rho_i\mu_i + \mu_x = 0, \tag{3b}$$

where the influence functions ψ and the parameters μ are described by the equations

$$\left\{\begin{aligned} &\Delta\psi_i + B_0^2\psi_i + \frac{\Phi_0}{M_0^2}(F_i - \mu_i) = 0;\\ &(\psi_i,\ \Phi_0) = 0;\quad \mu_i = \frac{(\Phi_0 F_i,\ \Phi_0)}{(\Phi_0,\ \Phi_0)};\ i = 1,\ 2,\ \ldots\ N; \end{aligned}\right. \tag{4}$$

$$\left\{\begin{aligned} &\Delta\psi_x + B_0^2\psi_x + \frac{\Phi_0}{M_0^2}(x - \mu_x) = 0;\\ &(\psi_x,\ \Phi_0) = 0;\ \mu_x = \frac{(\Phi_0 x,\ \Phi_0)}{(\Phi_0\Phi_0)};\ i = 1,\ 2,\ \ldots\ N \end{aligned}\right. \tag{5}$$

with the previous boundary conditions. All the ρ_i are determined from Eq. (1b) after the substitution of Eq. (3a) and after taking Eq. (3b) into account.

It is quickly evident that the operator acting on the unknowns Ψ and ρ in Eq. (1) is not symmetric. Conversely, the operator acting on ψ in Eq. (4) or (5) is symmetric, and its difference analog is positive-definite. Therefore, the influence function ψ may be calculated by any iterative method developed for positive-definite matrix operators. In this case, all the ψ_i are calculated once, and in each cycle of the external iteration it is necessary to recalculate only ψ_x and ρ_i.

Since ψ_x is of large dimensionality and is calculated iteratively (internal iteration), all the time involves in performing one external iteration is in fact taken up by this. An important moment in performing this procedure is the choice of the initial vector. Note that this problem is associated with the complex form of the required solution. If it were real, the solution obtained in the preceding step would be a completely suitable initial vector, and the number of internal iterations would rapidly reduce from cycle to cycle. To ensure reduction in the number of internal iterations in the process of isolating the intrinsic solution, regardless of whether it is real or complex, the initial vector in deter-

mining ψ_x at the n-th step of the external iteration is taken to be $f_n^{(0)}$, defined by the relation

$$f_n^{(0)} = -\frac{p_n}{k_n}\psi_x^{(n-1)} - \frac{q_n}{k_n k_{n-1}}\psi_x^{(n-2)}, \tag{6}$$

where $\psi_x^{(n-1)}$ and $\psi_x^{(n-2)}$ are the values of ψ_x, found from the two preceding external iterations; p_n and q_n are the coefficients of the equation for the desired eigenvalue ω_n

$$\omega_n^2 + p_n\omega_n + q_n = 0, \tag{7}$$

and are determined in the BASIRA program, as in the IRINA program [4, 5], from the condition of a minimum of the vector modulus [6]

$$\varepsilon_n^{(3)} = k_n k_{n-1}\mathbf{R}_n + p_n k_{n-1}\mathbf{R}_{n-1} + q_n\mathbf{R}_{n-2}, \tag{8}$$

where $\mathbf{R}_n$ is the orthonormalized total vector of the problem variables at the n-th external iteration, and k_n is a coefficient formed in its normalization.

The method of conjugate gradients is used to solve Eqs. (4) and (5) [7]. In the given case, a special feature is that the desired solution must be orthogonal to the steady distribution Φ_0. Formally, the solution scheme retains its orthogonality if it is ensured for the initial vector. However, for the sake of reliability, and to eliminate the noise arising, e.g., because of rounding, the solutions are periodically orthogonalized. In choosing the method of solving Eqs. (4) and (5), some other methods were investigated as well as that already noted. The method of conjugate gradients and the method of Chebyshev polynomials were the best, and almost equal in speed [8]. Although the first requires twice as many arithmetic operations to be performed at each step of the iterative process, it requires half as many iterations to attain the same degree of accuracy. This economy of iteration is the reason for its choice, although it also requires a larger memory. A procedure based on the Chebyshev polynomial proves most effective for the solution of Eq. (2) [8].

Termination of the process of isolating the principal eigenvalue is verified primarily from the collinearity of the vectors $\mathbf{R}_n$ and $\mathbf{R}_{n-1}$ in two successive iterations. It indicates that the solution is real. In its absence, coplanarity of the vectors $\mathbf{R}_n$, $\mathbf{R}_{n-1}$, and $\mathbf{R}_{n-2}$ in Eq. (8) is verified. Then the pair of roots (complex or real) is determined from Eq. (7). With high azimuthal symmetry of the reactor load, it may be expected that the principal eigenvalue has a multiple pair, to which corresponds a pair of identical linear elementary divisors. However, with weak symmetry violation, splitting occurs, and two close complex pairs of roots may be formed. Therefore, the following verification is performed for the smallness of the modulus of the vector

$$\varepsilon_n^{(5)} = k_n k_{n-1} k_{n-2} k_{n-3}\mathbf{R}_n + a_1 k_{n-1} k_{n-3}\mathbf{R}_{n-1} + a_2 k_{n-2} k_{n-3}\mathbf{R}_{n-2} + a_3 k_{n-3}\mathbf{R}_{n-3} + a_4\mathbf{R}_{n-4}. \tag{9}$$

The eigenvalues are determined here from the equation

$$\omega_n^4 + a_1\omega_n^3 + a_2\omega_n^2 + a_3\omega_n + a_4 = 0, \tag{10}$$

and the coefficients a_i are chosen from the condition that the modulus of the vector $\varepsilon_n^{(5)}$ be a minimum.

The BASIRA program is found to be a powerful instrument for analyzing the potentialities of different kinds of regulatory systems in ensuring the stability of the neutron distribution in the horizontal plane of large reactors. As an example, the stability of an RBMK-1000 reactor with an operating LAR control system and the possibilities for its modification are considered.

The map of the load, CR positions, and in-core sensors is adopted on the basis of the data of [9, 10], i.e., as in the first unit of Leningrad atomic power station. The calculation is performed for a reactor with a square lattice and 1884 cells. The steady neutron distribution in accordance with [9] is well equalized in the central region; the coefficient of radial nonuniformity is ∿1.1. The area of neutron migration M_0^2 = 550 cm²; the reactivity power coefficient $\alpha_\varphi = 0.005$. The reactivity coefficient over the graphite temperature α_C = 0.013 with a time constant of 1 h; the xenon reactivity coefficient α_{Xe} = 0.0298. With the standard automatic regulator switched on and the given parameters, according to a calculation by the BASIRA program, the reactor has several unstable eigenmodes, and the accelera-

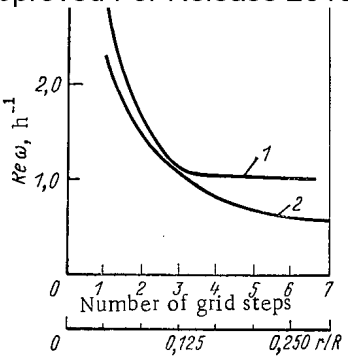

Fig. 1

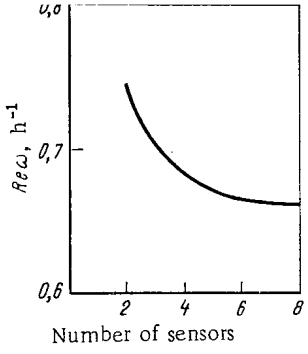

Fig. 2

Fig. 1. Dependence of Re ω on the distance between the LAR control rod and the surrounding sensors with 6 (1) and 7 (2) regulators; R is the active-zone radius of the reactor.

Fig. 2. Dependence of Re ω on the number of sensors placed around the LAR control rod.

tion time constant of the most unstable of these (the first azimuthal) τ_{01} = 2 min.* Some results of the analysis are now given. In Fig. 1, the real part of the principal eigenfrequency is shown as a function of the distance between sensors and control rods. In the calculation, it is assumed that around each rod, at equal distances, four sensors are placed. Curves are shown for seven standard LAR control rods, and for the case when the central LAR is switched off. They quantitatively confirm the earlier [2] qualitative investigation of the effect of amplifying the stabilizing action of the LAR system as the sensors are moved away from the rods. For the given reactor, as shown in [2] and as evident in Fig. 1, moving the sensors more than 6-7 grid steps from the LAR control rod is inexpedient. The maximum stabilizing effect of seven LAR, as is evident from Fig. 1, is such that the acceleration period of the most unstable mode is reduced to ∿1.7 h; for six LAR, this period is ∿1 h.

In Fig. 2, the influence of the number of sensors surrounding each LAR control rod is shown. The curve is plotted for seven rods, and the distance between rods and sensors is five reactor grid steps. It is evident that, with increase in the number of sensors, the stability of the calculation increases, but using more than six sensors does not in fact improve the stability. Other investigations have been performed for sensors that are non-uniform in their angle of orientation, sensors placed at different distances from the rods, etc. Without dwelling on this in detail, it may simply be noted that when sensors are placed at different distances around a rod the stability is mainly due to the closest sensors.

In [2], in addition to the usual LAR, there was also a qualitative investigation of a system of spatial regulation in external ionization chambers, consequently referred to as LAR–EIC. In Fig. 3, on the basis of calculations by the BASIRA program, it is shown how in this system of regulation the instability of the neutron distribution is weakened with increasing distance of the CR from the external chambers. For six rods, the limiting stabilizing effect is practically reached when they are half the radius of the reactor active region away from the chambers. The characteristic acceleration time of the most stable mode is ∿1.8 h. In Fig. 3, the influence of different positions with respect to the external chambers of a system of three rods on the stability is also shown (curves 1-3). It is evident that, in this case, the maximum stabilizing effect (admittedly less than for six rods) is reached when the rods are placed at a distance from the center equal to half the active-region radius and when their angular coordinates differ by 60° from the angular coordinates of the external chambers. Placing the rods and sensors on the same paths markedly worsens the stability. This effect was also investigated in [11]. Some discrepancy of the results

*Calculations have also been performed for the set of parameters ensuring τ_{01} = 7.8 min. The dependences obtained are unchanged in form. In the given range, the characteristic time for the development of the processes is increased, roughly speaking, by approximately 5.5 min.

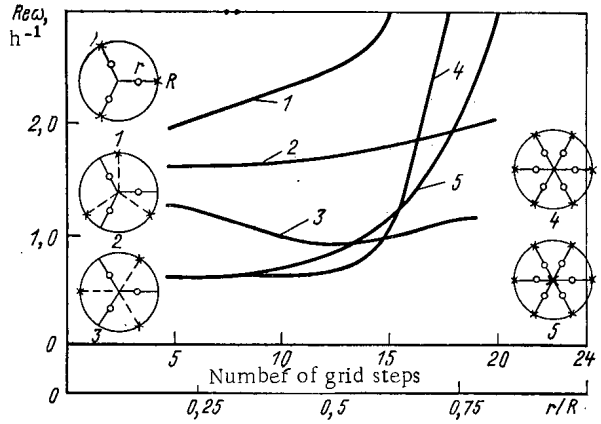

Fig. 3. Dependence of Re ω on the radius at which LAR–EIC rods are placed on the reactor: the crosses correspond to sensors and the circles to CR.

with the results of [11] may probably be explained by small differences in the calculational models. The position of the rods with respect to the sensors at which the corresponding angular coordinates do not coincide was called zone-asymmetric in [11]. For three regulators, such a configuration allows the stabilizing influence of the system to be somewhat amplified. This assertion also holds for other systems with an odd number of regulators. Zone-asymmetric positioning of the rods in this case leads to deterioration in the conditionality* of the matrix characterizing the influence of the rods on the sensors (it may even become singular, with a zero determinant), and correspondingly the problem becomes incorrect. Physically, this must be regarded as noise-instability of the system. In this sense, the LAR system has an undoubted advantage over the LAR–EIC system, in which, to a large extent, the stabilizing properties of moving the chamber away from the rods are used. The noise-stability may be increased using any of the following methods: 1) control by means of the regulating rods in each sector according to the signal from the group of external chambers monitoring the neutron distribution in the same sector; 2) forming a control signal for any rod from all the external chambers appearing in the system (which must be more than the rods in the system) as the sum of the off-balance signals, with weighting factors determined from the optimization condition for the stability or the quality of the transient process [2, 12, 13]; 3) as in the preceding case, but adding the off-balance signals from the internal sensors, with their own weighting factors, to the sum of off-balance signals forming the control signal. Calculations of a system with six rods have been performed for these three variants. No marked change in stability in comparison with the LAR–EIC method is observed. A certain difference in the curves of the stability as a function of the radius of the rod positions in the presence and absence of a central sensor is seen in Fig. 3 (curves 4 and 5). It is evident that the central sensor has no influence on the limiting possibilities of the system, but may significantly affect the stability with close positions of the rods and external chambers.

In conclusion, results are given for the calculation of a system of 12 LAR positioned uniformly in the CR grid of an RBMK reactor (see the map in [9]). Each rod of the LAR system is controlled according to the disbalance of the total current of four sensors placed at equal distances from the rod. Whereas in all the previous examples aperiodic instability is observed, in this case the instability is oscillatory in character, with an oscillation period of 36 h and a maximum acceleration period of ∿7.5 h when the sensors are removed to a distance of ∿5.5 grid steps from the rod. If this distance is reduced to one and a half grid steps, the instability becomes aperiodic with a period of ∿1.8 h.

*Generally speaking, this assertion is invalid with regard to other forms of asymmetric positioning of rods and sensors in the reactor. In the present work, no consideration is given to the results of investigations by means of the BASIRA program, theoretically confirming the possibility of significant suppression of the instability of the neutron distribution in the RBMK reactor, for example, by using only two rods and two sensors appropriately positioned in the active region.

LITERATURE CITED

1. B. Z. Torlin, At. Énerg., 45, No. 6, 457 (1978).
2. B. Z. Torlin, At. Énerg., 48, No. 5, 297 (1980).
3. A. M. Afanas'ev and B. Z. Torlin, At. Énerg., 43, No. 4, 243 (1977).
4. A. M. Afanas'ev and B. Z. Torlin, At. Énerg., 44, No. 6, 487 (1978).
5. A. M. Afanas'ev and B. Z. Torlin, Preprint ITEF-2 [in Russian], Moscow (1978).
6. J. Wilkinson, Algebraic Problem of Eigenvalues [in Russian], Nauka, Moscow (1970).
7. D. K. Faddeev and V. N. Faddeeva, Computational Methods of Linear Algebra [in Russian], Fizmatgiz, Moscow (1960).
8. G. I. Marchuk and V. I. Lebedev, Numerical Methods in the Theory of Neutron Transport [in Russian], Atomizdat, Moscow (1981).
9. N. A. Dollezhal' and I. Ya. Emel'yanov, Channel Nuclear Power Reactor [in Russian], Atomizdat, Moscow (1980).
10. I. Ya. Emel'yanov, V. V. Postnikov, and Yu. N. Volod'ko, At. Énerg., 48, No. 6, 360 (1980).
11. I. Ya. Emel'yanov et al., At. Énerg., 47, No. 6, 370 (1979).
12. B. Z. Torlin, At. Énerg., 47, No. 6, 415 (1979).
13. A. M. Afanas'ev and B. Z. Torlin, At. Énerg., 48, No. 2, 121 (1980).

MEASUREMENT OF THE NEUTRON TOTAL CROSS SECTIONS OF ^{109}Ag AND ^{110m}Ag

V. A. Anufriev, S. I. Babich, and V. N. Nefedov

UDC 621.039.556

The neutron total cross sections of stable ^{109}Ag and radioactive ^{110m}Ag ($T_{1/2}$ = 254 days) were measured on the neutron spectrometer at the SM-2 reactor. Information on the ^{109}Ag and ^{110m}Ag cross sections is of interest for calculating the effect of fission products on reactor characteristics [1, 2] and for the development of optimum conditions for the accumulation of the commercially useful isotope ^{110m}Ag in reactors [3].

The neutron total cross sections of silver isotopes were determined by measuring the transmission of samples by the time-of-flight method [4]. The best resolution of the neutron spectrometer on a flight path of 91.76 m was 58 nsec/m. Work with ^{110}Ag was performed by remote control, using a device for measuring highly active samples [5]. In all the measurements of transmission a fixed exit collimator was used to form a neutron beam with a rectangular cross section 1 × 6 mm.

A 1200 mg sample of silver metal enriched to 99.4% in ^{109}Ag was sealed in an aluminum can having inside dimensions of 1.5 × 7.8 × 24 mm. Measurements were made with the sample in two positions differing in thickness (nuclei/cm^2) by a factor of 16. From the results of the measurements of the neutron cross section in the energy range up to 210 eV, 13 levels of ^{109}Ag were identified and their resonance parameters $2g\Gamma_m$, E_0, and Γ_γ calculated (Table 1).

The results obtained were compared with published data [7-10] and with values recommended in [6]. In the main the resonance parameters agree with the values in [7-10] within the limits of error, except for differences of factors of 1.5-2 in $2g\Gamma_n$ and Γ for neutron levels with E_0 = 88.1 and 172.6 eV. From an analysis of the distribution of neutron widths and distances between levels of ^{109}Ag (Figs. 1-3) the following average characteristics were obtained: $\bar{D}$ = (15.6 ± 1)eV; $2g\Gamma_n^0$ = 2.82 meV; $S_0 = (9.0 \pm 0.3)\cdot 10^{-5}$; Γ_γ = (143 ± 10) meV. On the basis of the experiment and the average characteristics the total resonance capture integral of ^{109}Ag was calculated to be I_γ = (1480 ± 10)b (1b = 10^{-28} m^2). For measurements with neutron energies in the thermal region (0.02-1 eV) "thin" silver samples were used. The energy dependence of the total cross section is shown in Fig. 4. The values of the

Translated from Atomnaya Énergiya, Vol. 53, No. 1, pp. 29-31, July, 1982. Original article submitted July 16, 1981.

 0038-531X/82/5301-0478$07.50

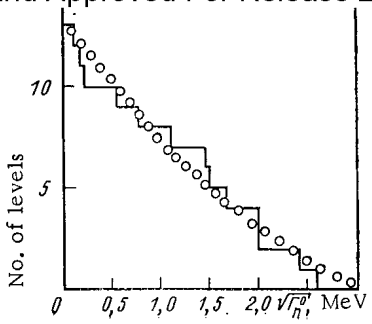

Fig. 1

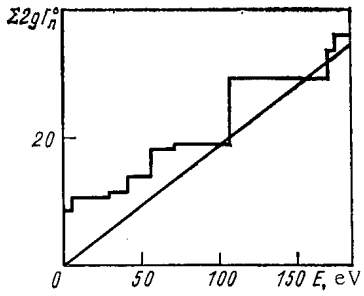

Fig. 2

Fig. 1. ○) distribution of values of reduced neutron width of ^{109}Ag resonances; ——) Porter-Thomas distribution [11].

Fig. 2. Dependence of sum of values of reduced neutron width of ^{109}Ag on neutron energy.

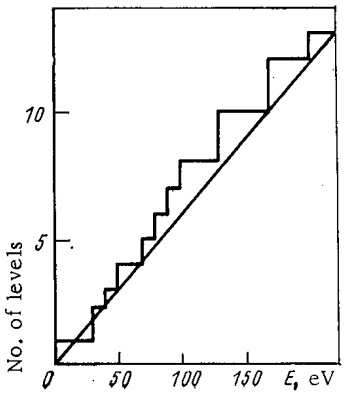

Fig. 3

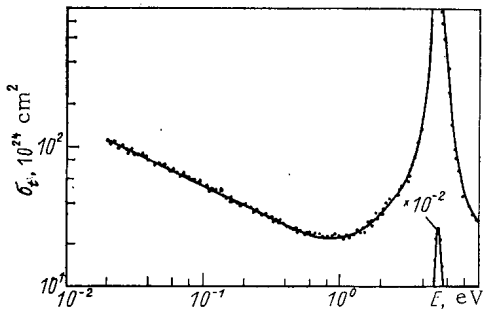

Fig. 4

Fig. 3. Distribution of number of observed levels for ^{109}Ag as a function of neutron energy.

Fig. 4. Neutron total cross section of ^{109}Ag for neutron energies in the range 0.02-10 eV.

TABLE 1. Neutron Resonance Parameters, meV

E_0, eV	Γ	Γ_γ	$2g\Gamma_n$	Γ [6]	Γ_γ [6]	$2g\Gamma_n$ [6]
5,145±0,003	156±20	143±20	19,3±0,6	146±6	137±6	19,1±0,3
30,7±0,3	145±7	132±7	11,0±0,4	137±6	130±6	11,0±0,6
40,5±0,4	152±13	147±13	7,4±0,5	136±7	131±7	7,5±0,2
56,0±0,7	200±19	172±19	16,6±1,1	176±9	139±7	18,6±1,5
71,1±0,9	175±9	149±9	38,5±1,6	147±5	120±5	40±3
88,1±1,3	260±76	258±76	4,7±1,0	136±15	130±15	9,4±0,3
91,3±1,5	148	—	0,052	—	—	0,05±0,01
106,8±1,7	141±35	141±35	0,22±0,08	—	—	0,20±0,03
134,3±2,4	240±16	159±16	121±4	200±7	120±5	120±6
139,9±2,5	135±21	134±21	3,2±0,9	135±46	133±46	2,4±0,3
170,0±3,4	148	—	0,41	—	—	0,39±0,13
172,6±3,4	202±30	164±30	57±5	188±20	140±15	72±6
207,6±4,5	165±47	140±47	37,6	157±20	133±15	36±2

cross sections for v_o = 2200 m/s, σ_t = (95 ± 4)b, σ_s = 5.9b, and σ_γ = (91 ± 4)b, are in complete agreement with the values recommended in [6].

The radionuclide ^{110m}Ag was obtained by bombarding ^{109}Ag with neutrons in the vertical channel of the SM-2 reactor. The samples used were those initially employed in the measurement of the neutron cross section of ^{109}Ag. The fluence of thermal neutrons in the bombardment was calculated from a Co monitor ($1.07 \cdot 10^{21}$ neutrons/cm^2). The ^{110m}Ag content was determined from a balance of all isotopes present in the silver samples which had been bom-

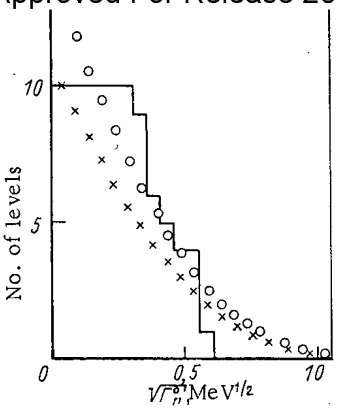

Fig. 5

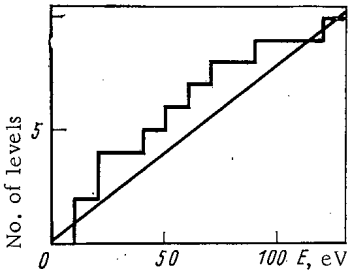

Fig. 6

Fig. 5. Integral distribution of reduced neutron width of ^{110m}Ag; ×, ○) Porter–Thomas distribution for 13 and 10 levels, respectively.

Fig. 6. Distribution of number of observed levels for ^{110m}Ag as a function of neutron energy.

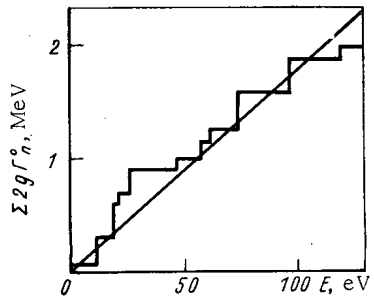

Fig. 7. Dependence of sum of values of reduced neutron width of ^{110m}Ag on neutron energy.

TABLE 2. Characteristics of Silver Samples

Nuclide	Not bombarded			Bombarded		
	%	nuclei/cm², 10^{-20}		%	nuclei/cm², 10^{-20}	
		thick	thin		thick	thin
^{107}Ag	0,6	3,7±0,2	0,23±0,01	0,57	3,6±0,2	0,23±0,01
^{109}Ag	99,4	620±15	38,8±0,8	77,6	484±8	30,3±0,5
^{110m}Ag	—	—	—	1,48	9,2±2,1	0,58±0,13
^{110}Cd	—	—	—	20,2	126±2	7,87±0,13
^{111}Cd	—	—	—	0,1	0,6±0,1	0,040±0,006

barded and those which had not. The number of isotopes was calculated from their neutron resonances, namely: ^{109}Ag from levels with E_0 = 5.15, 30.7, 40.5, and 56.2 eV; ^{107}Ag from E_0 = 16.46, 41.05, 46.1, 51.7 eV; ^{110}Cd from E_0 = 89.6, 230 eV; ^{111}Cd from E_0 = 27.7 eV. We note that by using data obtained with silver samples which had not been bombarded, the systematic error in the resonance parameters of ^{109}Ag and ^{107}Ag was eliminated. The complete composition of samples which had been bombarded and those which had not is shown in Table 2.

For a reliable identification of neutron resonances the transmission of bombarded silver samples was measured twice — 15 and 170 days after bombardment was stopped. For the first time 11 levels of ^{110m}Ag were observed for neutron energies up to 120 eV (Table 3). The resonance parameters were calculated, as for ^{109}Ag, by the "shape" method, using the

TABLE 3. Resonance Parameters of ^{109}Ag ($T_{1/2}$ = 254 days), meV

E_0, eV	Γ	$2g\Gamma_n$	$2g\Gamma_n^0$
11,54±0,05	133±45	0,26±0,05	0,076±0,015
19,45±0,13	224±41	1,14±0,25	0,26±0,04
21,20±0,15	168±36	1,3±0,2	0,28±0,04
26,5±0,2	90±11	0,55±0,12	0,11±0,02
45,7±0,5	148	1,2±0,4	0,18±0,06
58,5±0,7	148	0,86±0,42	0,11±0,06
62,5±0,7	148	1,03±0,52	0,13±0,06
78,4±1,1	148	1,1±0,8	0,12±0,09
98,4±1,5	148	3,2±1,6	0,32±0,20
120,2±1,9	148	3,1±1,5	0,28±0,15
152±3	148	—	—

one-level Breit–Wigner formula. The resonance capture integral for ^{110m}Ag is I_γ = (20 ± 4)b. Statistical processing of the distribution of resonance parameters (Figs. 5-7) enabled us to calculate the average characteristics of this isotope: $\overline{D}$ = (12 ± 1)eV; $2g\overline{\Gamma_n^0}$ = 0.19 meV; $S_0 = (1.1 \pm 0.5)\cdot 10^{-5}$. The values obtained for the average of the parameter S_0 for ^{109}Ag and ^{110m}Ag confirm the conclusions of the statistical model of the existence of a minimum of the strength function in the region of mass numbers 85-115 ($5\cdot 10^{-5}$) [12]. At the same time we note an appreciable difference in the experimental values of S_0 for ^{109}Ag and ^{110m}Ag ($9\cdot 10^{-5}$ and $1.1\cdot 10^{-5}$, respectively). From a comparison of measurements of silver samples which had been bombarded and those which had not, the ^{110m}Ag cross section in the thermal energy region was estimated as σ_t < 200b.

LITERATURE CITED

1. Y. Kikushi, in: Proc. Int. Conf. on Fast Reactor Physics, NB-4, Tokyo (1973).
2. J. Tyror, in: Panel Meeting on Fission Nuclear Data, IAEA-169, Vol. 1, Rev. Paper No. 3, Bologna, Aug. 26-30 (1973).
3. C. Weitkamp, in: Proc. Int. Conf. on Interaction of Neutrons with Nuclei, Vol. II, Lowell, July 6-9 (1976), p. 975.
4. T. S. Belanova et al., Preprint NIIAR P-6, 272, Dimitrovgrad (1976).
5. V. A. Anufriev et al., Preprint NIIAR P-11, 345 Dimitrovgrad (1978).
6. BNL-325, Third Edition (1973).
7. J. Desjardins et al., Phys. Rev., 120, 2214 (1960).
8. R. E. Chrien, Phys. Rev., 141, 1129 (1966).
9. J. Garg et al., Phys. Rev., 137B, 547 (1965).
10. G. V. Muradyan and Yu. V. Adamchuk, in: Nuclear Data for Reactors, Vol. 1, Vienna (1976), p. 79.
11. C. Porter and R. Thomas, Phys. Rev., 104, 483 (1956).
12. K. Seth, Nucl. Data, Section A, 2, 300 (1966).

SEPARATION OF HYDROGEN ISOTOPES BY METAL MEMBRANES

V. V. Latyshev, V. A. Gol'tsov, and S. A. Fedorov

UDC 621.039:621.385:533.15

The problem of providing engineering equipment for controlled thermonuclear synthesis requires the solution of a number of problems in the purification and separation of hydrogen isotopes [1], including the utilization of the tritium contained in waste water and discharge gases [2]. Many problems in the ultrafine purification, recovery, and separation of hydrogen isotopes can be successfully solved by using methods of hydrogen membrane technology [3], in which special alloys of palladium are used as the material of the diffusion cell [4]. The method of diffusive enrichment of hydrogen isotopes in the tritium cycle of thermonuclear reactors is all the more effective because in this case it is sufficient to use only a known amount of enrichment with high purity of the isotope mixture. An analysis of the experimental material [5-7] shows that the method of diffusion through palladium-alloy membranes in the diffusion regime of filtration can be used to achieve a separation coefficient of $\alpha = 1.5$-2.0. The protium flow through a membrane 0.1 mm thick is 0.2 $cm^3/(cm^2 \cdot sec)$ for a working temperature of 800°K, an inlet pressure of 0.1 MPa, and a vacuum at the membrane outlet. Thus, the method seems highly economical and requires more thorough analysis.

In the present paper we consider the scientific foundations of the diffusion method of separation. Since the rate of penetration of the hydrogen isotopes through a membrane is different for different metals (Table 1), the theoretical possibility of separating isotopes by this method is fairly clear. However, this approach is not a trivial one. In the separation of isotopes by diffusion through porous membranes, the fundamental process bringing about the separation is molecular diffusion of the gas. In the case under consideration we are dealing with the separation of isotopes as a result of a complex process taking place with dissociation of molecules when they are sorbed by the metal. Therefore the process of diffusive separation is a multistage process. The following stages should be distinguished: transport of the isotope mixture to the inlet side of the membrane, physical and chemical adsorption with subsequent dissociation of the molecule on the surface of the membrane, penetration of the atoms into the lattice of the metal, diffusion of the atoms from the inlet side of the membrane to the outlet side, exit of atoms from the metal, and their association into molecules on the outlet surface.

Any of the above-mentioned stages may be decisive for the effect of separation of hydrogen atoms when they penetrate through the membrane. Depending on the parameters of the process and on the construction and characteristics of the apparatus, the coefficient of separation by the membrane may be represented as the produce of the separation coefficient of the individual stages. However, the most hopeful results are obtained for a diffusion regime of separation, when the decisive stage is the diffusion of the atoms in the metal from the inlet side to the outlet side of the membrane. For a protium–deuterium mixture this process is described analytically in the present paper.

Let us consider a closed system consisting of metal atoms in a condensed state and an isotope mixture of protium and deuterium in the gaseous phase. The transition of the protium and deuterium atoms from the gaseous phase into the metal is described by the following reaction equations:

$$\frac{1}{2}\,H_2 \rightleftarrows H; \tag{1}$$

$$\frac{1}{2}\,D_2 \rightleftarrows D; \tag{2}$$

$$HD \rightleftarrows H + D, \tag{3}$$

Translated from Atomnaya Énergiya, Vol. 53, No. 1, pp. 32-35, July, 1982. Original article submitted November 28, 1980; revision submitted June 1, 1981.

 0038-531X/82/5301-0482$07.50

TABLE 1. Isotope Effects ($\eta = p_H/p_D$) and Permeability of Hydrogen and Deuterium in Some Metals and Alloys, $cm^3 \cdot mm/(cm^2 \cdot sec \cdot \sqrt{kPa})$

Material	Constants	T, °C					
		200	300	400	500	600	700
Ni	p_H	$3,8 \cdot 10^{-8}$	$3,6 \cdot 10^{-7}$	$1,9 \cdot 10^{-6}$	$5,7 \cdot 10^{-6}$	$1,3 \cdot 10^{-5}$	$2,6 \cdot 10^{-5}$
	p_D	$2,3 \cdot 10^{-8}$	$2,2 \cdot 10^{-7}$	$1,1 \cdot 10^{-6}$	$3,4 \cdot 10^{-6}$	$7,8 \cdot 10^{-6}$	$1,5 \cdot 10^{-5}$
	η	1,7	1,7	1,7	1,6	1,7	1,7
Pd	p_H	$2,36 \cdot 10^{-4}$	$5,1 \cdot 10^{-4}$	$9,2 \cdot 10^{-4}$	$1,3 \cdot 10^{-3}$	$1,8 \cdot 10^{-3}$	$2,6 \cdot 10^{-3}$
	p_D	$1,41 \cdot 10^{-4}$	$3,24 \cdot 10^{-4}$	$5,9 \cdot 10^{-4}$	$8,6 \cdot 10^{-4}$	$1,2 \cdot 10^{-3}$	$1,7 \cdot 10^{-3}$
	η	1,7	1,6	1,6	1,6	1,5	1,5
PdNi10	p_H	—	—	$4,4 \cdot 10^{-4}$	$7,3 \cdot 10^{-4}$	—	$1,5 \cdot 10^{-3}$
	p_D	—	—	$3,1 \cdot 10^{-4}$	$5,2 \cdot 10^{-4}$	—	$1,1 \cdot 10^{-3}$
	η	—	—	1,4	1,4	—	1,4
PdNi65	p_H	—	—	$9,0 \cdot 10^{-6}$	$2,5 \cdot 10^{-5}$	$5,6 \cdot 10^{-5}$	$1,0 \cdot 10^{-4}$
	p_D	—	—	$6,8 \cdot 10^{-6}$	$1,9 \cdot 10^{-5}$	$4,1 \cdot 10^{-5}$	$7,7 \cdot 10^{-5}$
	η	—	—	1,4	1,4	1,4	1,4
PdAg15	p_H	—	—	$1,2 \cdot 10^{-3}$	$1,6 \cdot 10^{-3}$	—	$3,1 \cdot 10^{-3}$
	p_D	—	—	$8,3 \cdot 10^{-4}$	$1,0 \cdot 10^{-3}$	—	$1,9 \cdot 10^{-3}$
	η	—	—	1,5	1,6	—	1,6
Steel 25	p_H	—	—	$3,8 \cdot 10^{-6}$	—	—	—
	p_D	—	—	$2,7 \cdot 10^{-6}$	—	—	—
	η	—	—	1,4	—	—	—
V-1 alloy	p_H	$2,7 \cdot 10^{-4}$	$5,7 \cdot 10^{-4}$	$9,6 \cdot 10^{-4}$	$1,2 \cdot 10^{-3}$	$1,5 \cdot 10^{-3}$	$2,0 \cdot 10^{-3}$
	p_D	$1,8 \cdot 10^{-4}$	$3,8 \cdot 10^{-4}$	$6,3 \cdot 10^{-4}$	$8,1 \cdot 10^{-4}$	$9,8 \cdot 10^{-4}$	$1,4 \cdot 10^{-3}$
	η	1,5	1,5	1,5	1,5	1,5	1,4
V-2 alloy	p_H	—	$9,1 \cdot 10^{-4}$	$1,4 \cdot 10^{-3}$	$1,9 \cdot 10^{-3}$	$2,4 \cdot 10^{-3}$	$2,9 \cdot 10^{-3}$
	p_D	—	$5,3 \cdot 10^{-4}$	$0,8 \cdot 10^{-3}$	$1,1 \cdot 10^{-3}$	$1,4 \cdot 10^{-3}$	$1,8 \cdot 10^{-3}$
	η	—	1,7	1,7	1,7	1,7	1,6

where H_2, D_2, and HD are, respectively, the molecules of protium, deuterium, and protium–deuterium in the gaseous state; H and D are the atoms of protium and deuterium dissolved by the metal.

The isotope exchange reaction in the gaseous phase is described by the equation

$$\frac{1}{2}H_2 + \frac{1}{2}D_2 \rightleftarrows HD. \quad (4)$$

The chemical potentials of the molecules of the ideal gaseous phase and the atoms in the metallic matrix are described as follows:

$$\mu_{H_2} = \mu^0_{H_2} + RT \ln P_{H_2}; \quad (5)$$

$$\mu_{D_2} = \mu^0_{H_2} + RT \ln P_{D_2}; \quad (6)$$

$$\mu_{HD} = \mu^0_{HD} + RT \ln P_{HD}: \quad (7)$$

$$\mu_H = \mu^0_H + RT \ln \gamma_H x_H; \quad (8)$$

$$\mu_D = \mu^0_D + RT \ln \gamma_D x_D, \quad (9)$$

where P_{H_2}, P_{D_2}, and P_{HD} are, respectively, the partial pressures the protium, the deuterium, and the protium–deuterium; x_H and x_D are the ratios of the number of atoms of protium and deuterium dissolved in the metal to the number of atoms of metal; γ_H and γ_D are the coefficients of activity of the atoms of protium and deuterium dissolved by the metal; μ° is the chemical potential of the corresponding atoms and molecules in the standard state.

Making use of the condition of thermodynamic equilibrium and material balance, we can describe a system of five independent equations in the concentrations (x_H; x_D; $x_{H_2} = P_{H_2}/P$; $x_{D_2} = P_{D_2}/P$; $x_{HD} = P_{HD}/P$):

$$\gamma_H x_H / \sqrt{P x_{H_2}} = \exp(\Delta G^0_H / RT); \quad (10)$$

$$\gamma_D x_D / \sqrt{P x_{D_2}} = \exp(\Delta G^0_D / RT); \quad (11)$$

$$x_{HD} / x_{H_2} x_{D_2} = \exp(\Delta G^0_{HD} / RT); \quad (12)$$

$$2x_{H_2} \frac{PV}{kT} + x_{HD} \frac{PV}{kT} + x_H N_{Me} = N^0_H; \quad (13)$$

$$2x_{D_2} \frac{PV}{kT} + x_{HD} \frac{PV}{kT} + x_D N_{Me} = N^0_D. \quad (14)$$

We use the following notation:

$$\Delta G_{\mathrm{H}}^{0}=\frac{1}{2}\mu_{\mathrm{H}_2}^{0}-\mu_{\mathrm{H}}^{0}; \tag{15}$$

$$\Delta G_{\mathrm{D}}^{0}=\frac{1}{2}\mu_{\mathrm{D}_2}^{0}-\mu_{\mathrm{D}}^{0}; \tag{16}$$

$$\Delta G_{\mathrm{HD}}^{0}=\frac{1}{2}\mu_{\mathrm{H}_2}^{0}+\frac{1}{2}\mu_{\mathrm{D}_2}^{0}-\mu_{\mathrm{HD}}^{0}; \tag{17}$$

$$P=P_{\mathrm{H}_2}+P_{\mathrm{D}_2}+P_{\mathrm{HD}}, \tag{18}$$

where ΔG° is the difference between the corresponding standard molar isobaric–isothermal potentials; V, volume of the system; k, Boltzmann constant; N_{Me}, number of atoms of metal; N_H^0, N_D^0, total numbers of atoms of protium and deuterium in the system.

The system of equations (10)-(14) can be solved by numerical methods. However, if the concentration of the gaseous phase is kept constant (i.e., if we can disregard the number of atoms dissolved in the metal in comparison with the number of atoms in the gaseous phase), we can obtain analytically an exact solution for the ratio of concentrations of the isotopes in the metal:

$$\frac{x_{\mathrm{H}}}{x_{\mathrm{D}}}=\frac{\gamma_{\mathrm{D}}}{\gamma_{\mathrm{H}}}\exp\left[(\Delta G_{\mathrm{H}}^{0}-\Delta G_{\mathrm{D}}^{0})/RT\right]\quad\left[\frac{\sqrt{k_0}}{4}\left(\frac{N_{\mathrm{H}}^{0}}{N_{\mathrm{D}}^{0}}-1\right)+\sqrt{\frac{k_0}{16}\left(\frac{N_{\mathrm{H}}^{0}}{N_{\mathrm{D}}^{0}}-1\right)^{2}+\frac{N_{\mathrm{H}}^{0}}{N_{\mathrm{D}}^{0}}}\right], \tag{19}$$

where

$$k_0=\frac{P_{\mathrm{HD}}^{2}}{P_{\mathrm{H}_2}P_{\mathrm{D}_2}}=\exp\left(\frac{2\Delta G_{\mathrm{HD}}^{0}}{RT}\right) \tag{20}$$

is the constant of the isotope-exchange reaction.

The values of ΔG° may be calculated, in principle, on the basis of known model representations, and thus, the expression (19) enables us to find the equilibrium concentration of the isotopes in the metal from their known concentration in the gaseous phase.

The separation coefficient of protium and deuterium in the dissolution process,

$$\alpha_L=\frac{x_{\mathrm{H}}}{x_{\mathrm{D}}}:\frac{N_{\mathrm{H}}^{0}}{N_{\mathrm{D}}^{0}} \tag{21}$$

takes the form

$$\alpha_{\mathrm{L}}=\frac{\gamma_{\mathrm{D}}}{\gamma_{\mathrm{H}}}\left[\frac{\sqrt{k_0}}{4}\left(1-\frac{N_{\mathrm{D}}^{0}}{N_{\mathrm{H}}^{0}}\right)+\sqrt{\frac{k_0}{16}\left(1-\frac{N_{\mathrm{D}}^{0}}{N_{\mathrm{H}}^{0}}\right)^{2}+\frac{N_{\mathrm{D}}^{0}}{N_{\mathrm{H}}^{0}}}\right]\exp\left(\frac{\Delta G_{\mathrm{H}}^{0}-\Delta G_{\mathrm{D}}^{0}}{RT}\right). \tag{22}$$

In this case the coefficient of separation depends on the isotopic effect of solubility, the constant of the isotope-exchange reaction, and the ratio of the concentrations of the isotopes in the gaseous phase.

In the diffusion regime of penetration the flow of an isotope is proportional to its solubility and its coefficient of diffusion in the metal. Therefore, the coefficient of separation of the isotopes in penetration through a membrane can be represented in the form:

$$\alpha_{p}=\frac{D_{\mathrm{H}}\gamma_{\mathrm{D}}}{D_{\mathrm{D}}\gamma_{\mathrm{H}}}\left[\frac{\sqrt{k_0}}{4}\left(1-\frac{N_{\mathrm{D}}^{0}}{N_{\mathrm{H}}^{0}}\right)+\sqrt{\frac{k_0}{16}\left(1-\frac{N_{\mathrm{D}}^{0}}{N_{\mathrm{H}}^{0}}\right)+\frac{N_{\mathrm{D}}^{0}}{N_{\mathrm{H}}^{0}}}\right]\exp\left(\frac{\Delta G_{\mathrm{H}}^{0}-\Delta G_{\mathrm{D}}^{0}}{RT}\right). \tag{23}$$

In this case also, the separation coefficient depends, among other things, on the ratio of the coefficients of diffusion of the isotopes.

We consider the solubility of the isotopes to be represented by the functions:

$$L_{\mathrm{H}}=\gamma_{\mathrm{H}}^{-1}P_{\mathrm{H}_2}^{1/2}\exp\left(\Delta G_{\mathrm{H}}^{0}/RT\right); \tag{24}$$

$$L_{\mathrm{D}}=\gamma_{\mathrm{D}}^{-1}P_{\mathrm{D}_2}^{1/2}\exp\left(\Delta G_{\mathrm{D}}^{0}/RT\right). \tag{25}$$

The isotopic effects of the diffusion on the solubility (these are calculated for the condition $P_{H_2} = P_{D_2}$ from experiments carried out for each isotope) can be written in the form

TABLE 2. Values of K for Different Values of N_D^0/N_H^0 and k_0

N_D^0/N_H^0	k_0							
	4	3,75	3,5	3	2	1	10^{-1}	10^{-3}
10^{-6}	1	0,97	0,935	0,87	0,71	0,5	0,16	0,016
10^{-3}	1	0,97	0,93	0,86	0,7	0,5	0,16	0,04
10^{-1}	1	0,973	0,947	0,89	0,77	0,61	0,39	0,32
1	1	1	1	1	1	1	1	1
10^3	1	1,03	1,07	1,15	1,41	1,99	6,1	24,7
10^6	1	1,06	1,1	1,16	1,45	1,99	6,326	63

TABLE 3. Variation of α_p as a Function of Temperature

T, °C	α_p	T, °C	α_p
300	1,8	500	1,6
400	1,7	610	1,6
460	1,6		

$$\eta_L = \frac{L_H}{L_D} = \frac{\gamma_D}{\gamma_H} \exp\left(\frac{\Delta G_H^0 - \Delta G_D^0}{RT}\right); \tag{26}$$

$$\eta_D = D_H/D_D. \tag{27}$$

If we write

$$K = \frac{\sqrt{k_0}}{4}\left(1 - \frac{N_D^0}{N_H^0}\right) + \sqrt{\frac{k_0}{16}\left(1 - \frac{N_D^0}{N_H^0}\right)^2 + \frac{N_D^0}{N_H^0}}, \tag{28}$$

then

$$\alpha_p = \eta_L \eta_D K. \tag{29}$$

Here η_L and η_D are constants of the material of the membrane, and K depends on the constant of the isotope-exchange reaction and the initial concentration of the mixture. In Table 2 we give the calculated value of K for all possible values of k_0 and N_D^0/N_H^0. Thus, in the limiting cases, when $k_0 \to 4$,

$$\alpha_p = \eta_L \eta_D, \tag{30}$$

and when $k_0 \to 0$,

$$\alpha_p = \eta_L \eta_D \sqrt{N_D^0/N_H^0}. \tag{31}$$

The separation coefficient is inversely proportional to the square root of the ratio of partial pressures of the isotopes in the gaseous mixture at the inlet of the membrane. For example, if $P_{D_2}/P_{H_2} = 10^6$, then $\alpha_p = 10^3$. In reality this can happen only when the gaseous phase is nonequilibrium (when there are no HD molecules). Under equilibrium conditions $k_0 \approx 4$, and in that case $\alpha_p = 1.3$-2.0.

In our study we made direct measurements of the separation coefficients of an equilibrium isotope mixture (H_2—HD—D_2) for penetration through a membrane made of a special palladium-based alloy called V-2 [4]. Diffusive filtration of the isotope mixture was carried out at a total pressure of 0.1 MPa at the inlet and a temperature from 300 to 610°C (Table 3). The composition of the initial fraction and the diffused fraction was analyzed with an MKh-1302 mass spectrometer. The choice of the regime (accelerating voltage, emission current, pressure) and the design of the inlet devices enabled us to reduce substantially the memory effects and the "diaphragm" effects.

The results obtained showed that in the region of most efficient operation of the alloy (T = 500°C) we have $\alpha_p = 1.6 \pm 0.2$. For the given temperature and initial fraction composition (in this case $N_D^0/N_H^0 = 1$) this result is in good agreement with the calculated results [see Eq. (29)]. When the temperature is reduced to 300°C, the separation coefficient in-

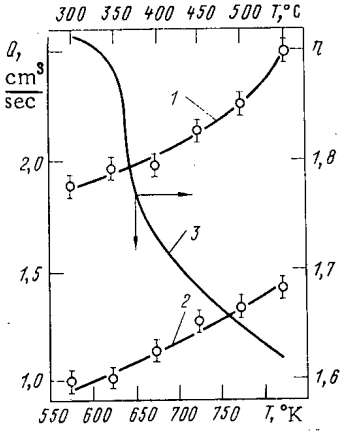

Fig. 1. Output of a diffusion filter for hydrogen isotopes with respect to protium (1), deuterium (2), and the isotopic effect (3).

creases to 1.8 ± 0.2. However, the output of the membrane decreases somewhat faster than exponentially. These effects apparently can be attributed to the interaction between the hydrogen atoms and to the formation of "groups" of hydrogen atoms in the metal. This metal-physics aspect of the problem will require further investigation.

A further study of the method of diffusion separation of hydrogen isotopes was carried out using a filter with an output of 2 liters/h, whose elements were made of industrial capillary tubes. The filter was tested on a special stand [8]. The results of the tests are shown in Fig. 1, from which it can be seen that the outputs of protium and deuterium increase exponentially with temperature. At the working temperature of the apparatus, the protium and deuterium output values were 2.2 and 1.3 liters/h. Thus, the isotopic effect of the output is equal to 1.7, which, in view of Eq. (29), ensures an equally high separation coefficient for the given conditions.

The permeability of the V-2 alloy to protium at a working temperature of 500°C was $1.8 \cdot 10^{-3}$ $cm^3 \cdot mm/(cm^2 \cdot sec \cdot \sqrt{kPa})$, which yields an output of 1 liter/h per gram of industrially produced capillary tubing. It should be borne in mind that when the membrane does not operate properly, precious metals may be used. This ensures that they can be almost completely regenerated.

Thus, the above-described experiments confirm the possibility and high efficiency of separating hydrogen isotopes by the method of diffusion through a metal membrane.

LITERATURE CITED

1. Z. V. Ershova et al., in: Reports of the All-Union Conference on Engineering Problems of Controlled Thermonuclear Synthesis [in Russian], Vol. 4, Izd. NIIEFA, Leningrad (1975), p. 14.
2. N. F. Myasoedov and V. K. Popov, At. Tekh. za Rubezhom, 8, 26 (1974).
3. V. A. Gol'tsov, Problems of Atomic Energy and Technology [in Russian], Atomic and Hydrogen Power Engineering Series, No. 1 (2), 65 (1977).
4. V. A. Gol'tsov et al., Izv. Vyssh. Uchebn. Zaved. Chern. Metall., No. 1, 117 (1977).
5. V. V. Latyshev et al., in: Methods of Investigation and Determination of Gases in Metals and Inorganic Materials. Theses of the Reports of the Fourth All-Union Conference [in Russian], Leningrad (1979), p. 151.
6. F. Altenhein, et al., in: Proc. Int. Conf. on Radiation Effects and Tritium Technol. Fusion Reactors, Gatlinburg, Oak Ridge, 1976, Vol. 3, p. 175.
7. C. Pierce and H. Howe, in: 7th Symp. Eng. Probl. Fusion Res., Vol. 1, Knoxville (1977), p. 101.
8. V. A. Gol'tsov, V. V. Latyshev, and A. A. Alekhov, Fiz.-Khim. Mekh. Mater., 13, No. 3, 116 (1977).

EXPERIMENTAL INVESTIGATION OF THE NEUTRON FLUX REGULATION BY MEANS OF A TWO-PHASE EQUILIBRIUM REACTION

I. G. Gverdtsiteli, A. G. Kalandarishvili,
V. B. Klimentov, M. N. Korotenko,
S. D. Krivonosov, B. A. Mskhalaya,
A. V. Nikonov, and V. D. Popov

UDC 621.039.515

The autonomy of each channel inspected must be considered in nuclear research reactors when several experiments requiring different neutron flux densities are made at the same time.

In order to match the reactor power with the required neutron flux density in a cell, one can successfully employ the earlier [1] described method of regulating the neutron flux by means of a two-phase equilibrium reaction in which neutron absorbing materials are kept in layer structures transparent for neutrons. The method may be supplemented by using porous structures, e.g., activated carbon. A profile of the neutron flux over the height of the core can be obtained in neutron flux regulation by means of a two-phase equilibrium reaction.

We chose cadmium and its compounds, as well as boron trifluoride gas, as absorbers. Studies of the sorption kinetics involved weight and volume techniques applied to the activated carbon-cadmium system; the studies have shown that the particular pair can be efficiently used to regulate the neutron flux at temperatures above 600°C, whereas the pair consisting of activated carbon and boron trifluoride can be employed in the temperature range 20-300°C.

In order to check the possible neutron flux regulation in the apparatus with the aid of sorption systems, we developed a tube with the activated carbon—cadmium system. The channel was designed in the form of several coaxial cylinders. The inner cylinder 1 contained a calorimeter assembly [2] with two thermal dispersers of radiation which were filled with material capable of undergoing fission (uranium dioxide with 2% ^{235}U enrichment). Cylinders 2 and 5 formed an autonomous evacuated volume communicating with a cadmium thermostat mounted below the core. The 0.65 cm wide gap between cylinder 5 and the perforated partition was filled with activated carbon; the space between cylinder 2 and the partition served for admitting the cadmium vapor phase through four distributors into the plane of the core center. A jacket formed around the entire assembly a protected cavity which was evacuated by pumping during the entire experiment. The temperature of the individual components was kept constant with four electric heaters and checked with Chromel-Alumel thermocouples. A directly charged sensor was attached to the outer surface of the jacket for measuring the neutron flux in the cell.

The experimental tube for regulating the neutron flux density was tested in the VVR-M reactor of the Institute of Nuclear Research of the Academy of Sciences of the Ukrainian SSR. The degree of attenuation of this particular sorption system was measured at various power ratings of the apparatus and for various temperature conditions of the sorbent and the absorber.

The results of this research (Fig. 2) have shown that the change in the degree of attenuation is correlated to the change in the temperature of sorbent and absorber, the temperature determining the specific cadmium concentration in the activated carbon. The degree of attenuation of the sorption system was defined as the ratio of neutron flux density required for obtaining the experimentally measured liberation of heat in the calorimeters to the neutron flux density in the experimental cell. The flux density of the thermal neutrons in the cell was determined from the external directly charged sensors (sensitivity of $3.15 \cdot 10^{-20}$ A·cm²·sec).

Translated from Atomnaya Énergiya, Vol. 53, No. 1, pp. 36-37, July, 1982. Original article submitted August 20, 1980.

0038-531X/82/5301-0487$07.50

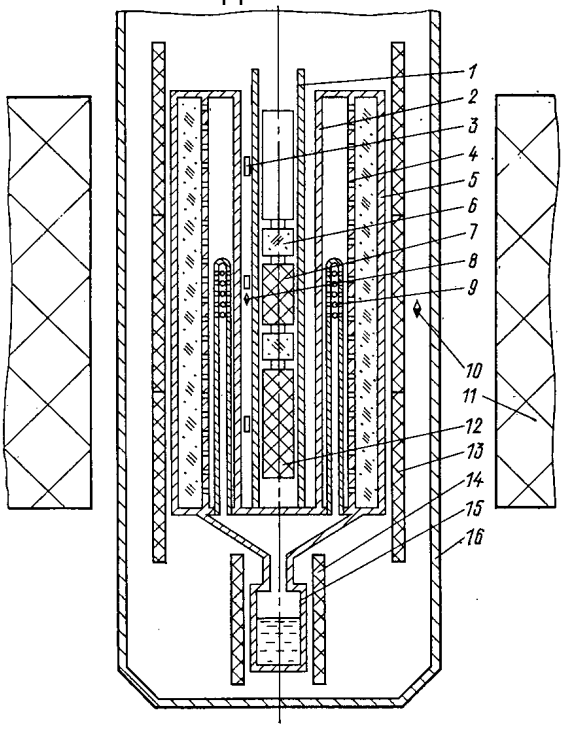

Fig. 1

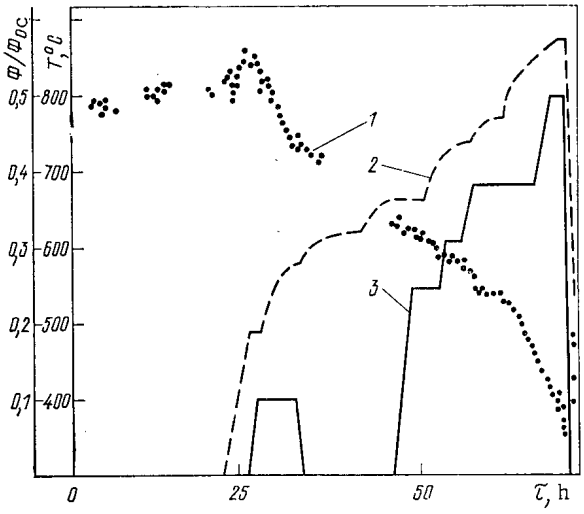

Fig. 2

Fig. 1. Experimental tube for regulating the neutron flux with an activated carbon–cadmium system: 1, 2, 5) cylinders; 3) sensor of thermal neutrons; 4) partition; 6) simulator; 7, 12) thermal dispersers of radiation; 8, 10) directly charged sensors; 9) distributor; 11) core; 13, 14) electric heaters; 15) cadmium thermostat; 16) jacket.

Fig. 2. Dependence of the degree of attenuation (1) upon the temperature conditions of the sorbent (2) and the absorber (3) (Φ denotes the neutron flux density behind an adsorbing shield, the flux density being determined from the heat liberated; O_{oc} denotes the neutron flux density before the shield (subscript "0"), as measured with the directly charged sensor (the subscript c refers to the center plane of the core)).

The liberation of heat in the thermal dispersers of radiation was converted into neutron flux densities with a formula of [3], taking into account the temperature coefficient of the sensitivity:

$$Q = a\overline{\Phi}N_0\sigma_F V,$$

where a denotes the energy (MeV) liberated in a single ^{235}U fission event; $\overline{\Phi}$, average thermal-neutron flux density (neutrons/cm^2·sec); N_0, number of ^{235}U atoms per cm^3; σ_F, effective fission cross section (cm^2); V, volume (cm^3) of the material undergoing fission; and Q, heat liberation in the calorimeter (W).

In order to eliminate the influence of the cadmium vapor phase upon the degree of attenuation of the neutron flux density, the neutron flux and temperature conditions existing while the power of the apparatus is raised were reproduced. Cadmium condensation was produced by a sharp inflection of the heat liberation, which resulted in a redistribution of the neutron flux density in the core and a subsequent rapid return of the calorimeter readings to the state before the reduction of the apparatus power and to cooling of the cadmium, i.e., an attenuation of the neutron flux density was obtained basically via the cadmium absorbed by the activated carbon.

Our investigations have confirmed that the neutron flux density of a reactor can be efficiently regulated by sorption and desorption processes involving neutron-absorbing materials. It is suggested to investigate in the future the possibility of regulating the neutron flux density of a reactor with sorption systems consisting of activated carbon and boron trifluoride or pyrolytic graphite and an alkali metal.

LITERATURE CITED

1. I. G. Gverdtsiteli et al., At. Énerg., 48, No. 3, 187 (1980).
2. V. N. Avaev et al., Experimental Investigations of Fields of Gamma Radiation and Neutrons [in Russian], Atomizdat, Moscow (1974).
3. R. Alami and P. Augeron, Heat Removal and Generation of Heat in Nuclear Reactors [Russian translation], Gosatomizdat, Moscow (1961).

DEVICE FOR CONTINUOUS MONITORING OF BURNING OF NUCLEAR FUEL

I. G. Gverdtsiteli, A. G. Kalandarishvili, and V. A. Kuchikhidze

UDC 621.039.546

The breeding of fuel is of great importance in the design of modern nuclear power reactors. This requires the exact calculation of a number of neutron-physical parameters of the reactor. In particular, one must know the degree of burning of the nuclear fuel in recycling of the core and in order to optimize the recycling of the spent fuel.

The known destructive [1-3] and nondestructive [4] methods of determining the burning of nuclear fuel require fuel rods to be removed from the reactor, which is inconvenient and often also undesirable from a technological point of view. Further, they do not permit burning to be monitored continuously while the reactor is operating.

In the present communication we discuss the possibility of determining the degree of burning of nuclear fuel through the accumulation of the nuclides $^{133,137}Cs$ and $^{85,87}Rb$ in a sensing element based on layered graphite compounds. These nuclides, with the exception of ^{137}Cs, are stable [5] and satisfy the requirements that have to be met by monitors of fuel burning [6].

As a monitor of burning we propose using nuclides of the alkali metals cesium and rubidium, and as a sensing element we propose anisotropic pyrolitic graphite, which is selectively sensitive to the alkali metals [7]. The alkali metals (cesium and rubidium) intercalate into the spaces between the graphite layers and so give rise to a considerable expansion of the geometrical dimensions along the C axis of the layered graphite structure [8, 9]. By measuring the absolute expansion of the graphite along the C axis we can determine the number of cesium and rubidium atoms that have been introduced and thereby determine the degree of burn-up of the fuel.

The sensing element of anisotropic pyrolitic graphite is located between two flanges in a fuel rod (Fig. 1). One of the flanges is movable along the C axis of the graphite. The quantity of fission products present (cesium and rubidium) increases as the nuclear fuel is burned up. By diffusion the fission products find their way into the graphite element, where, by intercalation, they cause the graphite to expand along the C axis. This expansion is transmitted by a rod to a special device mounted in the can, where it is recorded.

To estimate different characteristics of the device, a calculation was carried out for a water-cooled water-moderated reactor fuel rod type VVÉR-440 with 3.5% ^{235}U enrichment (dimensions of nuclear fuel: d = 0.77 cm, h = 250 cm) for a mean thermal neutron flux of $\sim 10^{13}$ neutrons/cm^2·sec [10].

The number of stable and long-lived isotopes emitted from the fuel during the time of irradiation τ was calculated by solving the diffusion equation [11]:

$$\partial N_i/\partial\tau = D\Delta N_i + fY_i, \quad (1)$$

where N_i is the number of atoms of the i-th isotope in the solid fuel rod (atoms·cm^{-3}); f is the fission rate of ^{235}U (nuclei·cm^{-3}·sec^{-1}); Y_i is the relative output of the i-th isotope per single fission act; and D is the diffusion coefficient (cm^2·sec^{-1}).

The solution of this equation for stable and long-lived nuclides subject to the initial [$N_i(r, 0) = 0$] and boundary [$N_i(d, \tau) = 0$] conditions has the following form [11] for

Translated from Atomnaya Énergiya, Vol. 53, No. 1, pp. 37-38, July, 1982. Original article submitted March 13, 1981.

0038-531X/82/5301-0489$07.50

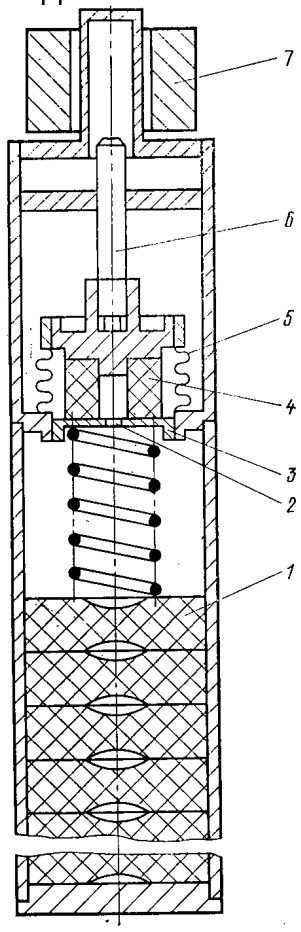

Fig. 1

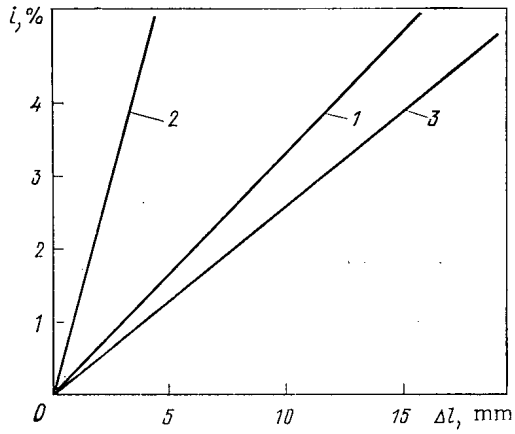

Fig. 2

Fig. 1. Fuel rod with continuous monitoring of burn-up by described scheme. 1) Fuel assembly; 2) channel for removal of vapor; 3) screen; 4) graphite block; 5) bellows; 6) rod; 7) device for recording expansion of graphite.

Fig. 2. Plot of burn-up of nuclear fuel versus absolute elongation of graphite block for intercalation by nuclides of cesium (1), rubidium (2), and a mixture of cesium and rubidium nuclides (3).

the number of atoms N_i' of the i-th isotope emitted from volume V during the irradiation time, allowing for burning of the fuel:

$$N_i' = fY_i\tau V \exp(-\sigma_f\Phi\tau)\left[1-\frac{6a^2}{90D\tau}+\frac{6a^2}{\pi^4 D\tau}\sum_{n=1}^{\infty}\frac{1}{n^4}\exp\left(-\frac{n^2\pi^2 D\tau}{a^2}\right)\right], \quad (2)$$

where the diffusion coefficient D is determined from the formula:

$$D = 6.6\cdot 10^{-6}\exp\left(-\frac{71700}{RT}\right). \quad (3)$$

The results of the calculations were used to plot burn-up versus the absolute elongation (Fig. 2) of a graphite block in the form of a washer with d_{outer} = 0.725 cm, d_{inner} = 0.3 cm, l = 4 cm. The sensitivity of such a block is 0.385 cm at 1% burn-up for intercalation of the graphite by a mixture of cesium and rubidium nuclides. The sensitivity of burn-up measurements can be increased by optimizing the construction of the sensing element.

LITERATURE CITED

1. L. I. Golubev et al., At. Énerg., 41, No. 3, 197 (1976).
2. Yu. V. Sivintsev, At. Tekh. za Rubezhom, No. 6, 30 (1979).

3. V. M. Gryazev et al., Preprint NIIAK No. 25 (359) [in Russian], Dmitrovgrad (1978).
4. H. Ramthun, in: Proc. 2nd ASTM-EURATOM Int. Symp. on Reactor Dosimetry. Dosimetry Methods for Fuels-Cladding and Structural Materials, Held at Palo Alto, California, Washington, Oct. 3-7, 1977, Vol. 1, s.a. 433.
5. O. F. Nemets and Yu. V. Gofman, Reference Book on Nuclear Physics [in Russian], Naukova Dumka, Kiev (1975).
6. A. Fudge, in: Proc. IAEA Symp. on Analytical Methods in the Nuclear Fuel Cycle, Vienna (1971), p. 442.
7. A. R. Ubbelode and P. A. Lewiss, Graphite and Its Crystalline Compounds [Russian translation], Mir, Moscow (1965).
8. I. G. Gverdtsiteli et al., Zh. Fiz. Khim., 49, No. 1, 217 (1975).
9. I. G. Gverdtsiteli et al., Zh. Fiz. Khim., 50, No. 11, 2926 (1976).
10. E. P. Anan'ev, Atomic Installations in Power Engineering [in Russian], Atomizdat, Moscow (1978).
11. B. Lastman, Radiation Phenomena in Uranium Dioxide [in Russian], Atomizdat, Moscow (1964).

KINETIC CONSTANTS OF RADIATION GAS FORMATION IN POLYETHYLENE

N. N. Alekseenko, P. V. Volobuev, and S. B. Trubin

UDC 541.28:621.039.538

In the biological shield of small-scale nuclear power facilities, polyethylene is widely used as a material with excellent moderating properties with respect to reactor neutron radiation. However, polyethylene is characterized by a relatively low radiation stability, as a result of which during its operation, intense gas release is observed, which can lead to the origination of an explosion-hazardous situation. It is necessary, therefore, to conduct a comprehensive study of the process of radiation gas release from polyethylene.

It is well-known that by the action of ionizing radiation, radiation–chemical reactions take place in polyethylene, leading to the formation of molecular hydrogen. The presence of atomic hydrogen in the polymer matrix has not been detected [1]. It may be supposed, therefore, that the hydrogen in polyethylene is formed according to a biradical mechanism. A certain amount of the hydrogen formed leaves the material by means of diffusion, and another part as the result of recombination reaction is returned to the polymer matrix. In this trivial concept, the process of radiation gas formation in polyethylene can be described by quasichemical reactions of the type

$$\Pi \underset{k_2}{\overset{k_1}{\rightleftarrows}} \Pi' + H_2; \tag{1}$$

$$\Pi' \to \Pi_p, \tag{2}$$

where Π is a gas formation center (a pair of hydrogen atoms in the polyethylene); Π' is a pair of radicals, formed after the breakaway of hydrogen atoms; Π_p, pair of radicals, recombined with one another; H_2, hydrogen molecule; and k_1, k_2, k_3, reaction velocity constants.

The system of kinetic equations corresponding to the process, described by reactions (1) and (2), taking account of diffusion of the gas formed, can be written in the form

$$\frac{\partial n}{\partial t} = D\Delta n - \frac{\partial N}{\partial t}; \tag{3}$$

$$\frac{\partial N}{\partial t} = -k_1 N + k_2 N_n'; \tag{4}$$

Translated from Atomnaya Énergiya, Vol. 53, No. 2, pp. 38-40, July, 1982. Original article submitted March 10, 1981.

0038-531X/82/5301-0491$07.50

$$\frac{\partial N'}{\partial t} = k_1 N - k_2 N' - k_3 N'. \tag{5}$$

Here n is the number of hydrogen molecules formed in unit volume of polyethylene; N, number of gas formation centers in unit volume of polyethylene; N', number of radical pairs, originating as the result of the formation of hydrogen; t is the time, and D is the diffusion coefficient.

The system of equations (3)-(5) can be converted to a system of two equations, one of which is Eq. (3) and the other is

$$\frac{\partial N}{\partial t} = -(k_1 + k_2 n) N + k_2 N_0 n e^{-k_3 t} + k_2 k_3 n e^{-k_3 t} \int_0^t N(\tau) e^{-k_3 \tau} d\tau. \tag{6}$$

The solution of the system obtained is a problem of considerable complexity. Therefore, we shall consider the simplest special cases. The simplest case, obviously, will be the case of quasiequilibrium, isochoric process of gas release. By quasiequilibrium is understood the part of the isochoric radiation gas release process, where the concentration of gas dissolved in any point of the sample, with the quasiequilibrium isochoric gas release negligibly small by comparison with the concentration.

In order to derive the quasiequilibrium criterion, we shall consider the case when the process of diffusion of the gas, which has formed, from the sample is steady. Without reducing the generality of the discussions, it can be supposed that the strength of the gas release sources $\nu = -dN/dt$ is independent of the time. This is fulfilled if the time of observation is significantly less than the characteristic time of gas release τ_ν — the time during which the intensity of the gas release is decreased by a factor of e. It is shown in [2] that this time amounts to $(3\text{-}7)\cdot 10^4$ sec. Assuming uniformity of the dose intensity distribution throughout the sample, which is equivalent to independence of the function on the coordinates, for the diffusion equation with boundary conditions

$$n|_{\substack{x=0 \\ x=l}} = k_S p \tag{7}$$

we can obtain

$$n = \frac{\nu}{2D}(lx - x^2) + k_S p, \tag{8}$$

where k_S is the solubility constant of the gas (hydrogen) in the sample; p, gas pressure; and l, thickness of the sample.

The nonuniformity of the concentration throughout the sample is defined as the ratio of the maximum concentration at the center of the sample, to the minimum concentration at the boundary

$$\varphi = \frac{n_{\max}}{k_S p} = 1 + \frac{\nu}{2D} \frac{1}{k_S p} \frac{l^2}{4}. \tag{9}$$

It is necessary that the nonuniformity φ is close to unity or

$$(\varphi - 1) \ll 1. \tag{10}$$

In order to satisfy condition (10), as it follows from Eq. (9), it is most effective to reduce the thickness of the sample l. We shall suppose that condition (10) is satisfied. Then the gas release process can be assumed to be in quasiequilibrium, the diffusion mechanism of gas transfer in general can be neglected and, consequently, the whole gas-release process can be described by the one equation (6). As, in the case of quasiequilibrium between the pressure in the gas phase and the gas concentration in the sample, there exists an unambiguous conformity; then having assumed that the process of dissolution is described by Henry's Law (7), the concentration in Eq. (6) can be substituted by the pressure p.

However, in Eq. (6), a further number of gas formation centers occur. In order that this quantity also can be substituted by the pressure, we shall use the equation of balance. Taking into account that the ampul with the sample being investigated and the gas vacuum measurement system have a different temperature [3], we can write

$$nV_S + p\frac{V_1}{kT_1} + \frac{V_2}{kT_2} p = V_S (N_0 - N), \tag{11}$$

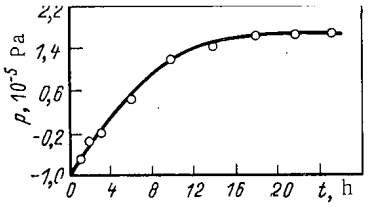

Fig. 1. Variation of pressure of the gas released during radiolysis of polyethylene in a closed system (dose intensity 0.64 Gy/sec).

where V_S is the volume of the sample; V_1, free volume of the ampul, being at temperature T_1; V_2, volume of the measurement system, being at temperature T_2; k, Boltzman's constant; and $(N_0 - N)$, number of destroyed gas formation centers.

With independence on the coordinates of the absorbed dose intensity, the concentration of destroyed gas formation centers also is independent of the coordinates. Taking account of Henry's Law, we find

$$N = -\frac{p}{V_S}\left(k_S V_S + \frac{V_1}{kT_1} + \frac{V_2}{kT_2}\right) + N_0$$

or

$$N = N_0 - p\varkappa, \tag{12}$$

where

$$\varkappa = k_S + \frac{V_1}{V_S}\frac{1}{kT_1} + \frac{V_2}{V_S}\frac{1}{kT_2}.$$

Whence we obtain

$$\frac{dN}{dt} = -\frac{dp}{dt}\varkappa. \tag{13}$$

Relation (6) can now be written in the form

$$-\frac{dp}{dt}\varkappa = -k_1 N_0 + k_1 \varkappa p - N_0 k_2 k_S p + k_2 k_S \varkappa p^2 + N_0 k_2 k_S p e^{-k_3 t} + k_2 k_S N_0 p\,(1 - e^{-k_3 t}) - \varkappa k_2 k_3 k_S p e^{-k_3 t}\int_0^t p(\tau)\,d\tau. \tag{14}$$

In the experiment, the isochoric gas release curves are observed (see Fig. 1). The presence of a horizontal section means that in Eq. (1) and (2) the constant k_3 either is very small, or is equal to zero. We shall assume that $k_3 = 0$. Then the gas release process must have a section where $dp/dt = 0$. Consequently, we can write

$$\varkappa k_2 k_S p_m^2 + k_1 \varkappa p_m - k_1 N_0 = 0. \tag{15}$$

We find from this expression k_1, and we substitute in the relation for dp/dt:

$$\frac{dp}{dt} = -\frac{k_2 k_S p_m^2 N_0}{N_0 - \varkappa p_m} + \frac{\varkappa k_2 k_S p_m^2}{N_0 - \varkappa p_m} + k_2 k_S p^2. \tag{16}$$

Hence,

$$k_2 = \frac{dp}{dt}\left[-\frac{\varkappa k_S p_m^2 N_0}{N_0 - \varkappa p_m} + \frac{\varkappa^2 k_S p_m}{N_0 - \varkappa p_m}p + \varkappa k_S p^2\right]^{-1}. \tag{17}$$

The value of dp/dt as a function of p is not difficult to calculate from the experimental curve of $p = p(t)$, and the value of p_m is found also from experiment. Thus, from the experimental results of the investigation of the isochoric radiation gas release, it is found to be possible to determine the constants of the forward and reverse reactions of gas formation.

The study conducted of the kinetics of isochoric gas release from polyethylene of low density, has enabled the values of the kinetic constants to be determined: $k_1 = (7.4 \pm 0.6)\cdot 10^{-7}$ sec^{-1} and $k_2 = (2.8 \pm 0.2)\cdot 10^{-29}$ m^3/sec, and the latter coincides well with the

known data for the kinetics of destruction of alkyl radicals [4]. Unfortunately, there are no published data about the numerical values of the constant k_1.

The experiments were conducted with the following thermodynamic conditions: $T_1 = 328°K$, $T_2 = 301°K$; $V_S = 0.31 \cdot 10^{-4}$ m^3; $V_1 = 0.21 \cdot 10^{-3}$ m^3; $V_2 = 0.56 \cdot 10^{-3}$ m^3; $l = 10^{-4}$ m; 10^{28} $(m^3)^{-1}$; $k_S = 0.68 \cdot 10^{19}$ $(m^3)^{-1} \cdot Pa$. The values of p_m and $dp/dt \sim f(p)$ were determined from experimental data, shown in Fig. 1.

LITERATURE CITED

1. G. N. P'yankov, in: Radiation Modification of Polymer Materials [in Russian], Tekhnika, Kiev (1969), p. 77.
2. P. V. Volobuev et al., in: Radiation Safety and Protection of Nuclear Power Stations [in Russian], No. 1, Atomizdat, Moscow (1975), p. 244.
3. N. N. Alekseenko et al., in: Radiation Safety and Protection of Nuclear Power Stations [in Russian], No. 1, Atomizdat, Moscow (1975), p. 251.
4. M. Doul, Radiation Chemistry of Macromolecules, Atomizdat, Moscow (1978).

CHARACTERISTICS OF THE DISTRIBUTION OF HELIUM BUBBLES IN A DISLOCATION NETWORK

A. M. Parshin, S. A. Fabritsiev, and V. D. Yaroshevich

UDC 669.785:546.291

The high-temperature helium embrittlement of structural steels and alloys is accompanied, as a rule, by intercrystalline failure. This proves irrefutably that the grain boundaries (natural sinks for helium atoms) are the most vulnerable structural elements of these materials. All the measures which allow the helium atoms to be held in the body of the grain, and thereby preventing its collection at the boundaries, should promote the suppression or weakening of high-temperature helium embrittlement. The latter undoubtedly requires studies of the detailed mechanism of interaction of the helium atoms with both the grain boundaries and with other imperfections of the crystal structure of the grain itself (different type of dislocations, twins, packing defects, carbides, nitrides, etc.).

In the present paper, the distribution of helium in samples of the alloy Kh20N45M4B, containing $3 \cdot 10^{-3}$ at. % He, was studied by the methods of the transmission electron microscope. Samples with this quantity of helium were investigated in the following states: 1) in the original state; 2) after annealing at a temperature of 1050°C during 30 min; 3) after their deformation up to $\varepsilon = 10\%$, and 4) after deformation up to $\varepsilon = 10\%$ and subsequent annealing at 1050°C during 30 min.

In the original state, the structures of the samples containing helium, do not differ from the structures of the samples without helium. Figure 1 shows the structure of samples containing helium after their annealing (state 2). It can be seen that after annealing, helium bubbles have been formed. They are all due to defects of the crystal structure. The distribution of the bubbles by size has two maxima in the region of 50 and 300 Å (1 Å = 10^{-10} m), the first is related with bubbles at dislocations and the second with bubbles at boundaries and inclusions.

In the microstructure of the samples containing helium after their deformation up to $\varepsilon = 10\%$ (state 3), no significant differences are detected from the structure of samples without helium and with this same degree of deformation. The distribution of dislocations in both cases is identical, and their density is $\sim 9 \cdot 10^{10}$ cm^{-2}. However, subsequent annealing of these samples leads to completely different structures. If, in the samples not containing helium, the dislocations are completely annealed, then in the samples with helium their density is reduced by not more than a factor of 2. This indicates that the helium is a powerful stabilizer of the dislocation structure.

Translated from Atomnaya Énergiya, Vol. 53, No. 1, pp. 40-41, July, 1982. Original article submitted March 18, 1981.

 0038-531X/82/5301-0494$07.50

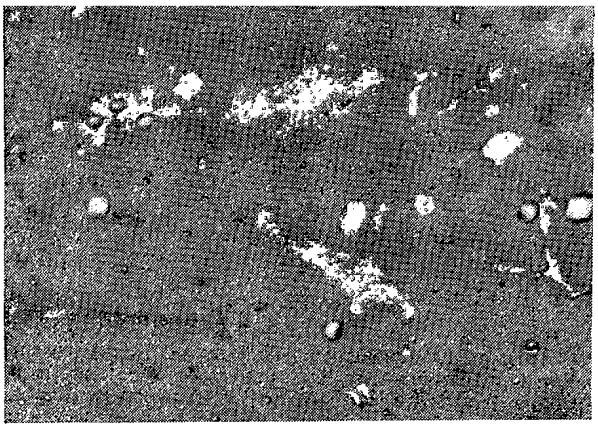

Fig. 1. Structure of the alloy Kh20N45M4B, after annealing at a temperature of 1050°C during 30 min.

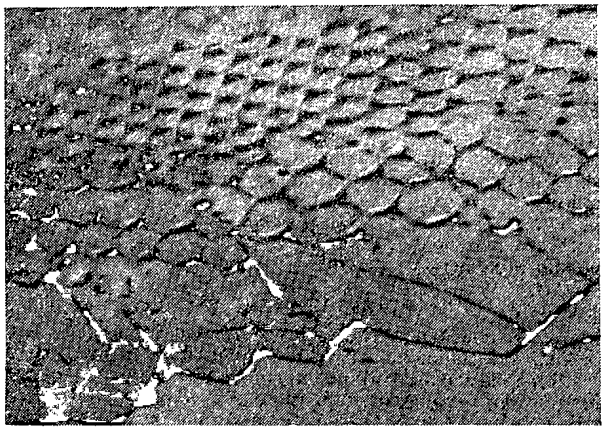

Fig. 2. Distribution of helium bubbles in a dislocation network.

When studying the distribution of helium in samples, annealed after deformation, the following interesting characteristics are found. First and foremost, it was found that in contrast from the annealed samples, not subjected to previous deformation, the sizes and density of the helium bubbles at the grain boundaries in the deformed samples, are significantly lower, and the density of the bubbles found in the dislocations in the body of a grain, is significantly higher. This indicates that the dislocation structure created by previous deformation, is a quite powerful acceptor, effectively retaining the helium in the body of the grain.

Figure 2 shows the characteristic structure of a sample containing helium (state 4). In addition to the characteristics listed above, it can be seen from the figure that annealing leads to the formation of numerous dislocation networks, in which obviously are found a previously unobserved uniformity of distribution of the helium bubbles, namely: the helium bubbles are found only in collapsed nodes of the dislocation networks; the sizes of the helium bubbles are identical (50 ± 10 Å).

The causes, leading to the observed mechanisms, at the present time are still not completely explained. It can be said only that one of the possible causes of this distribution of helium bubbles is a different solubility of helium in expanded and collapsed nodes of the dislocation networks. The results of this investigation show that the dislocation structure, stabilized by helium, is a reliable means for preventing the escape of helium at the grain boundaries and for weakening high-temperature helium embrittlement.

ABSORBED ELECTRON DOSES IN MIXED LIQUID-PHASE SYSTEMS

É. D. Grushkova, V. V. Krayushkin, and Yu. D. Kozlov

UDC 539.12.08

One of the most pressing problems at present is the purification of the sewage and waste water from towns, factories, and large livestock complexes. Intensive development of technology for the purification of effluent using various sources of ionizing radiation has led to the conclusion that the use of electron accelerators is promising [1]. In connection with this, it is important to investigate the characteristics of the absorbed electron energy in the irradiation of mixed liquid-phase systems.

The absorbed dose (AD) of electrons at any depth of the irradiated medium may be calculated by the Monte Carlo method, using the kinetic equation with definite boundary conditions [2]. Relatively simple semiempirical methods of calculating the AD have now also been developed [3]. In [4], an experimentally determined universal function was proposed, allowing the dose rate in the depth of a semiinfinite absorber to be calculated when a broad beam of electrons with a known initial angular and energy distribution is incident. These calculational and experimental methods, however, are cumbersome and complicated for the practical solution of technological problems and for use in calculations of the basic parameters of radiation–chemical plants (RCP).

The aim of the present work is to develop a sufficiently simple method of AD calculation in liquid-phase systems in designing RCP using electron accelerators.

As is known [5], the distribution of the absorbed-dose rate (ADR) over the depth of an unmixed object, with irradiation by a normally incident beam of monoenergetic electrons, is described by the function

$$P(x)=\frac{P_M}{2}[1+\sin(0.2+\Theta x)] \text{ for } \Theta x \leqslant 4.5, \quad (1)$$

where x is the thickness coordinate of the irradiated object, g/cm^2; P_M and Θ are defined in [6] in terms of the parameters of the radiation source

$$\Theta=\begin{cases}\dfrac{1.05}{E(E+0.48)} & \text{for } 0.03\leqslant E\leqslant 0.35 \text{ pJ, , cm}^2/\text{g}\\ 1.3E^{-1} & \text{for } 0.35<E\leqslant 0.8 \text{ pJ; ;}\end{cases} \quad (2)$$

$$P_M=2.3jE\Theta, \text{ kg·R/sec.} \quad (3)$$

Here E is the electron energy, pJ; j is the current density at the surface of the irradiated object, μA/cm^2.

It is assumed that the ADR distribution of the electron raidation in a water-equivalent absorber has the same form as in unmixed systems [3], that irradiated liquid-phase systems are similar to water in their physical properties, and that the AD distribution in the irradiated layer of liquid is homogeneous (confirmed experimentally [7]). Under these assumptions, two cases of the irradiation of a liquid flux by a broad electron beam are considered: 1) when the thickness of the liquid layer does not exceed the path length of electrons of the given energy; 2) when the thickness of the liquid layer is greater than the electron path length.

The mean AD in the irradiated liquid layer is determined by integrating the ADR distribution function over the depth of the layer. It is assumed here that the parameters of the radiation source, and hence also the value of P(x), are constant over time. Then the AD is determined from the formula (the subscripts 1 and 2 denote the two cases of irradiation)

$$\overline{D}_{1,2}=\frac{D_M}{a_0}\int_{x'}^{x''}\frac{P(x)}{P_M}dx. \quad (4)$$

Translated from Atomnaya Énergiya, Vol. 53, No. 1, pp. 41-42, July, 1982. Original article submitted April 14, 1981.

 0038-531X/82/5301-0496$07.50

Here $x'_1 = x'_2 = a_f$; $x''_1 = a_f + a_0$, $x''_2 = R$; P(x) is the ADR distribution according to Eq. (1): a_f, thickness of the absorbing filter; a_0, thickness of the liquid layer; R, maximum path length of electrons of the given energy in the irradiated liquid. The factor D_M is determined from the formula

$$D_M = \frac{2.3I\Theta E}{Lv}\,10^3, \text{kg·R}; \tag{5}$$

where I is the total yield current of the electron beam in the atmosphere, mA; L is the transverse (relative to the direction of liquid flow) dimension of the irradiation zone, cm; v is the velocity of liquid flow, cm/sec.

If the walls of the radiation-chemical apparatus are made of materials of atomic number $Z_{ef} > 10$, then reflection of the radiation from the opposite walls must be taken into account in conditions where the thickness of the irradiated liquid layer does not exceed the electron path length [8].

Integrating, and taking into account that R = 4.5/Θ [6], Eqs. (2) and (4) yield the relations

$$\overline{D}_1 = \frac{D_M}{2a_0}\left[a_0 + \frac{2}{\Theta}\sin\left(0.2 + a_f\Theta + \frac{a_0\Theta}{2}\right)\sin\frac{a_0\Theta}{2}\right];$$
$$\overline{D}_2 = \frac{D_M}{2a_0}\left[\frac{4.5a_f}{\Theta} + \frac{2}{\Theta}\sin\left(2.45 + \frac{a_f\Theta}{2}\right)\sin\left(2.25 - \frac{a_f\Theta}{2}\right)\right]. \tag{6}$$

In the general case, when the ADR varies over time τ and over the width of the radiation source l, the mean AD in the irradiated liquid is determined by integration over all these parameters

$$\overline{D} = \frac{D_M}{a_0 L(\tau_2 - \tau_1) P_M}\int_{a_f}^{R}\int_{0}^{L}\int_{\tau_1}^{\tau_2} P(x, l, \tau)\,dx\,dl\,d\tau. \tag{7}$$

For a series of specific radiation-engineering processes, the mean values of the AD and ADR have been determined experimentally, and may be regarded as given in calculating RCP parameters. Then, from Eqs. (1)-(7), with the substitution of the mean values of the AD and ADR, the basic parameters of the RCP may be determined: the current density and total current of the electron beam, the electron energy, liquid flow rate, layer thickness, etc.

Thus, a sufficiently simple method of calculating the AD and ADR of electron radiation in mixed liquid-phase systems has been proposed, allowing RCP design parameters to be determined.

LITERATURE CITED

1. Radiation for a Clean Environment, Symposium Proceedings, IAEA, Vienna (1975).
2. M. Berger, Methods Comput. Phys., 1, 135 (1963).
3. V. F. Baranov, Electron-Beam Dosimetry [in Russian], Atomizdat, Moscow (1974).
4. G. B. Radzievskii and D. P. Osanov, in: Problems of Dosimetry and Radiation Protection [in Russian], No. 3, Atomizdat, Moscow (1964), p. 125.
5. L. V. Chepel', At. Énerg., 30, No. 1, 70 (1971).
6. V. V. Krayushkin and V. P. Suminova, in: Papers of Second All-Union Conference on the Use of Charged-Particle Accelerations in the National Economy [in Russian], Vol. 1, Izd. NIIÉFA, Leningrad (1976), p. 347.
7. E. Proksch, Kerntechnik, 18, No. 1, 20 (1976).
8. V. V. Krayushkin, At. Énerg., 47, No. 1, 46 (1979).

INFLUENCE OF REACTOR RADIATION AND γ RADIATION UPON THE OPTICAL PROPERTIES OF QUARTZ GLASS

I. Kh. Abdukadyrova

UDC 666.192:535.372.343

The dose dependence of the intensity of the three well-known [1, 2] photoluminescence peaks λ = 290, 470 (λ_{exc} = 252-258 nm), and 520 (λ_{exc} = 320 nm) was earlier studied in various quartz glass varieties to determine their possible utilization as detectors of reactor radiation. The latter two bands have the greatest region of monotonic growth of the light yield as a function of the thermal neutron flux and are almost independent of uncontrollable impurities. It was established that the results are well reproducible (5%) and that no aftereffect exists even when the samples are exposed for several months; the influence of the temperature in a short heating (200°C), of the dose rate of neutron radiation, and of ^{60}Co gamma radiation (up to 10^8 Gr) have been studied. In order to precisely determine the limits of measurement and the details of the production of radiation defects, the growth of the luminescence intensity I during a subsequent increase in the flux F to $6\cdot10^9$ neutrons/cm^2 was studied. It was found that the function I(F) has a maximum with a characteristic position. The maximum of the ultraviolet band occurs earlier (at about $6\cdot10^{18}$ neutrons/cm^2), that of the other bands at about $(2-3)\cdot10^{19}$ neutrons/cm^2. In order to establish the reason for these changes, we analyzed the kinetics of the absorption spectra. The optical density of an irradiated sample increases in the ultraviolet (260-300 nm) up to fluxes of $6\cdot10^{19}$ neutrons/cm^2. In the visible range, there appears a band at λ = 620 nm for E $\approx$ 10^{18} neutrons/cm^2, and a band near 500 nm at 10^{19} neutrons/cm^2 (Fig. 1). The similarity between the changes in the intensity of the photoluminescence spectra and the optical absorption leads to the conclusion that the corresponding spectra can overlap. According to estimates made for 520 and 470 nm, the reabsorption of the emission at visible color centers is insignificant (10-12%). Therefore, it was concluded that the reduced light yield of the long-wave photoluminescence bands at F > $3\cdot10^{19}$ neutrons/cm^2 is often caused by overlapping of the spectra. Most likely there exist other reasons such as radiation annealing and superposition of the nearest absorption band upon λ_{exc}. It has been established for the ultraviolet peak of the luminescence that I_{290} maintains its value at low doses and increases substantially thereafter; the maximum of the I(F) curve was shifted toward higher doses (toward F = $3\cdot10^{19}$ neutrons/cm^2). Reabsorption must be considered the basic effect which accounts for the earlier noted reduction of the light yield at doses of up to $3\cdot10^{19}$ neutrons/cm^2. The photoluminescence peaks under consideration can be employed in dosimetry up to doses of F = $3\cdot10^{19}$ neutrons/cm^2 (a correction for reabsorption must be introduced for the case λ = 290 nm).

It was noted in [2-4] that glasslike silica can exhibit photoluminescence at 615 or 668 nm (upon excitation in the ultraviolet part of the spectrum and in the 620 nm band). Therefore, the generation of a fourth photoluminescence peak by radiation was studied in three quartz glass varieties. It was observed that the long-wave photoexcitation of previously irradiated glass of a fourth type (F = $5\cdot10^{17}$-10^{18} neutrons/cm^2) produces a luminescence band with λ = 651-658 nm; this is in good agreement with the results of [3]. An increase in the flux up to $2\cdot10^{19}$ neutrons/cm^2 implies a substantial increase in the light yield (Fig. 2, curve 1). At high flux (up to $6\cdot10^{19}$ neutrons/cm^2) saturation was observed. The optical density of the color centers with λ = 620 nm changes almost linearly at F = $0.5\cdot10^{18}$-$2\cdot10^{19}$ neutrons/cm^2 (see Fig. 2, curve 2). It is a characteristic feature that the saturation region of this center corresponds to that noted for the photoluminescence: $(2-6)\cdot10^{19}$ neutrons/cm^2. A comparison of curves 1 and 2 (see Fig. 2) reveals that a correlation between the change of the photoluminescence intensity at 658 nm and the absorption band at 620 nm is observed in each stage of irradiation of quartz glass. Similar peaks were found in the spectrum of neutron-irradiated glass of the first type. These results confirm the assumption [3] that the two bands are caused by the same defect which is of the type of a nonbridging Si—O oxygen atom. The form of the I_{620}(F) curve was thereafter more precisely

Translated from Atomnaya Énergiya, Vol. 53, No. 1, pp. 42-44, July, 1982. Original article submitted July 7, 1981.

 0038-531X/82/5301-0498$07.50

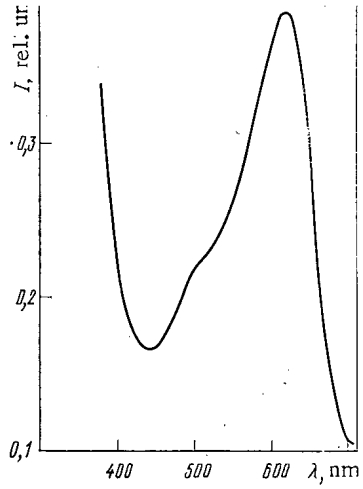

Fig. 1. Absorption spectrum of quartz glass in the range 400-700 nm at a neutron flux of $2 \cdot 10^{19}$ neutrons/cm^2.

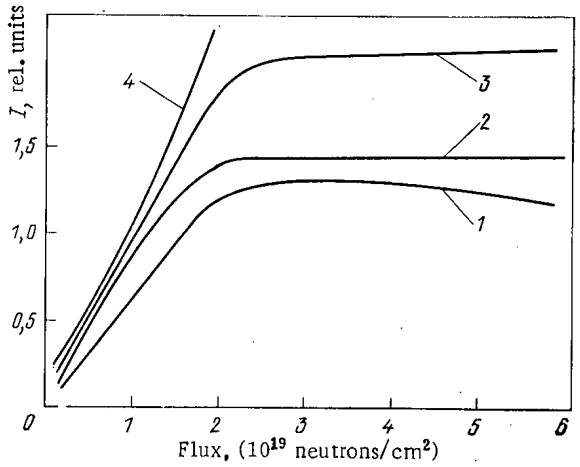

Fig. 2

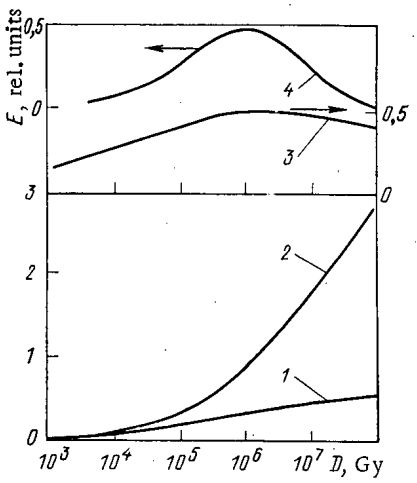

Fig. 3

Fig. 2. Dependence of the intensity of optical spectra of quartz glass of the fourth type upon the flux: 1) photoluminescence at λ = 658 nm; 2) absorption at λ = 630 nm; 3) EPR signal with g_{eff} = 2.0013; 4) absorption at λ = 215 nm.

Fig. 3. Growth of the optical density of glass of the first type exposed to gamma radiation (curves 1 and 3) and to reactor radiation (curves 2 and 4) in the maximum of the 215 nm (curves 1 and 2) and 540 nm (curves 3 and 4) bands.

determined by calculation with the Smakula formula [5] with which the approximate concentration of the color centers with λ = 620 nm was calculated. The values obtained show that the concentration N of the centers does increase up to $2.8 \cdot 10^{18}$ cm^{-3} at $2 \cdot 10^{19}$ neutrons/cm^2 and that it changes only slightly thereafter (to about N = $3.0 \cdot 10^{18}$ cm^{-3}).

A structure-sensitive technique, viz., electron-paramagnetic resonance (EPR), was used for the subsequent investigation of the accumulation and destruction of defects in the samples under consideration. In all irradiated plates, the usual axially symmetric signal of the E' center with g_{eff} = 2.0013 was observed at room temperature. The intensity of these signals (see Fig. 2, curve 3) is proportional to the dose of the reactor radiation in the range $5 \cdot 10^{17}$-$2 \cdot 10^{19}$ neutrons/cm^2. The $I_{EPR}(F)$, $I_{658}(F)$, and $I_{620}(F)$ curves (see Fig. 2, curves 3, 1, and 2, respectively) obey a unique law. The density of the optical absorption with λ = 215 nm increases linearly up to F = $2 \cdot 10^{19}$ neutrons/cm^2 in the plates examined (see

TABLE 1. Stability of the Readings of the (E_1-E_5) System Based on Quartz Glass of Type 1 During Variations of the External Conditions (a_1-a_5)

Parameter	Number of the measurement			
	1	2	3	4
a_1, h	0,5	2	15	1000
E_1	0,30	0,33	0,31	0,30
a_2, h	0,25	0,30	0,45	0,70
E_2	0,32	0,32	0,29	0,26
a_3, °C	30	90	150	180
E_3	0,31	0,33	0,30	0,29
a_4, °C	40	70	200	220
E_4	0,30	0,32	0,32	0,28
a_5, R/sec*	20	80	1000	4000
E_5	0,32	0,32	0,30	0,27

*1 R = $2.58 \cdot 10^{-4}$ C/kg.

Fig. 2, curve 4). Our results, along with the published data on the suggested nature of the defects produced, lead to the conclusion that the defect formation in quartz glass of increased purity is dominated by a well-known mechanism: rupture of Si—O bonds with simultaneous formation of two defects of the Si—O or Si type, the defects being traps of charge carriers. Indeed, the reactor irradiation of glass of the fourth type produces a large number of centers with g_{eff} = 2.0013 and λ = 215 nm while at the same time a significant concentration of centers with λ = 620 and 658 nm is observed. This means that the corresponding structural defects are stable and interrelated and that the kinetics of their accumulation are similar.

In our opinion, there is all reason to use the range of proportionate intensity increase of the signals considered for the dosimetry of reactor radiation in the range of $5 \cdot 10^{17}$-$2 \cdot 10^{19}$ neutrons/cm^2.

The glasses were irradiated with ^{60}Co photons in order to assess the contribution of the gamma component of the composite radiation during the development of, say, ultraviolet absorption centers. The result is that the absorption at 215 nm is extremely weak. This attests to selective recording of neutron radiation by the glasses of types 3 and 4. Similar experiments were made with glass of type 1. The corresponding induced optical absorption at λ = 215 nm is represented (Fig. 3) by curves 1 and 2 which indicate the accumulation of defects upon gamma and gamma-neutron irradiation, respectively. The functions $E_\gamma(D)$ and $E_{\gamma,n}(D)$ differ considerably in the very wide dose range from 10^3 to 10^8 Gy. The curve $E_\gamma(D)$ (Fig. 3, curve 1) is characterized by a proportionate increase up to $3 \cdot 10^6$ Gy and a slight reduction of the slope thereafter. Such kinetics are extremely interesting for the determination of the absorbed gamma radiation dose in practice. Therefore the operational characteristics of the glass were investigated. It follows from Table 1 that the glass of type 1 is characterized by high reproducibility of the readings (a_1) in the four measurement cycles listed, by stability during variations of the irradiation temperature and the storage temperature (a_3, a_4), and by a slight decrease in density at increasing times of optical bleaching (a_2) and at increasing dose rates (a_5). The possibility of "healing" the induced band by heating up to T = 500°C and the subsequent use of the sample was assessed. In the case of γ,n-irradiation, the coloring (Fig. 3, curve 2) is first characterized by a small color-center generation rate which thereafter increases with increasing dose. The curve depicting the accumulation of color centers under the influence of reactor radiation rises higher than that obtained with γ radiation and does not reach saturation. This feature can be employed to determine the contribution of neutron radiation when unknown curves are evaluated.

Irradiation in cadmium sheaths did not strongly modify the concentration of the centers. In the visible part of the spectrum, an absorption band with λ = 540 nm is induced in the gamma-irradiated samples (Fig. 3, curve 3). It follows from Fig. 3 that the degree to which the sample is darkened increases proportionately to the dose up to $7 \cdot 10^5$ Gy (as we had observed previously), and thereafter saturation of the visible coloring is observed at 10^6-10^8 Gy. The defect-formation process seems to become stable because the unknown centers

are of the impurity type. A similar curve was obtained for samples irradiated in a reactor. In the first stage, the form of the kinetics and the rate of darkening resemble the case of gamma irradiation (Fig. 3, curve 4), and the curve reaches a maximum. This can be caused by the γ radiation field of the core. Thereafter, the sample is bleached. This effect seems to result from an intense migration of metallic impurities at high doses of reactor radiation (10^7-10^8 Gy), i.e., from radiation annealing. This feature of the function $E_{540}(D)$, i.e., the fact that the centers are related to impurities, makes the earlier suggested colorimetric gamma dosimeter from glass of type 1 (λ = 540 nm) unsuitable for the determination of the gamma component in the case of γ,n-irradiation. In the latter case, one should better employ the color centers of this glass with the maximum at 215 nm in the interval of 10^3-10^8 Gy of composite radiation or of ^{60}Co gamma radiation, with the color centers resulting from intrinsic structural defects.

LITERATURE CITED

1. A. V. Amosov et al., in: Abstracts of the 3rd All-Union Scientific-Technical Conference on Quartz Glass "New Inorganic Materials and Coatings on the Basis of Glass and Refractory Compounds" [in Russian], Moscow (1973), p. 15.
2. W. Primak and R. Uphaus, Chem. Phys., 29, No. 4, 972 (1958).
3. L. Skuja and A. Silin, Phys. Status Solidi (1), 56 (1979).
4. P. Keiser, Opt. Soc. Am., 64, No. 4, 475 (1974).
5. F. Seitz, Modern Theory of Solids [Russian translation], Gostekhteorizdat, Moscow (1949), p. 693.

TAKING INTO ACCOUNT THE VARIABLE BACKGROUND OF DELAYED NEUTRONS IN REACTIVITY MEASUREMENTS WITH THE AID OF PULSED NEUTRON TECHNIQUES

A. G. Shokod'ko and V. M. Sluchevskaya

UDC 621.039.51

It is generally accepted that when the reactivity is measured with integral pulse techniques, the timewise integral count F_d of the neutron detector in the delayed neutron flux resulting from the irradiation of the reactor by a pulsed neutron source must be determined [1, 2]. These measurements are usually made in reactors with a rather small lifetime of the instantaneous (flash) neutrons so that the inequalities

$$\alpha \gg R \gg \lambda_i \qquad (1)$$

are satisfied to the greatest possible extent, where α denotes the basic (smallest) attenuation coefficient of the instantaneous neutrons; λ_i, decay constant of the precursors of the delayed neutrons of the i-th group; and R, frequency of switching on the time analyzer recording the response of the detector in the reactor to detector irradiation from the source (the frequency of flashes of the pulsed source can be any integer times smaller than R).

Thus, with conditions (1) the time analyzer records the decay of the instantaneous component of the neutron flux on an almost constant background resulting from the delayed component; the F_d value is obtained from the following elementary relationship (in the zeroth approximation):

$$F_d^{(0)} = n_{1,2} \frac{1/R}{t_2 - t_1}, \qquad (2)$$

where $n_{1,2}$ denotes the total number of counts in the time analyzer channels comprising the selected time interval from t_1 to t_2 at the end of the time analyzer cycle when the instantaneous component has practically ceased.

Translated from Atomnaya Énergiya, Vol. 53, No. 1, pp. 44-45, July, 1982. Original article submitted July 16, 1981.

0038-531X/82/5301-0501$07.50

TABLE 1. Correction Factor K_{max} and Degree to which It is Approximated by the Factor K_{max}^{eff}

R, Hz	K_{max}	$\frac{K_{max}^{eff}-K_{max}}{K_{max}}$, %	R, Hz	K_{max}	$\frac{K_{max}^{eff}-K_{max}}{K_{max}}$, %
	$\rho/\beta_{eff}=1$			$\rho/\beta_{eff}=10$	
2	1,05118	0,500	2	1,09532	0,955
4	1,02648	0,119	4	1,04879	0,224
6	1,01785	0,050	6	1,03275	0,093
10	1,01080	0,016	10	1,01975	0,030
14	1,00774	0,007	14	1,01413	0,013
20	1,00544	0,002	20	1,00991	0,005
	$\rho/\beta_{eff}=5$			$\rho/\beta_{eff}=-20$	
2	1,08698	0,869	2	1,09980	1,035
4	1,04458	0,207	4	1,05097	0,255
6	1,02994	0,087	6	1,03419	0,112
10	1,01807	0,029	10	1,02061	0,040
14	1,01293	0,013	14	1,01474	0,020
20	1,00907	0,005	20	1,01033	0,010

Naturally, Eq. (2) is an approximation. An F_d determination of greater accuracy has been provided in [3-6] where the delayed component of the detector count was represented as a sum of exponentials the number of which is equal to the number of groups of delayed neutrons:

$$N(t)=N_0\sum_j A_j\exp(-\alpha_j t);\quad j=1,\ \ldots,\ 6, \tag{3}$$

where α_j denotes the roots of the Nordheim equation which result from the decay constants λ_i:

$$\frac{\rho}{\beta_{eff}}+\sum_i\frac{a_i\alpha}{\lambda_i-\alpha}+\frac{\alpha\Lambda}{\beta_{eff}}=0 \tag{4}$$

at given reactivities ρ/β_{eff} and ratios Λ/β_{eff}; Λ denotes the time of generation of instantaneous neutrons in the reactor; and a_i denotes the relative fraction of delayed neutrons in the i-th group. The amplitudes A_j are given by the equation

$$A_j=\left\{\Lambda/\beta_{eff}+\sum_i\left[a_i\lambda_i/(\lambda_i-\alpha_j^2)\right]\right\}^{-1}. \tag{5}$$

Under these assumptions a correction factor K for $F_d^{(o)}$ was obtained in [2] with the aid of Eq. (2) for the case in which $t_2 - t_1$ is equal to the channel width of the time analyzer:

$$K=\frac{\sum_j A_j/\alpha_j}{\sum_j\{A_j\exp(-\alpha_j t_2)/(R\,[1-\exp(-\alpha_j/R)])\}}. \tag{6}$$

When t_2 increases, the correction factor grows and reaches its maximum K_{max} at the limit $t_2 = 1/R$. This method of obtaining the correction of Eq. (6) is not very advantageous because a Nordheim of 7th order must be solved.

The goal of the present work was to obtain the maximum simplification of the formula for the correction factor and, accordingly, to simplify the calculations at an insignificant loss of accuracy of the correction. This was obtained by using a single group of delayed neutrons with an effective decay constant:

$$\lambda=\sum_i a_i\lambda_i. \tag{7}$$

This form of λ can be generally justified for the given conditions by considering only the form of the neutron yield curve of the sample in experiments in which the parameters a_i and λ_i are being determined [7]. Indeed, in flash irradiation of a sample, the curve has the form $n(t) = c\Sigma a_i\lambda_i\exp(-\lambda_i t)$, where c = const. For a time analyzer, the curve is converted into the curve $n'(t) = c\,\Sigma\,a_i\lambda_i\,[1-\exp(-\lambda_i/R)]^{-1}\exp(-\lambda_i t)\approx cR\,(1-t\Sigma a_i\lambda_i)$, under the conditions of Eq. (1), and from this curve results the efficient parameter λ in Eq. (7).

For a single group of delayed neutrons, Eq. (4) becomes a second-order equation or even a first-order equation at $\alpha\Lambda/\beta_{eff} \approx 0$; $\alpha \equiv \alpha_d$ can be easily calculated by hand for known λ and ρ/β_{eff}. After that, the unknown correction factor can be easily determined.

In order to verify the degree of accuracy of this approach, K_{max} was calculated with a "MIR" computer for six groups of delayed neutrons and K_{max}^{eff} was calculated for a single group with an effective λ and with Eq. (7). The calculations were made for several ρ/β_{eff} and R values (see Table 1). The delayed-neutron data were taken from [7] for ^{235}U ($\lambda = 0.435\ sec^{-1}$). It follows from Table 1 that for all reactivity values and for the majority of frequencies, K_{max}^{eff} differs from the true K_{max} by at most 0.25%. This means that the approximation with a single effective group of delayed neutrons renders good results in this case, and F_d can be found in this approximation either with the formula

$$F_d = n_{1,2}\frac{1-\exp(-\alpha_d/R)}{\exp(-\alpha_d t_1)-\exp(-\alpha_d t_2)}, \tag{8}$$

or with the formula

$$F_d = F_d^{(0)}\eta, \tag{9}$$

in which the correction factor η is defined by the formula

$$\eta \equiv \frac{1-\exp(-\alpha_d/R)}{\exp(-\alpha_d t_1)-\exp(-\alpha_d t_2)}\frac{t_2-t_1}{1/R}. \tag{10}$$

When the factor K of Eq. (6) is taken for a single exponential, the factor is a particular case of the factor η.

In an experiment, α_d should be obtained by iteration. In zeroth iteration, the reactivity is determined with F_d^0 (see Eq. (2)) in a pulse technique; after that, α_d is determined, then η or F_d in the first iteration, etc. The iteration process converges very rapidly. One or two iterations suffice to obtain accuracy. Interestingly enough, the approximation with a single effective group of delayed neutrons with $\lambda = 1/\sum_i (a_i/\lambda_i)$ [6] in place of λ according to Eq. (7) reduces λ by a factor of about 5.5 and results in an almost 100% deviation of $(K_{max}^{eff} - 1)$ from $(K_{max} - 1)$.

Therefore, our work suggests an extremely simple and, at the same time, adequately accurate approximation which takes into account the variable background of delayed neutrons in pulsed neutron experiments.

LITERATURE CITED

1. E. Garelis, in: Proc. IAEA Symposium on Pulsed Neutron Research, Karlsruhe, May 10-14, 1965, Vol. 2, p. 3.
2. É. A. Stumbur, I. P. Matveenko, and A. G. Shokod'ko, in: Theoretical and Experimental Problems of Nonstationary Neutron Transfer [in Russian], Atomizdat, Moscow (1972), p. 245.
3. A. Fraude, Nukleonik, 4, No. 2, 84 (1962).
4. C. Sastre, Nucl. Sci. Eng., 20, No. 3, 359 (1964).
5. Y. Kaneko and K. Sumita, J. Nucl. Sci. Technol., 4, No. 8, 400 (1967).
6. I. F. Zhezherun, in: Theoretical and Experimental Problems of Nonstationary Neutron Transfer [in Russian], Atomizdat, Moscow (1972), p. 244.
7. G. R. Keepin, Physics of Nuclear Kinetics, Addison-Wesley (1965).

MEASUREMENT OF TRANSIENT VARIATIONS OF THERMOELECTROMOTIVE FORCE

E. P. Volkov, V. I. Nalivaev,
S. V. Priimak, I. I. Fedik,
O. P. Tselykovskii, and V. Ya. Yakubov

UDC 536.532

Certain methodological difficulties arise in the investigation of the effect of nuclear radiations on the thermoelectromotive force (transient variations) of thermocouples in pulsed reactors. The distinctive features of these reactors impose specific demands on the technique of measuring transient variations.

The rate at which energy is released per unit volume q_V in the constructional materials and reference metals needs to be known for the thermal analysis of the irradiation device and to provide a basis for the measurement technique. The quasiadiabatic method of measurement [1] is simple, reliable, and sufficiently accurate. As shown in [1], the specific energy released q_V can be calculated through the formula:

$$q_V = c\rho \frac{dt}{d\tau} \text{ W/m}^3,$$

where c is the specific heat (kJ/kg·°K); ρ, density (kg/m³); and dt/dτ, rate of variation of temperature on the linear part of the heating curve (°K/sec). This method was used to measure q_V for aluminum, graphite, stainless steel, silver, and tantalum.

The construction of the calorimetric sensor is shown in Fig. 1. A thermocouple of diameter 0.7 mm is located in the calorimetric body, made from the material under investigation. Contact between the thermocouple and the calorimetric body is provided by low temperature solder. The calorimetric body is centered in the casing by means of a needle support and an annular disk with needle-shaped lugs. The support and the disk are made from asbestos. The sensor casing was made from graphite, to minimize the absorption of reactor radiation. The thermoelectromotive force was amplified by a normalizing converter and displayed on a cathode ray oscilloscope. The relative error of the measuring circuit was not more than ±1%.

The irradiation device together with the calorimetric sensors was installed in the reactor. The calorimetric body was allowed to come to ambient temperature, after which the reactor was switched on and the temperature of the calorimetric body recorded. The reactor power was arranged so that the temperature of the calorimetric body remained low (not more than 400°K), when heat loss due to radiation is negligible.

The results of the measurements of q_V in aluminum, grpahite, steel, silver, and tantalum are presented in Fig. 2, from which it can be seen that the specific energy released is proportional to reactor power. We note that nuclear radiation has no effect on the thermoelectromotive force of thermocouples mounted in the calorimetric body and on the measurements of q_V, since this effect is independent of temperature in the working temperature range of calorimetric sensors [2].

Our results and also those of [3] indicate that the specific energy released by substances of atomic number Z close to those investigated is sufficiently well described by a linear dependence of q_V on Z. This enabled us to find q_V for copper, using experimental values.

The results on the specific energy released in the reference metals enabled us to solve the questions of principle involved in the measurement of the transient variations ΔE, namely: the choice of the initial temperature T_{init} of the reference metal, the calculation of the time required to melt it, and the choice of the recording instrument.

Translated from Atomnaya Énergiya, Vol. 53, No. 1, pp. 45-47, July, 1982. Original article submitted July 28, 1981.

 0038-531X/82/5301-0504$07.50

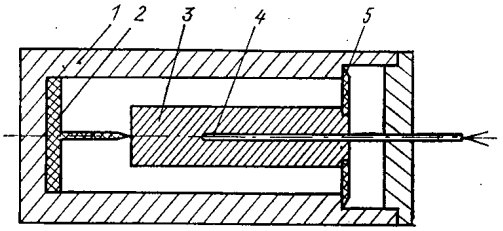

Fig. 1

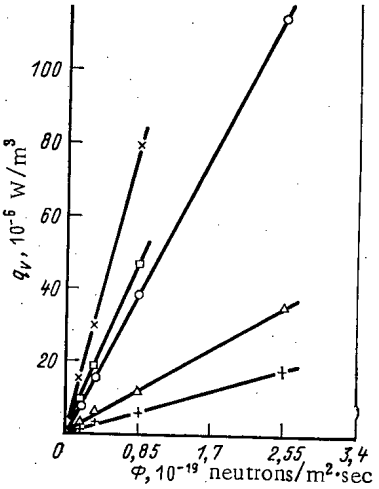

Fig. 2

Fig. 1. Calorimetric sensor: 1) casing; 2) needle support; 3) calorimetric body; 4) thermocouple; 5) annular disc.

Fig. 2. Plots of specific energy released versus flux density of thermal neutrons. +) C; Δ) Al; ○ steel Kh18N10T; □) Ag; ×) Ta.

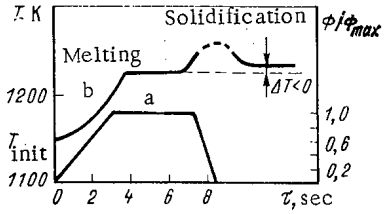

Fig. 3. Variation with time after reactor switched on for (a) power for thermal neutron flux density $\Phi_{max} \approx 3.5 \cdot 10^{19}$ neutrons/m^2·sec; and (b) temperature of silver.

TABLE 1. Time of Melting and Initial Temperature of Silver and Copper for Different Thermal Neutron Flux Densities

Reference metal	$\Phi = 1{,}75 \cdot 10^{19}$ neutrons/m^2·sec		$\Phi = 3{,}5 \cdot 10^{19}$ neutrons/m^2·sec	
	τ_{melt}, sec	T_{init}, °K	τ_{melt}, sec	T_{init}, °K
Ag	14,8	1190	7,4	1140
Cu	24,0	1320	12,0	1300

The initial temperature of the reference metal is chosen below the melting point by an amount such that the reference metal is heated up to the melting point T_{melt} in the time taken by the reactor to reach steady power:

$$T_{init} = T_{melt} - \frac{q_V^{unit} \int_0^{\tau_0} N(\tau)\, d\tau - Q}{c\rho},$$

where q_V^{unit} is the specific energy released per unit reactor power; $N(\tau)$, reactor power; τ_0, time taken by the reactor to reach steady power conditions; and Q, heat losses due to radiation and conduction per unit volume of reference metal.

The construction of the irradiation device provides the necessary screening of the sample of reference metal. This enables Q to be neglected. The time required to melt the reference metal is found from the relationship

$$\tau_{melt} = \gamma_{melt}\rho/q_V,$$

where γ_{melt} is the specific heat of fusion.

The initial temperature of the reference metals and the time required to melt them are given in Table 1. It can be seen from these results that thermoelectromotive force can be recorded using a pen recorder with a speed of response of ∿0.5 sec.

Transient variations were measured in VR 5/20 thermocouples of diameter 1.6 mm, the working joints of which were obtained by direct welding of the thermoelectrodes to the molybdenum sheath. The irradiation device held a container with samples of the reference metals — silver and copper — together with thermocouples, and a heater with which to set the temperature of the reference metals T_{init} prior to switching on the reactor. The measuring setup and the radiation conditions of the tests are described by Volkov et al. in the following article of the present issue.

A typical temperature curve in the measurement of ΔE is shown in Fig. 3, where ΔE is defined as the difference $\Delta E = E_{melt} - E_{solidification}$. It was established that the values of the transient variations of the thermoelectromotive force of VR 5/20 thermocouples of the tested construction at the melting points of silver and copper are negative and do not exceed 0.6% of the measured value.

Summarizing, the specific energy released in the reference and constructional materials of the irradiation device were measured in the course of the tests. This enabled methodological questions relating to the measurement of the transient variations of the thermoelectromotive force of thermocouples under pulsed reactor conditions to be resolved.

LITERATURE CITED

1. N. S. Shimanskaya, The Calorimetry of Ionizing Radiations [in Russian], Atomizdat, Moscow (1973).
2. V. I. Vlasov et al., At. Énerg., 43, No. 4, 293 (1977).
3. V. M. Kolyada and V. S. Karasev, The Calorimetry of Nuclear Reactor Radiations [in Russian], Atomizdat, Moscow (1974).

THERMOELECTROMOTIVE FORCE OF VR 5/20 THERMOCOUPLES OF VARIOUS CONSTRUCTIONS

E. P. Volkov, V. I. Nalivaev,
S. V. Priimak, I. I. Fedik,
O. P. Tselykovskii, and V. Ya. Yakubov

UDC 536.532

The effect of nuclear radiations on the thermoelectromotive force (the transient variations ΔE) of thermocouples has been investigated in many papers [1]. The results cited in these papers are often contradictory, both in absolute magnitude and in sign, which renders their practical exploitation difficult. It is no easy matter to establish the reasons for these discrepancies, since the published papers do not always consider the contructional features of the investigated thermocouples and the tests are carried out in reactors with different radiation spectra.

In the work reported here we investigated the transient variations of the thermoelectromotive force of VR 5/20 thermocouples of various constructions under pulsed reactor conditions. The VR 5/20 type thermocouple is one which is widely used to measure temperatures up to 2000°K in vacuo and in inert and carbon-containing media.

Translated from Atomnaya Énergiya, Vol. 53, No. 1, pp. 47-48, July, 1982. Original article submitted July 28, 1981.

 0038-531X/82/5301-0506$07.50

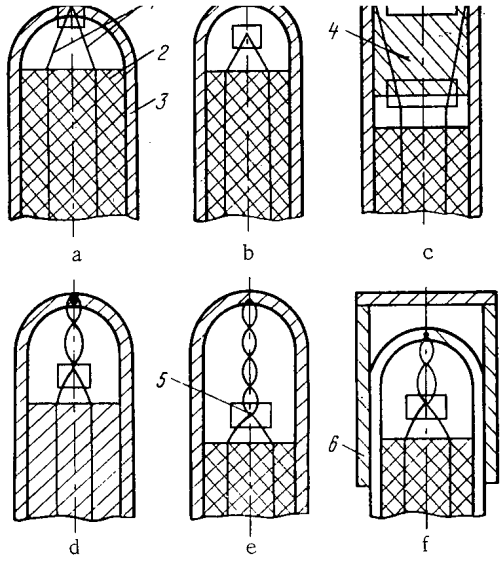

Fig. 1. Various forms of working junction. (a) Thermoelectrodes welded to sheath; (b) isolated junction; (c) cork with shaped slots; (d), (e) junction with two- and three-loop structure, respectively; (f) thermocouple mounted in ZrC bush.

The various thermocouple constructions are shown in Fig. 1, where 1 denotes the thermoelectrodes, of diameter 0.2 or 0.35 mm; 2 is an insulator of BeO; 3 is a protective sheath of Mo, of diameter 1.6 or 2.0 mm. The working junction is of various forms: welded to the sheath, isolated from the sheath, or located in a cork 4 with shaped slots [2]. The latter variant improves the reliability of the thermocouple as it avoids having to weld the thermoelectrodes to the sheath, and contact of the thermoelectrodes with the sheath is over the surface of the sheath, the thermoelectrodes, and the cork; the working junction is displaced, however, into the sheath. This type of junction was thus modeled in the tests by the constructions shown in Fig. 1d, e. The thermal resistance between the electrical contact 5 of the thermoelectrodes and the protective sheath is clearly increased in this model on account of the radiative heating. We also tested thermocouples with a protective bush 6 of ZrC, a construction often used in temperature measurements in pulsed reactors.

The tests were carried out on 30 thermocouples (3 of each type at the melting points of each of the reference metals — silver and copper). The irradiation device incorporated a graphite container with a central hole and a number of nonthrough holes around the periphery containing chemically pure (reference) metals and the thermocouples. An electrical heater was mounted in the central hole. Two coaxial screens of molybdenum foil were mounted in the gap between the container and the casing of the irradiation device, which was cooled by the flowing reactor water.

The tests were carried out at a reactor power giving the following conditions: thermal neutron flux density $\sim 3.5 \cdot 10^{19}$ neutrons/$m^2 \cdot$sec; fast neutron flux density $\sim 6 \cdot 10^{17}$ neutrons/$m^2 \cdot$sec; γ radiation dose rate $\sim 2 \cdot 10^6$ rad/sec (1 rad = $2.58 \cdot 10^{-4}$ Cal/kg); duration of irradiation pulse — not more than 10 sec.

The thermoelectromotive force was measured by the precision setup described in [3]. Instrumental error in the measurement of temperature in the range 1230-1350°K by the VR 5/20 thermocouple did not exceed 9 μV. Transient variations were defined as $\Delta E = E_R - E_o$, where E_R and E_o are the mean values of the thermoelectromotive force at nominal and zero reactor power respectively. The mean-square error of the measurements of ΔE amounted to ±0.6°K. Each type of thermocouple gave a linear dependence of ΔE on reactor power.

An analysis of the results of the tests showed that the transient variations of the thermoelectromotive force of thermocouples with a working junction of type (a), characterized

by minimum thermal resistance between the electrical contact of the thermoelectrodes and the protective sheath, are negative at the melting points of silver and copper and do not exceed −5.6°K, which agrees with the conclusions of [4] as regards the sign of the transient variations. The difference in absolute value must apparently be ascribed to the constructional differences of the thermocouples and the features of the irradiation conditions.

The transient variations of thermocouples of types (b) were not more than 5°K, which can be explained by the fact that the thermal resistance between the junction and the reference metal results in an increase in the component of ΔE due to radiative heating [5].

The maximum values of ΔE of thermocouples types (d) and (e), which model type (c), are −2.5 and −5.1°K respectively. The electrical contact of the thermoelectrodes of these thermocouples is removed from the place of welding to the sheath but is in the immediate vicinity of the insulator. The thermal resistance between the electrical contact and the protective sheath is thus small and the variations of ΔE due to radiative heating are consequently insignificant.

Variations of the thermoelectromotive force of thermocouples type (f) did not exceed +10°K at the melting point of silver and copper. They are cuased by the effect of the contact thermal resistance between the protective sheath and the protective ZrC bush, which increases the component due to radiative heating.

In this manner, if the thermal resistance between the electrical contact of the thermoelectrodes and the protective sheath is negligibly small, then the transient variations of the thermoelectromotive force of VR 5/20 thermocouples are negative: from −2.5 to −5.6°K. VR 5/20 thermocouples with an isolated junction or with a protective ZrC bush have transient variations which are positive (5-10°K). The sign and the absolute value of the transient variations of the thermoelectromotive force depend not only on the irradiation conditions but also on the construction of the thermocouple and on how it is mounted in the object.

LITERATURE CITED

1. B. V. Lysikov and V. K. Prozorov, in: Reactor Thermometry [in Russian], Atomizdat, Moscow (1980), p. 79.
2. S. A. Anisimov, V. A. Neverov, and Yu. G. Spiridonov, Inventor's Certificate No. 537260, Byull. Izobret., No. 44 (1976).
3. V. I. Vlasov, et al., At. Énerg., 43, No. 4, 293 (1977).
4. N. V. Markina, Features of Temperature Measurement in Nuclear Installations with High Radiation Flux Densities [in Russian], Author's Abstract, NIIAR, Dmitrovgrad (1974).
5. S. V. Priimak and I. I. Fedik, At. Énerg., 51, No. 3, 158 (1981).

DEPENDENCE OF SPATIAL DISTRIBUTION OF NEUTRONS UNDER MODERATION IN POLYETHYLENE OF THICKNESS UP TO 5 cm ON THEIR INITIAL ENERGY

S. P. Makarov

UDC 539.125.5

In order to estimate how the capture of neutrons under moderation (resonance neutrons) and thermal neutrons influences the energy dependence of the neutron counting efficiency, we require to know how the space-energy distribution within a polyethylene moderator depends on the initial energy of the neutrons incident upon the moderator.

The neutron current density to the detector is reduced as a result of the capture by the absorber of neutrons under moderation and thermal neutrons, i.e., the neutron counting efficiency is reduced. For each value of the initial neutron energy, the proportion of neutrons captured depends, firstly, on the type of absorber (thermal or resonance neutrons), and, secondly, on where the plate-abosrber is located within the interior of the moderator. If the difference between the proportions of neutrons captured at any two values of their initial energy is nonzero, then the introduction of the absorber into the interior of the moderator changes the form of the energy dependence of the neutron counting efficiency. This is possible if the space–energy distribution of the thermal neutrons and neutrons under moderation depends on the initial neutron energy.

The accuracy of computation depends greatly on how well the spatial distribution of points of formation (sources) of thermal neutrons is knwon. The results of the computation cited in Table 1 were obtained allowing for the relative contribution made by epithermal neutrons to the count rate (a 1/v detector).

The fact that Δ_T is nonzero is due mainly to the dependence of the spatial distribution of thermal neutrons and neutrons under moderation on their initial energy. The largest value of $\Delta_T = 0.15$ was obtained at $x \approx 1.5$ cm, while the largest (by more than a factor of one and a half) variation of the relative counting efficiency for fast (E_{o1}) and intermediate (E_{o2}) neutrons, important for practical purposes, is attained with a thermal-neutron absorber and is located a few millimeters from the detector.

Resonance absorbers, unlike thermal absorbers, do not screen thermal neutrons and only partially reduce their source density. They are thus less effective than thermal absorbers.

Allowing for the capture of thermal neutrons by an indium plate of thickness 0.5 mm and for the relative contribution of epithermal neutrons to the count rate, we find that $\Delta_{In}(1, 0) = 0.09$; when $t = 2$ cm, $E_{o1} = 5$ MeV, $E_{o2} = 0.024$ MeV. For a silver plate of thickness 0.9 mm under the same conditions, $\Delta_{Ag}(1, 0) = 0.04$.

Experimental determination of the values of Δ confirmed the results of the calculation.

Table 2 presents the results of measurements taken under conditions close to optimum, when the values of Δ, the difference between the proportions of neutrons captured, are at their greatest. In the energy range of SbBe and PoBe neutron sources, the optimum thickness of a polyethylene moderator is $\sim$2 cm (at a diameter of 7 cm); the optimum (experimental) value of x is $\sim$0.5 cm and is the same for any absorber (cadmium, indium, silver). It does not depend on the thickness of the moderator (the greatest neutron count rate for the SbBe source is observed when $t = 3.5$ cm). The thicknesses of the plate-absorbers are also the optimum (with respect to Δ). The measurements were repeated many times. The error in the cited values of $\eta_{abs}(x, E_o)/\eta(E_o)$ is not more than unity in the second decimal place.

The values of η' and Δ' cited in Table 2 (the contribution of recoil protons to the count rate is subtracted) refers to moderated and themal neutrons, the registration of which is affected by resonance absorbers. Resonance absorbers have hardly any effect on fast neutrons.

Translated from Atomnaya Énergiya, Vol. 53, No. 1, pp. 48-49, July, 1982. Original article submitted August 3, 1981; revision submitted December 30, 1981.

0038-531X/82/5301-0509$07.50

TABLE 1. Relative Reduction of Neutron Count Rate as Function of x and Initial Neutron Energy E_0, where x is Distance between Detector and Thermal-Neutron Plate-Absorber in a Polyethylene Moderator of Thickness 3.5 cm

x, cm	$\frac{\eta_T(x, E_{01})}{\eta(E_{01})}$	$\frac{\eta_T(x, E_{02})}{\eta(E_{02})}$	$\Delta_T(x)$	x, cm	$\frac{\eta_T(x, E_{01})}{\eta(E_{01})}$	$\frac{\eta_T(x, E_{02})}{\eta(E_{02})}$	$\Delta_T(x)$
0,0	0,11	0,08	0,03	2,0	0,71	0,56	0,15
0,5	0,28	0,18	0,10	2,5	0,80	0,69	0,11
1,0	0,43	0,30	0,13	3,0	0,91	0,84	0,07
1,5	0,57	0,42	0,15	3,5	1,00	1,00	0,00

Note. Here $\Delta_T(x)$ is the difference between the proportions of thermal neutrons captured, $E_{01} \gg 1$ MeV; $E_{02} < 0.01$ MeV.

TABLE 2. Ratio of Neutron Count Rates with Absorber and Without It $[\eta_{abs}(x, E_0)/\eta(E)]$

t Absorber thickness (mm)	$\frac{\eta_{abs}(0,5;\ PoBe)}{\eta(PoBe)}$	$\frac{\eta_{abs}(0,5;\ SbBe)}{\eta(SbBe)}$	Δ	$\frac{\eta'_{abs}(0,5;\ PoBe)}{\eta'(PoBe)}$	Δ'
$t_{Cd} = 0,2$	0,80	0,52	0,28	0,60	$0,08 \pm 0,02$
$t_{In} = 0,5$	0,84	0,58	0,26	0,68	$0,10 \pm 0,02$
$t_{Ag} = 0,9$	0,84	0,65	0,19	0,68	$0,03 \pm 0,02$

Experimentally determined values of Δ' are in good agreement with the results of the calculations. The tentative estimate of Δ obtained for a wide energy interval E_0 and thermal absorbers (see Table 1) is greater than Δ'_{Cd} (see Table 2) due to the narrower energy interval E_0 in the latter case.

If resonance absorbers are combined, then, ignoring screening, Δ_Σ can be described by the formula:

$$\Delta_\Sigma \approx (\Delta - \Delta')_{Cd} + \sum_i \Delta'_i,$$

i.e., Δ_Σ can be increased only by combining absorbers having resonances. If, e.g., $x_{In} \gg x_{Cd}$, then a cadmium plate of thickness 0.5 mm completely screens the indium plate. If $(x_{In} - x_{Cd}) < 0.5$ cm, then partial screening is observed.

As shown by the results of calculations and measurements, the most effective absorbers are those for which the energy of the resonances $E_i < 5$ eV. For a uniform distribution of resonance absorbers over the thickness of the polyethylene moderator, the proportion of neutrons captured is increased, which is what one would expect from theoretical considerations. The values of Δ' in this case are, however, less than if the same quantity (in terms of the number of nuclei) of absorber had been used in the form of a plate. It follows from this that a uniform distribution of absorbers in the volume of the moderator results in the loss of the effect connected with the different spatial density distributions of thermal neutrons and neutrons under moderation for different E_0.

The values of Δ' become close to zero when the thickness of the polyethylene absorber $t \geqslant 5$ cm. Accordingly, the above features could not be observed, e.g., when a cadmium absorber was used in the moderators of known neutron sensors under conditions much different from optimum (t > 5 cm).

If a boron absorber is introduced into a moderator of any thickness, the values of Δ_B' are close to zero. In this case, as before, the neutron counting efficiency is reduced to the same extent for any value of E_0.

In this manner, the introduction of resonance absorbers into the interior of the moderator and the determination of the difference between the proportion of neutrons captured Δ from measurements provides a way of detecting the dependence of the spatial distribution of thermal neutrons and neutrons under moderation on their energy. Furthermore, this method enables the physical conditions necessary for the existence of this dependence to be determined together with the optimum conditions for which the value of Δ is greatest.

The method of varying the energy dependence of the neutron counting efficiency by introducing resonance absorbers into comparatively thin hydrogen-containing moderators has found practical application. It was used to develop a portable "wide-range" neutron counter [1, 2] in which the neutron counting efficiency varies within the limits ±14% over a wide energy range. Allowing for the energy dependence of the wide-range Hansen and MacKibben neutron counter used as a monitor, this variation is less than ±11%, i.e., lies almost within the same limits as the known wide-range counter [3].

The author wishes to thank N. I. Laletin for valuable remarks in the course of the calculations and also B. M. Gokhberg and S. N. Serbinov for their assistance with the experimental part of the work.

LITERATURE CITED

1. S. P. Makarov, Metrologiya, No. 5, 63 (1974).
2. S. P. Makarov, Inventor's Certificate No. 468553, Byull. Izobret., No. 9, 215 (1976).
3. V. I. Fominykh, Proc. Metrological Institute of the USSR [in Russian], No. 89 (149), Izd. Standartov, Moscow (1967).

Corrigenda: The author of "Fourth Congress on the Use of New Nuclear Physics Methods in the National Economy" (Vol. 52, No. 4, p. 227) is Yu. S. Zamyatin.

IMPLANTATION OF RADIOACTIVE CESIUM IONS IN SOLID MATERIALS

Yu. V. Bulgakov, V. P. Petukhov,
and L. M. Savel'eva

UDC 516.236

In using the method of radioactive indicators in experiments with solid objects, it is often difficult to introduce the active impurity into the sample on account of its inadequate solubility. In such cases, the method of ionic implantation opens broad possibilities, allowing any impurities to be introduced into any solid substrate. However, the use of standard implanters acting on the principle of the magnetic separation of nuclides for this purpose is complicated by considerations of radiation safety and by the low use coefficient of the working material. The problem is significantly simplified if implantation is restricted to ions of cesium, rubidium, and potassium, which have the smallest ionization potentials. For these ions, there exist simple and highly efficient (~100%) sources, operating on the basis of surface ionization [1]. Thanks to the selectivity of the ionization process, such sources do not require subsequent separation of the ions, which significantly simplifies the whole equipment, and provides radiation safety when working with ions of radioactive nuclides. The above elements have a set of radioactive isotopes (see Table 1 of [2]), and therefore the method is sufficiently universal. Below, an implanter of radioactive ions used in investigations of the durability of materials is described [3, 4], and some data are reported on the behavior of cesium introduced in solid materials.

The basic component of the implanter is an ion source, shown diagrammatically in Fig. 1. Ionization of atoms of the working material occurs at a tungsten strip 1, coated by a layer of porous tungsten (tungsten sponge). The sponge is obtained by sintering tungsten powder moistened by distilled water, at the surface of the tape as a result of heating in vacuo at ~1700°C for 1-2 min. Before exposing the sample, the working material is applied to the surface of the tungsten sponge in the form of an aqueous solution of an appropriate compound (for example, a solution of the salt CsCl). On heating the tape to a sufficiently high temperature, the compound breaks down, and cesium (or another alkali metal) evaporates from the tungsten in the form of positive ions. These are accelerated in an electric field created in the gap between the ion-source screen 2 and the diaphragm 3, under which the activated sample is placed.

Implantation of ions is performed in a vacuum of ~7 mPa. The permissible residual pressure is determined mainly by the electric strength of the accelerating gap. It is possible to use an oil exhaust system without a nitrogen trap, but in this case it is desirable to maintain the temperature of the activated samples at 100-150°C for the removal of the oil film from their surface. The temperature to which the tungsten tape is heated on irradiation is chosen experimentally, taking the condition of maximum use of the working material into account. At low temperature, metallic cesium accumulates at the tungsten surface, reducing its working yield, and consequently the probability of the evaporation of cesium in ionic form is sharply reduced; at high temperature, the material evaporates too rapidly, which leads to breakdown of the accelerating gap and reduction is 900-1000°C, when an ion flux of $\sim 1 \cdot 10^{14}$ cm^{-2} may be produced in the course of a single implantation. The duration of ionic implantation in these conditions is 5-10 sec, and the use coefficient of the working material reaches 50%. With increase in ionic flux, the use coefficient falls, mainly because of the reduction in ionization probability and the breakdown of the accelerating gap.

The strength of retention of the radioactive ions in the samples is determined by the depth of their implantation. The latter, in turn, depends on the nature of the ions, their energy, and the target characteristics. In Fig. 2, the dependence of the mean projective path lengths R_p and their scatter ΔR_p on the atomic number of the target Z_2 is shown for cesium ions of various energies; the curves are obtained by the interpolation of tabular data [5]. In the experimental conditions (E = 50-70 keV), the implantation depth of the ions was 10-30 nm for different materials; this is sufficient to obtain strong radioactive markers

Translated from Atomnaya Énergiya, Vol. 53, No. 1, pp. 50-51, July, 1982. Original article submitted September 1, 1981.

 0038-531X/82/5301-0512$07.50

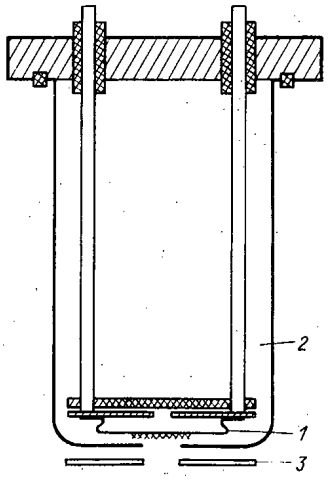

Fig. 1. Diagram of ion source.

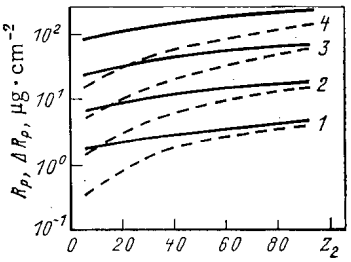

Fig. 2. Dependence of the mean protective path R_p and the scatter of the paths ΔR_p (dashed curves) of cesium ions on the atomic number of the target atoms Z_2 and the energy, keV: 1) 20; 2) 80; 3) 300; 4) 1000.

TABLE 1. Decay Characteristics of Long-lived ($T_{1/2} \geqslant 1$ day) Isotopes of Potassium, Rubidium, and Cesium [2]

A		$T_{1/2}$	E, keV		
			β^+	β^-	γ
K	40	$1{,}3 \cdot 10^9$ yr.	491	1321	1470
	43	0,94 days	—	830	627
Rb	83	83 days	—	—	521
	84	38 days	1700	908	890
	86	19 days	—	1795	1080
	87	$5{,}3 \cdot 10^{10}$ year	—	270	—
Cs	129	1,3 days	—	—	410
	131	9,7 days	—	—	355
	132	6,5 days	—	—	670
	134	2,1 days	—	657	625
	137	30 yr.	—	514	662

Note. Only the energies of the most intense spectral lines of the β^+, β^-, and γ radiation of the nuclides are shown.

at the surface of the activated objects. Experiments with targets of diamond, aluminum, silicon, iron, and copper and also of some alloys based on aluminum and iron showed that removal of the marker by mechanical or chemical means is impossible without also removing the substrate material. Thermal vaporization of the marker in conditions excluding oxidation of the materials is only observed at the melting point of the investigated materials.

It remains to thank academician G. N. Flerov for his interest in the work, and for valuable advice.

LITERATURE CITED

1. É. Ya. Zandberg and N. I. Ionov, Usp. Fiz. Nauk, 67, No. 4, 581 (1959).
2. B. S. Dzhelepov, L. K. Peker, and V. O. Sergeev, Decay Schemes of Radioactive Nuclei [in Russian], Izd. Akad. Nauk SSSR, Moscow–Leningrad (1963).
3. Yu. V. Bulgakov et al., in: Abstracts of the Proceedings of the First MGU–ZIL Scientific–Engineering Conference [in Russian], Izd. Mosk. Gos. Univ., Moscow (1978), p. 15.
4. Yu. V. Bulgakov et al., Abstracts of the Proceedings of the First Factory–University All-Union Scientific Conference [in Russian], Vol. 1, Izd. Mosk. Gos. Univ., Moscow (1980), p. 12.
5. M. A. Kumakhov et al., Projective Paths and Scatter of Paths for 1240 Ion–Target Combinations [in Russian], VINITI, Moscow (1974), Dep. No. 700-75.

How To Comply With The New Copyright Law

Participation in the Copyright Clearance Center (CCC) assures you of legal photocopying at the moment of need.

Libraries everywhere have found the easy way to fill photocopy requests legally and instantly, without the need to seek permissions, from more than 3000 key publications in business, science, humanities, and social science. You can:

Fill requests for multiple copies, interlibrary loan (beyond the CONTU guidelines), and reserve desk without fear of copyright infringement.

Supply copies from CCC-registered publications simply and easily.

The Copyright Clearance Center is your one-stop place for on-the-spot clearance to photocopy for internal use.

Its flexible reporting system accepts photocopying reports and returns an itemized invoice. You send only one convenient payment. CCC distributes it to the many publishers whose works you need.

And, you need not keep any records, the CCC computer will do it for you. Register now with the CCC and you will never again have to decline a photocopy request or wonder about compliance with the law for any publication participating in the CCC.

To register or for more information, just contact:

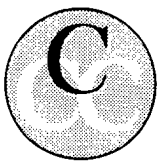

Copyright Clearance Center
21 Congress Street
Salem, Massachusetts 01970
(617) 744-3350

a not-for-profit corporation

NAME _____ TITLE _____

ORGANIZATION _____

ADDRESS _____

CITY _____ STATE _____ ZIP _____

COUNTRY _____ TELEPHONE _____

Declassified and Approved For Release 2013/03/04 : CIA-RDP10-02196R000300010001-0

CHANGING YOUR ADDRESS?

In order to receive your journal without interruption, please complete this change of address notice and forward to the Publisher, 60 days in advance, if possible.

(Please Print)

Old Address:

name

address

city

state (or country) zip code

New Address

name

address

city

state (or country) zip code

date new address effective

name of journal

THE LANGUAGE OF SCIENCE
Plenum
PUBLISHING CORPORATION

233 Spring Street, New York, New York 10013

MEASUREMENT TECHNIQUES
Izmeritel'naya Tekhnika
Vol. 25, 1982 (12 issues) $400

MECHANICS OF COMPOSITE MATERIALS
Mekhanika Kompozitnykh Materialov
Vol. 18, 1982 (6 issues) $330

METAL SCIENCE AND HEAT TREATMENT
Metallovedenie i Termicheskaya Obrabotka Metallov
Vol. 24, 1982 (12 issues) $420

METALLURGIST
Metallurg
Vol. 26, 1982 (12 issues) $435

PROBLEMS OF INFORMATION TRANSMISSION
Problemy Peredachi Informatsii
Vol. 18, 1982 (4 issues) $320

PROGRAMMING AND COMPUTER SOFTWARE
Programmirovanie
Vol. 8, 1982 (6 issues) $135

PROTECTION OF METALS
Zashchita Metallov
Vol. 18, 1982 (6 issues) $380

RADIOPHYSICS AND QUANTUM ELECTRONICS
Izvestiya Vysshikh Uchebnykh Zavedenii, Radiofizika
Vol. 25, 1982 (12 issues) $400

REFRACTORIES
Ogneupory
Vol. 23, 1982 (12 issues) $380

SIBERIAN MATHEMATICAL JOURNAL
Sibirskii Matematicheskii Zhurnal
Vol. 23, 1982 (6 issues) $495

SOIL MECHANICS AND FOUNDATION ENGINEERING
Osnovaniya, Fundamenty i Mekhanika Gruntov
Vol. 19, 1982 (6 issues) $380

SOLAR SYSTEM RESEARCH
Astronomicheskii Vestnik
Vol. 16, 1982 (4 issues) $275

SOVIET APPLIED MECHANICS
Prikladnaya Mekhanika
Vol. 18, 1982 (12 issues) $400

SOVIET ATOMIC ENERGY
Atomnaya Énergiya
Vols. 52–53 (12 issues) $440

SOVIET JOURNAL OF GLASS PHYSICS AND CHEMISTRY
Fizika i Khimiya Stekla
Vol. 8, 1982 (6 issues) $175

SOVIET JOURNAL OF NONDESTRUCTIVE TESTING
Defektoskopiya
Vol. 18, 1982 (12 issues) $485

SOVIET MATERIALS SCIENCE
Fiziko-khimicheskaya Mekhanika Materialov
Vol. 18, 1982 (6 issues) $345

SOVIET MICROELECTRONICS
Mikroélektronika
Vol. 11, 1982 (6 issues) $195

SOVIET MINING SCIENCE
Fiziko-tekhnicheskie Problemy Razrabotki Poleznykh Iskopaemykh
Vol. 18, 1982 (6 issues) $420

SOVIET PHYSICS JOURNAL
Izvestiya Vysshikh Uchebnykh Zavedenii, Fizika
Vol. 25, 1982 (12 issues) $400

SOVIET POWDER METALLURGY AND METAL CERAMICS
Poroshkovaya Metallurgiya
Vol. 21, 1982 (12 issues) $435

STRENGTH OF MATERIALS
Problemy Prochnosti
Vol. 14, 1982 (12 issues) $495

THEORETICAL AND MATHEMATICAL PHYSICS
Teoreticheskaya i Matematicheskaya Fizika
Vols. 50–53, 1982 (12 issues) $380

UKRAINIAN MATHEMATICAL JOURNAL
Ukrainskii Matematicheskii Zhurnal
Vol. 34, 1982 (6 issues) $380

Send for Your Free Examination Copy

Plenum Publishing Corporation, 233 Spring St., New York, N.Y. 10013
In United Kingdom: 88/90 Middlesex St., London E1 7EZ, England
Prices slightly higher outside the U.S. Prices subject to change without notice.

RUSSIAN JOURNALS IN THE PHYSICAL AND MATHEMATICAL SCIENCES

AVAILABLE IN ENGLISH TRANSLATION

ALGEBRA AND LOGIC
Algebra i Logika
Vol. 21, 1982 (6 issues) $270

ASTROPHYSICS
Astrofizika
Vol. 18, 1982 (4 issues) $320

AUTOMATION AND REMOTE CONTROL
Avtomatika i Telemekhanika
Vol. 43, 1982 (24 issues) issues) $495

COMBUSTION, EXPLOSION, AND SHOCK WAVES
Fizika Goreniya i Vzryva
Vol. 18, 1982 (6 issues) $345

COSMIC RESEARCH
Kosmicheskie Issledovaniya
Vol. 20, 1982 (6 issues) $425

CYBERNETICS
Kibernetika
Vol. 18, 1982 (6 issues) $345

DIFFERENTIAL EQUATIONS
Differentsial'nye Uravneniya
Vol. 18, 1982 (12 issues) $395

DOKLADY BIOPHYSICS
Doklady Akademii Nauk SSSR
Vols. 262–267, 1982 (2 issues) $145

FLUID DYNAMICS
Izvestiya Akademii Nauk SSSR, Mekhanika Zhidkosti i Gaza
Vol. 17, 1982 (6 issues) $380

FUNCTIONAL ANALYSIS AND ITS APPLICATIONS
Funktsional'nyi Analiz i Ego Prilozheniya
Vol. 16, 1982 (4 issues) $320

GLASS AND CERAMICS
Steklo i Keramika
Vol. 39, 1982 (6 issues) $460

HIGH TEMPERATURE
Teplofizika Vysokikh Temperatur
Vol. 20, 1982 (6 issues) $400

HYDROTECHNICAL CONSTRUCTION
Gidrotekhnicheskoe Stroitel'stvo
Vol. 16, 1982 (12 issues) $305

INDUSTRIAL LABORATORY
Zavodskaya Laboratoriya
Vol. 48, 1982 (12 issues) $400

INSTRUMENTS AND EXPERIMENTAL TECHNIQUES
Pribory i Tekhnika Eksperimenta
Vol. 25, 1982 (12 issues) $460

JOURNAL OF APPLIED MECHANICS AND TECHNICAL PHYSICS
Zhurnal Prikladnoi Mekhaniki i Tekhnicheskoi Fiziki
Vol. 23, 1982 (6 issues) $420

JOURNAL OF APPLIED SPECTROSCOPY
Zhurnal Prikladnoi Spektroskopii
Vols. 36–37 (12 issues) $420

JOURNAL OF ENGINEERING PHYSICS
Inzhenerno-fizicheskii Zhurnal
Vols. 42–43, 1982 (12 issues) $420

JOURNAL OF SOVIET LASER RESEARCH
A translation of articles based on the best Soviet research in the field of lasers
Vol. 3, 1982 (4 issues) $95

JOURNAL OF SOVIET MATHEMATICS
A translation of Itogi Nauki i Tekhniki and *Zapiski Nauchnykh Seminarov Leningradskogo Otdeleniya Matematicheskogo Instituta im. V. A. Steklova AN SSSR*
Vols. 18–20, 1982 (18 issues) $680

LITHOLOGY AND MINERAL RESOURCES
Litologiya i Poleznye Iskopaemye
Vol. 17, 1982 (6 issues) $420

LITHUANIAN MATHEMATICAL JOURNAL
Litovskii Matematicheskii Sbornik
Vol. 22, 1982 (4 issues) $205

MAGNETOHYDRODYNAMICS
Magnitnaya Gidrodinamika
Vol. 18, 1982 (4 issues) $325

MATHEMATICAL NOTES
Matematicheskie Zametki
Vols. 31–32, 1982 (12 issues) $400

continued on inside back cover